UASLP
Universidad Autónoma de San Luis Potosí

FACULTAD DE CIENCIAS

COMPLEXITY AS A MEASURE OF PATHS TO REGULARITY

Tesis que para obtener el grado de Doctor en Ciencias Interdisciplinarias presenta

Andrea Arlette España Tinajero

Línea de Investigación

Modelamiento Matemático y Computacional

Codirectores de Tesis

Dr. Xavier Leoncini, Aix-Marseille Université

Dr. Edgardo Ugalde Saldaña, Universidad Autónoma de San Luis Potosí

San Luis Potosí, San Luis Potosí, mayo de 2023

Aix*Marseille université
Socialement engagée

POSGRADO EN CIENCIAS INTERDISCIPLINARIAS

Instituto de Física

San Luis Potosí, a 9 de mayo del 2023

La presente tesis, titulada "COMPLEXITY AS A MEASURE OF PATHS TO REGULARITY", presentada por Andrea Arlette España Tinajero para obtener el grado de Doctor en Ciencias Interdisciplinarias, por la Universidad Autónoma de San Luis Potosí, ha sido realizada bajo la dirección conjunta de los siguientes codirectores de tesis:

- Dr. Xavier Leoncini, Aix-Marseille Université.
- Dr. Edgardo Ugalde Saldaña, Universidad Autónoma de San Luis Potosí.

Esta tesis se realizó en el marco de un doctorado en cotutela entre la Aix-Marseille Université y la Universidad Autónoma de San Luis Potosí. De la primera siguiendo el programa establecido por la Ecole Doctorale Physique et Sciences de la Matière, en colaboración con el Centre de physique théorique, bajo el título en francés: *Complexité définie comme une mesure des chemins conduisant à une certaine notion de régularité.*

Abstract

In this thesis, a way to quantify the synchronization of a system is introduced. It is made from a codification of the paths towards synchronization for synchronizing flows defined over a network. The collection of paths toward synchronization defines a combinatorial structure, called *the transition diagram*, the main object of study. The cardinality of this collection defines a measure of complexity which depends on the dimension of the system.

The transition diagram corresponding to the Laplacian flow over the complete graph K_N and the complete bipartite graph $K_{N,N}$ is described, through a coding: the feasible states by increasing functions, and the transitions between them by consecutive functions that follow certain rules. These results are applied to the Kuramoto flow (over the same graph) when a neighborhood close to the diagonal is considered. Furthermore, it generalizes to flows that are monotonic (that is, its coordinates and the differences of the coordinates maintain the order).

It is presented as well some numerical and analytical results concerning the Laplacian and Kuramoto flows over the cycle graph C_N, and the ring lattice family $C(N,k)$. In this case there are a different perspective, due to their no-monotonic behavior.

Keywords: Non-linearity, Synchronization, Laplacian, Kuramoto model

Contents

List of Figures

List of Tables

1 Introduction

The study of complex systems is currently in full expansion and we can find multiple examples as in Wang, Bu, Han, et al. 2016; Yu, Zeng, Gillard, et al. 2015; Hou, Small, and Lao 2015. In fact, the notion of complex systems can encompass a much broader field than those encountered in physics Wang, Bu, Han, et al. 2016; Z.-K. Gao and Jin 2012; Wu, Sun, and Z. Gao n.d.; Ni, Jiang, and Zhou 2009, ranging from biology Giuliani, Benigni, Zbilut, et al. 2002; Marwan, Wessel, Meyerfeldt, et al. 2002, to social sciences Davies, Fry, Wilson, et al. 2013; Baudains, Johnson, and Braithwaite 2013; Epstein 2002; Siegel 2009, economics and finance Kyrtsou and Vorlow 2005; Bigdeli and Afshar 2009.

With regard only to physics, complex systems can be considered as systems composed of many components, most often having non-linear interaction on a complex network for example. When dynamics is introduced, depending on the initial conditions and the considered system, the system may end up landing on a final given attractor, which in the most simple case is just some fixed point of the dynamical system as in Siegel 2009. One of the outstanding phenomena around complex systems is the one studied in this thesis: the synchronization phenomenon.

The synchronization of events seems to happen naturally, as if they were programmed in such a way that the interaction between them, even if it is very small, would result in an adjustment of their rhythms.

For example, imagine that we are in an auditorium, listening to an orchestra concert. The venue is full, and the musicians are doing a really great job. The minutes pass and we hear the final note of the melody. We are so excited, that we begin to applaud. Next, the person who is by our side, also applauds and in a few seconds, the whole audience is doing it. If we pay attention, it turns out that the sound, at the beginning is irregular and passed the time, it seems as if a single pair of enormous hands were applauding, with a higher volume. This phenomenon occurs, without the audience, at first, had agreed with how often they would applaud, just listening to the way others do it, naturally, causes synchrony.

Another example, and probably one of the most famous, was discovered by a Dutch astronomer, physicist, and mathematician: Christiaan Huygens (1629-1695). He was sick and resting in a room, when he noticed that there were two pendulum clocks hanging on the wall and they were perfectly synchronized. He analyzed the phenomenon and concluded that both clocks were interacting, and they did so because

of the only link that existed between them: the wall on which they were hanging.

There are many other examples that we can find in the literature Pikovsky, Rosenblum, and Jürgen Kurths 2001. Different types of tools and modelization will be then developed to understand typical synchronization phenomena occurring in these systems. These tools have been used to develop models in many different fields ranging from pure mechanical science to neuroscience or self-organization observed in flocking of birds or schooling of fishes.

Before the concept of synchronization, the frequency adjustment is described. Generally, the interaction between two oscillators is not symmetrical Zarauza Martínez 2016, this means that one of the oscillators is more powerful than the other. The frequencies of the two oscillators can be denoted as ω_1 and ω_2, which can be assigned an order, for example $\omega_1 < \omega_2$.

The observed frequencies Ω_i, defined as the average speed of phase rotation of the oscillators. That is $\langle \dot{\theta} \rangle = \Omega$. And,

$$\Omega_i = \lim_{T\to\infty} \frac{1}{T} \int_0^T \frac{d\theta_i}{dt} dt = \lim_{t\to\infty} \frac{1}{T} \left[\theta_i(T) - \theta_i(0)\right]. \tag{1.1}$$

If the coupling is strong enough, $\Omega_1 = \Omega_2 = \Omega$, where generally $\omega_1 < \Omega < \omega_2$.

When the frequencies ω_i of two decoupled systems are very similar, synchronization arises because the interaction force is sufficient. Furthermore, there must be a certain relationship between the phases of the oscillators. This condition means that the phase difference must be restricted. Let $\epsilon > 0$, then $|\theta_1 - \theta_2| < \epsilon$.

It is important to be able to distinguish the different cases that may occur in a system where coupled oscillators act, the first of them, and the most desired in the case study of this thesis, is where a state of synchronization is reached, that is, where the oscillators have the same phase from a certain instant. Another possible state is in which the oscillators are in a phase locked, that is, the difference between them is a fraction of the complete angle along their entire trajectory (or in other words, the differences between the phases of different oscillators remain constant in time), as for example, if the case of two pendulums is considered, with a difference of π radians, that is, when one goes to the left, the other goes to the right. This means that the system is always in balance, but without complete synchronization, to know more details of the case of dimension 2, see Pantaleone 2002. The last case is when the oscillators do not have any coherence with each other, that is, each one goes at their own pace and their behavior does not seem to have much influence on their partner.

This field of research when considering coupled dynamical systems on networks has been highly developed from the main article by Kuramoto published in 1975 Kuramoto 1975 that describes the synchronization of a group of coupled oscillators.

There are several studies considering homogeneously coupled systems like global coupling, completely random coupling or couplings according to a network Acebrón, Bonilla, Pérez Vicente, et al. 2005; Strogatz 2000; Fonseca and Abud 2018; DeVille and B. Ermentrout 2016; Delabays, Jacquod, and Dörfler 2019; Medvedev and Tang 2017; Moreno and Pacheco 2004, among other features van Hemmen and Wreszinski 1993; Sokolov and G. B. Ermentrout 2019 which study the conditions under which globally synchronized phases, phase locked and different degrees of incoherence can be observed.

As noticed by Arenas, Diaz-Guilera, Jurgen Kurths, et al. 2008, the way in which the connectivity of a synchronized subnetwork increases as time progresses, follows its linearized dynamics. From this perspective, in this thesis it is proposed to study the dynamics of the non-linear system from its linearization, that is, to study the path towards synchronization through the study of the Laplacian as a linear dynamical system, which has been extensively studied and of which many properties are known. On the other side, it is well known that the non-linear dynamics is not always fully synchronizing and some important differences between linear and non-linear interactions appear as we increase the size of the system, starting with the fact that in the case of the Laplacian, it is always possible to obtain global synchronization. Nevertheless, there is always a small volume around the synchronizing manifold where the linear behavior dominates, and synchronization takes place. There are also works that make a linear reformulation of the Kuramoto system as in Roberts 2008, so that its behavior can be explained from the linear point of view.

Due to the great difficulties that one has in itself to find the conditions under which a system can be synchronized, this work focuses on studying the systems that we know *a priori* that synchronizes, through a novel approach that focuses on studying the transitory state, that is, what happens while the system reaches synchronization. One can decide under what conditions one wants to start and eventually know what condition it will reach (which is a synchronized state). The novelty of this thesis is the description of the different ways in which the asymptotic state of a synchronizing system is reached, which are given the name of paths towards synchronization. Furthermore, an interesting feature in this thesis is to count the number of these paths, since it is a way of measuring the complexity of a system (in the case of transient dynamics), to study the transient behavior and characterize the complexity of the attractor's basin. Characterizing the complexity of the system by measuring the diversity of paths is a topic that has been studied in several works, as in Afraimovich and Zaslavsky 2003; Zaslavsky and Afraimovich 2005; X. Leoncini and Zaslavsky 2002.

The main objective of this work can be stated: to describe the transitory behavior of systems that synchronize, which are defined on a fixed network, through a well-defined coding that allows to globally describe the states by which an initial condition can be found. Using this coding, define a function that describes the complexity of the systems to be evaluated. In addition, this coding must allow describing the properties

and characteristics of the transitory state of the systems.

Specifically, the objectives of this thesis are:

— To analytically describe the combinatorial structures that are formed from the paths to synchronization.
— To give a qualitative description of these.
— To study how these combinatorial structures depend on:
  — The network.
  — The linearity or non-linearity of the system.
  — The distance between each pair of coordinates.
  — The time scale.
— To study the complexity of combinatorial structures.

To achieve the objectives of this thesis, the concept of synchronization sequences is introduced, which can be related to the connectivity matrix, defined in Arenas, Díaz-Guilera, and Pérez-Vicente 2006. If it is considered the case of a fully synchronizing system, the set of all synchronizing sequences is necessary to form a transition diagram, which encodes the full transient dynamics towards synchronization. Specifically, this thesis is dedicated to studying this combinatorial structure for the Laplacian system dynamics on the complete graph K_N in deep detail, and the case of the complete bipartite graph $K_{N,N}$ in some detail. The characterization is carried out through some topological and numerical properties of the corresponding transition diagrams, in addition to the qualitative properties of the generated paths.

This work, which describes how systems that we know how to synchronize reach this asymptotic state, provides a more complete explanation of the synchronization phenomenon. In this way, it is possible to understand not only macroscopically, but microscopically this phenomenon. In addition, the results of this thesis provide a measure of the complexity of the systems, according to the number of paths that can be generated, when the graph topology is changed.

The content of the thesis is organized as follows. After establishing the basic concepts in Chapter 2 in graph theory, linear algebra, combinatorics that will be used throughout this thesis, the two systems in question: the Laplacian system and the Kuramoto model are defined. Then, the methods are described and divided into two sections:

— The first focuses on the formal construction of the paths to synchronization, through successions of subgraphs, which is the main object of study in this thesis.

— The second section focuses on the computational analyzes, which were made to give an idea of the behavior of the transient state of the systems acting on the different types of graphs.

Next, in Chapter 3, the exploratory study of the Laplacian system and the Kuramoto model applied to the complete graph, the bipartite complete graph, the cycle graph and the family of ring lattices are presented. The behavior of a set of random initial conditions in different dimensions is evaluated, under the following margins:

— The depth of the transition graph.
— The number of possible states in the transition graph.
— The distribution of path lengths.
— The number of different paths towards synchronization.

To finish the section, a discussion between the differences and similarities found by varying the topology of the graph is presented. These subsections are intentionally repetitive, so that they can be read individually, depending on the needs of a future reader. In Chapter 4, the formal and rigorous results of this doctoral work are presented, organized in three important sections, each one of them focuses on the study of a combinatorial object.

— Firstly, the transition diagram of synchronization paths for the complete graph K_N is presented, from a complete rigorous and formal study based on a coding, made from increasing functions and the combinatorics around them.

— Secondly, results concerning the structure of the transition diagram for the complete bipartite graph $K_{N,N}$, for balanced initial conditions. This formulation allows a formal, but not complete, description of the space. This process is done from a coding of pairs of increasing functions, and the parallelo-polyminoes that are formed from these pairs.

— Thirdly, it is discussed the behavior of the Laplacian applied to the cycle graph C_N. In addition, the behavior of the transition diagram of the complete graph and of the complete bipartite graph when the Kuramoto model is applied, is discussed.

Finally, in Chapter 4.3.2 the conclusions and perspectives of this work are written, which can be taken for several future and productive works.

Note: This thesis was done in co-tutelage in the universities: Autonomous University of San Luis Potosí and Aix-Marseille Université. The version of the thesis that is presented is the Mexican version.

2 Theoretical and methodological frameworks

Contents

2.1 Basic concepts

This section presents the definitions that will be used throughout the thesis and provides examples of them for a better understanding. It begins with graph theory, linear algebra, the Laplacian system, the Kuramoto model and it is finalized with a section about combinatorics.

2.1.1 Graph theory

Throughout this thesis, it will be considered a system of coupled differential equations that acts on an initial condition, in which each of its components interacts with the others according to an interaction rule. For example, consider a fixed system, for which an initial condition has 4 components. The interaction rule in this case is as follows: component number 1 interacts with component 2 and 3 (and vice versa) and component 4 interacts with component 3 (and vice versa). This interaction rule can be seen in the following Figure 2.1.

This representation of the interaction rules between the components of an initial condition is called *graph* or *network*, and it will be defined formally below.

On the one hand, a *graph* or *network* refers to an undirected graph $G = (V, E)$, with vertices in V and edges in E. On the other hand, a *directed graph* is a couple $D = (V, A)$ of vertices in V and arrows in A. An *edge* is a set of two vertices (both are the start, and

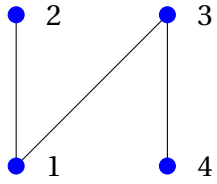

Figure 2.1 – Example of interaction rules between the components of a four-dimensional initial condition, in which it indicates that vertex 1 interacts with vertices 2 and 3 and vice versa, in addition, vertex 3 interacts with vertex 4 and vice versa.

both are the end), while an *arrow* is an ordered pair of vertices (the first indicates the start and the second indicates the end). It is denoted by $|V|$ the number of vertices that a graph has.

In this thesis I focus mainly on the study of three graphs: the complete graph, the bipartite complete graph, and the cycle graph (with their respective family called ring lattice), each of which is defined below. First, in the *complete graph* $K_N = (V, E)$ such that $|V| = N$, each of its vertices has an edge with all the others, that is $(v_i, v_j) \in E$ for all $v_i \in V$ where $1 \leq i, j \leq N$ and $i \neq j$. In Figure 2.2 (a), an example of the complete graph is shown where $N = 4$, that is, K_4. Continuing with the concept of the *complete bipartite graph* denoted by $K_{N,N} = (V, E)$, in this case $|V| = 2N$ and it is defined as follows, it is defined two disjoint subsets of V, let's say $V_1, V_2 \subset V$ such that $|V_1| = |V_2| = N$, and for all vertex in V_1 there exist an edge with all vertices in V_2, that is, $(v_1, v_2) \in E$, for all $v_1 \in V_1$ and all $v_2 \in V_2$. In Figure 2.2 (b), an example of the complete bipartite graph is shown where $N = 2$, that is, $K_{2,2}$. Finally, the *cycle graph* denoted by $C_N = (V, E)$ such that $|V| = N$, each vertex is connected to its consecutive, also the first vertex is connected to the last one. In other words $(v_i, v_{i+1}) \in E$ for all $v_i \in V$ with $1 \leq i < N$ and $(v_1, v_N) \in E$. In Figure 2.2 (c), an example of the cycle graph is shown where $N = 4$, that is, C_4.

There is a type of graph called *ring lattice*, that is a graph which is obtained by taking a cycle graph and connecting each vertex to its neighbors two "hops" away, which is written as $C(N, 2)$ giving as a result a 4-regular graph (that is, all its vertices have degree 4), as it can be seen in Figure 2.3, an example of the ring lattice $C(6, 2)$ is shown, where each of its vertices has degree 4. The definition can be generalized to other even numbers greater than 4 (connecting each vertex to its neighbors three hops away, that is $C(N, 3)$ giving a 6-regular graph, and so on: $C(N, k)$, the particular case when $k = 1$ is exactly the cycle graph C_N).

From the graphs, it can be defined their subsets to study each of their parts, hence the interest in the following concept. A *subgraph* of G (or *subnetwork*) it is also a graph,

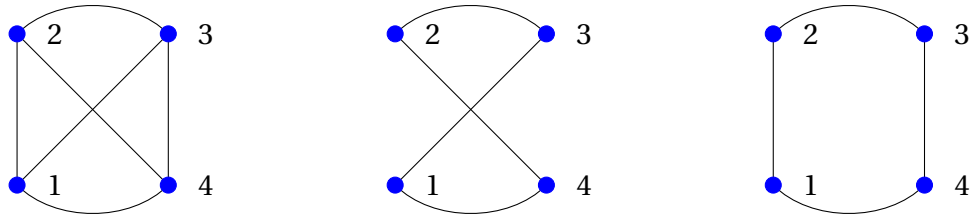

Figure 2.2 – Example of a complete graph, a bipartite complete graph and a cycle graph. In (a) the complete graph of dimension 4 is presented, denoted by K_4, in (b) the complete bipartite graph is shown with two sets of dimension two, which is denoted as $K_{2,2}$ and finally, in (c) the cycle graph of dimension 4 is shown, which is written as C_4.

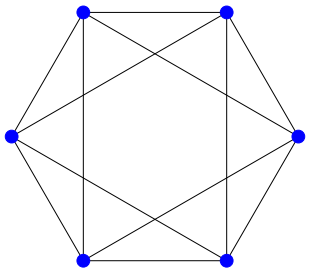

Figure 2.3 – Ring lattice example $C(6,2)$, which is made based on a cycle graph C_6 and each vertex is joined with its first two neighbors to the left and to the right.

which it is written $G' = (V', E')$ such that $V' \subset V$ and all the edges in $E' \subset E$ have end vertices in V'. As it is easy to infer, in general, each subgraph has multiple subgraphs, Figure 2.4 shows in (a) an example of a graph with 4 vertices and 4 edges, and in (b) one of its subgraphs composed of 3 vertices and 2 edges which are included in the sets of vertices and edges of the original graph (a). The set of vertices with which a fixed vertex v is connected, it is called *neighborhood*, and each one of them is called *neighbor*. For example, in Figure 2.4 (a), vertices 2 and 3 are neighbors of vertex 1. In addition, the number of neighbors that a vertex v has can be called the *degree* of v. In Figure 2.4 (a), all the vertices have degree 2, while in (b) the vertex 1 has degree 2 and vertices 2 and 3 have degree 1.

From the subgraphs, other types of graphs can be defined that preserve certain properties. For instance, an *induced subgraph* $G' = (V', E')$ of a graph $G = (V, E)$ is one subgraph such that for the vertices subset $V' \subset V$ all of the edges $E' \subset E$ connecting pairs of vertices in V'. In Figure 2.5, an example of a graph, an induced subgraph and a subgraph that is not induced is shown. For the same set of vertices. In (a) a graph is

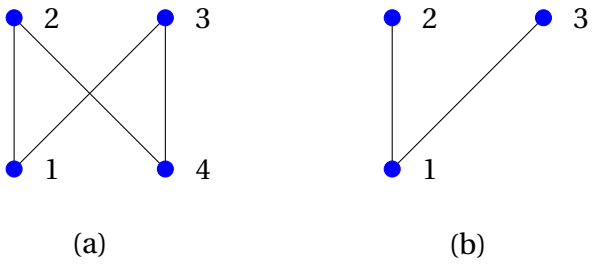

(a) (b)

Figure 2.4 – Example of a graph and one of its subgraphs. In (a) a graph is shown, which is the cycle graph of dimension 4 C_4 and in (b) a subgraph of it is shown. All the vertices that appear in (b) are in (a) and this happens analogously for the edges.

shown. In (b), an induced subgraph of it is shown, because all the edges connecting to the vertices in (a) appear in (b). In (c), a subgraph is shown that is not induced by (a), because not all the edges connecting the vertices in (a) appear in (c).

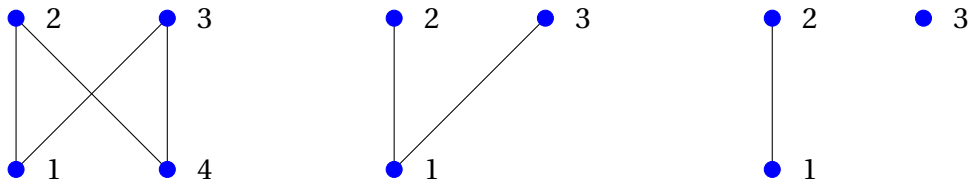

(a) (b) (c)

Figure 2.5 – Example of a graph, an induced subgraph and a not induced subgraph. In (a), a graph is shown. In (b), an induced subgraph of (a) is shown, because all the edges connecting to the vertices in (a) appear in (b). In (c), a subgraph of (a) is shown, but it is not induced by (a), because not all the edges connecting the vertices in (a) appear in (c).

Now, I am interested in exploring the type of connections that exist in the graph beyond the first neighbors. That is, if one vertex can be reached to another by following a succession of vertices in such a way that they are connected by an edge. This concept is called *path*, and more formally, it is a sequence of vertices in an undirected graph G such that each couple of consecutive vertices form an edge. On the other hand, a path in a directed graph D is an ordered sequence of vertices:

$$v_1 \to v_2 \to \cdots \to v_{n-1} \to v_n$$

such that, each couple of consecutive vertices form an arrow. In this case it is said

that v_1 is the *starting* vertex of the path and v_n the *ending* one. Furthermore, if the number of arrows in the sequence is counted, that is $n-1$, this amount is called *length of the path*. In Figure 2.6 it is shown an example of different paths that are in the same graph. They are two different paths to get from vertex 1 to vertex 3 highlighted in red. Explaining them in detail. In (a), the path $v_1 \to v_2 \to v_3$ is shown. In (b), the path $v_1 \to v_3$ is shown as well. The first path has length 2 and the second path has length 1. This is a very important concept for later definitions. Also, a path is said to be *maximal* if it cannot be added any new vertex to make it longer.

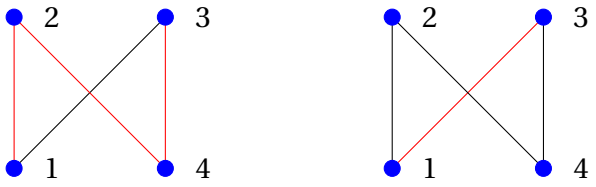

(a) (b)

Figure 2.6 – Example of two paths between two vertices in the same graph. Both in (a) and in (b) the same graph is shown, the difference between them is the red highlighted lines that denote different paths through which one can get from vertex 1 to vertex 3. In (a), there is a path of length 3, passing through vertices 1, 2, 4, and 3. In (b), a path of length 1 is shown, passing directly from vertex 1 to vertex 3.

From the definition of a path of a graph, it can be defined properties of it. In this case, it is said that a graph is *connected* if each couple of vertices belong to a path. If for a given graph there is a path through all its vertices, then the graph is connected. As can be seen in Figure 2.6, both graphs are connected. On the other hand, any graph G can be decomposed in a unique manner as a disjoint union of connected subgraphs $G_1, ..., G_n$, called *connected components*. As is depicted in Figure 2.7, a graph of 5 vertices and 4 edges, which has two connected components is shown. The first subgraph is composed of vertices 1 and 2 and the edge that joins them. The second subgraph is composed of vertices 3, 4 and 5 and the edges that go from vertices 3 to 4, 4 to 5 and 5 to 3. These subgraphs are disjoint, connected and they are the only ones that the graph is composed of, that is, they are its connected components.

Each of the directed or undirected graphs can be written as a square matrix with entries in the real numbers, in which each row and column represents a vertex, coded 0 if there are no edges or arrows between them, and 1 if there are some connection type. This object is called the *adjacency matrix* associated with the graph G. It can be written each of its entries as $a_{i,j}$ where i represents the row number and j represents the column number. The set of square matrices with N rows and N columns with

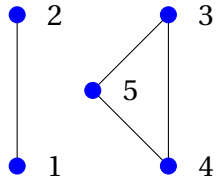

Figure 2.7 – Example of a graph with two connected components. This figure shows a graph with five vertices and 4 edges, in this case there are two connected components, the first is the one composed of vertices 1 and 2 and the edge that joins them, and the second is formed by the vertices 3,4 and 5 and the edges that join this set of vertices.

entries in the real numbers is written as $\mathscr{M}_{N\times N}(\mathbb{R})$. In Figure 2.8 (a), an example of an undirected graph is shown, and in (b), the adjacency matrix associated with this graph is shown as well. In blue, the numbering of the rows and columns are shown, with they each entry can be written if there is an edge between the associated vertices (with a 1) or not (with a 0).

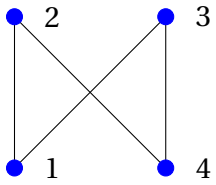

(a)

$$\begin{array}{c} \\ 1 \\ 2 \\ 3 \\ 4 \end{array} \begin{array}{c} \begin{array}{cccc} 1 & 2 & 3 & 4 \end{array} \\ \begin{pmatrix} 0 & 1 & 1 & 0 \\ 1 & 0 & 0 & 1 \\ 1 & 0 & 0 & 1 \\ 0 & 1 & 1 & 0 \end{pmatrix} \end{array}$$

(b)

Figure 2.8 – Example of an adjacency matrix associated to a graph. In (a) a cycle graph of dimension 4 is shown, and in (b) the adjacency matrix associated with this graph is shown. In blue, the numbering of the rows and columns of the matrix is shown, which serves to guide us in the construction of the matrix, which represents the vertices in the graph shown in (a), this construction is done as follows: at position i, j of the matrix a 1 is written when there is an edge connecting vertex i with vertex j and a 0 when there is no edge between them.

There are many types of matrices, and in this case, there are presented two types that will be useful later to define the system. First of all, it is the *diagonal matrix* that is denoted by $Diag(\{x_1, x_2, ..., x_N\})$ where $x_1, x_2, ..., x_N \in \mathbb{R}$, and is defined as follows $a_{i,j} = x_i$, if $i = j$ where $1 \leq i, j \leq N$, and 0 otherwise. Here is an example of a diagonal matrix.

$$Diag(\{1,2,3,4\}) = \begin{pmatrix} 1 & 0 & 0 & 0 \\ 0 & 2 & 0 & 0 \\ 0 & 0 & 3 & 0 \\ 0 & 0 & 0 & 4 \end{pmatrix}.$$

Second, the *degree matrix* associated with an adjacency matrix M_G that is denoted $Deg(M_G)$ is a diagonal matrix defined as follows, each entry $a_{i,j} \neq 0$ corresponds to the degree of the vertex v_i of G. As it can be seen in the example depicted in Figure 2.9. In (a), it is shown one graph, and in (b), is its degree matrix associated.

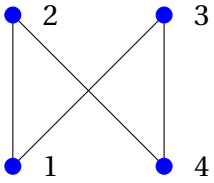

(a)

$$Deg(M_G) = \begin{pmatrix} 2 & 0 & 0 & 0 \\ 0 & 2 & 0 & 0 \\ 0 & 0 & 2 & 0 \\ 0 & 0 & 0 & 2 \end{pmatrix}$$

(b)

Figure 2.9 – Example of a degree matrix associated with a graph. In (a), an example of the cycle graph of dimension 4 C_4 is shown, and in (b), the degree matrix associated with its adjacency matrix (which can be seen in the Figure 2.8) is shown. In this case, all the vertices of the graph shown in (a) they have degree 2, then, in (b), there are only twos on the diagonal of the matrix.

From these definitions, is now in position to present the function called *Laplacian matrix* $L : \mathscr{M}_{N\times N}(\mathbb{R}) \to \mathscr{M}_{N\times N}(\mathbb{R})$, which is applied to the adjacency matrix M_G associated with a graph G and is defined as follows:

$$L(M_G) = M_G - Deg(M_G). \tag{2.1}$$

This is the finite matrix-analogue of the classical Laplacian operator in physics Cvetkovic, Doob, and Sachs 1995 that describe multiple phenomena such as heat conduction or wave propagation. In Figure 2.10 is shown in (a) a fixed graph and in (b) the computation of the Laplacian matrix associated with the adjacency matrix of (a), which in this case is nothing more than using the previous examples shown in Figures 2.8 and 2.9. Also, $L(M_G)$ is a *symmetric matrix*, that is, $a_{i,j} = a_{j,i}$ for all $1 \leq i, j \leq N$, this happens as long as G is undirected. Using this mathematical concept, it has been possible to study the vibration of a discrete membrane Cvetkovic, Doob, and Sachs 1995 and some chemical properties of substances Merris 1994. In addition, its spectrum has been widely studied when applied to different types of graphs, for example, in K. Das 2004; K. C. Das 2004; Liu, Dolgushev, Qi, et al. 2015, whose definitions are in the next section.

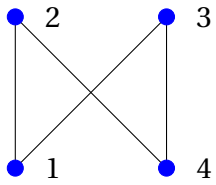

(a)

$$L(M_G) = \begin{pmatrix} -2 & 1 & 1 & 0 \\ 1 & -2 & 0 & 1 \\ 1 & 0 & -2 & 1 \\ 0 & 1 & 1 & -2 \end{pmatrix}$$

(b)

Figure 2.10 – Example of Laplacian matrix associated with a graph. In (a) an example of the cycle graph of dimension 4 C_4 is shown and in (b) shows the Laplacian matrix associated with its adjacency matrix, which is defined as the subtraction of the adjacency matrix (calculated in the Figure 2.8) and the degree matrix (calculated in the Figure 2.9), resulting in the matrix that is shown in (b).

As it is mentioned before, in this thesis there is an interest in the behavior of three graphs in particular, then it proceeds to write the Laplacian matrix of the complete graph K_N, the complete bipartite graph $K_{N,N}$ and the cycle graph C_N in a generalized manner for future reference.

It is recalled that in the Equation (2.1), the calculation of the Laplacian matrix depends on the adjacency matrix and the degree matrix, for the complete graph K_N the adjacency matrix is formed by ones in all the entries except the diagonal (which is formed only by zeros), furthermore, each one of the vertices is connected to all the others, that is why the degree of each vertex is $N-1$, then:

$$\left(L(M_{K_N})\right)_{i,j} = \begin{cases} -(N-1) & \text{if } i = j, \\ 1 & \text{otherwise.} \end{cases} \tag{2.2}$$

The matrix form of the Equation (2.2) is as follows.

$$L(M_{K_N}) = \begin{pmatrix} -(N-1) & 1 & \cdots & 1 & 1 \\ 1 & -(N-1) & \cdots & 1 & 1 \\ \vdots & & \ddots & & \vdots \\ 1 & 1 & \cdots & -(N-1) & 1 \\ 1 & 1 & \cdots & 1 & -(N-1) \end{pmatrix}.$$

Now, for the calculation of the Laplacian matrix in the case of the complete bipartite graph $K_{N,N}$, it is remembered that each vertex of V_i is joined with the N vertices of the other subset V_j where $i, j \in \{1,2\}$ with $i \neq j$. In addition, its adjacency matrix is composed of 2 blocks of zeros and 2 blocks of ones, then:

$$\left(L(M_{K_{N,N}})\right)_{i,j} = \begin{cases} -N & \text{if } i = j, \\ 1 & \text{if } N < i \leq 2N \text{ and } 0 < j \leq N \\ & \text{or } N < j \leq 2N \text{ and } 0 < i \leq N, \\ 0 & \text{otherwise.} \end{cases} \tag{2.3}$$

The matrix form of the Equation (2.3) is as follows.

$$L(M_{K_{N,N}}) = \begin{pmatrix} -N & 0 & \cdots & 0 & 1 & \cdots & 1 & 1 \\ 0 & -N & & 0 & 1 & \cdots & 1 & 1 \\ \vdots & & \ddots & & \vdots & & \vdots & \vdots \\ 0 & 0 & & -N & 1 & \cdots & 1 & 1 \\ 1 & 1 & \cdots & 1 & -N & & 0 & 0 \\ \vdots & \vdots & & \vdots & & \ddots & & \vdots \\ 1 & 1 & \cdots & 1 & 0 & & -N & 0 \\ 1 & 1 & \cdots & 1 & 0 & \cdots & 0 & -N \end{pmatrix}.$$

In the case of the cycle graph C_N, it is remembered that each vertex is joined to its two adjacent vertices, so each one has degree 2. In addition, the adjacency matrix is made up of two ones in each row and the other entries are zero. This is repeated cyclically and symmetrically in each of the rows, that is why there is the following Laplacian matrix:

$$\left(L(M_{C_N})\right)_{i,j} = \begin{cases} -2 & \text{if } i = j, \\ 1 & \text{if } i = j+1 \text{ and } 0 < j \leq N-1 \\ & \text{or } i = j-1 \text{ and } 1 < j \leq N, \\ & \text{or } i = 1 \text{ and } j = N, \\ & \text{or } i = N \text{ and } j = 1, \\ 0 & \text{otherwise.} \end{cases} \tag{2.4}$$

The matrix form of the Equation (2.4) is as follows.

$$L(M_{C_N}) = \begin{pmatrix} -2 & 1 & 0 & 0 & \cdots & 0 & 0 & 0 & 1 \\ 1 & -2 & 1 & 0 & \cdots & 0 & 0 & 0 & 0 \\ 0 & 1 & -2 & 1 & & 0 & 0 & 0 & 0 \\ & \ddots & & & \ddots & & & \ddots & \\ 0 & 0 & 0 & 0 & & 1 & -2 & 1 & 0 \\ 0 & 0 & 0 & 0 & \cdots & 0 & 1 & -2 & 1 \\ 1 & 0 & 0 & 0 & \cdots & 0 & 0 & 1 & -2 \end{pmatrix}.$$

Finally, in the case of the family of ring lattices $C(N,k)$, specifically when two neighbors to the left and two neighbors to the right are considered, that is, $C(N,2)$, the Laplacian matrix associated with its adjacency matrix is written as follows:

$$\left(L(M_{C(N,2)})\right)_{i,j} = \begin{cases} -4 & \text{if } i = j, \\ 1 & \text{if } i = j+1 \text{ and } 0 < j \leq N-1 \\ & \text{or } i = j-1 \text{ and } 1 < j \leq N, \\ & \text{or } i = j+2 \text{ and } 0 < j \leq N-2 \\ & \text{or } i = j-2 \text{ and } 2 < j \leq N, \\ & \text{or } i = 1 \text{ and } N-1 \leq j \leq N, \\ & \text{or } i = 2 \text{ and } j = N, \\ & \text{or } i = N-1 \text{ and } j = 1, \\ & \text{or } i = N \text{ and } 1 \leq j \leq 2, \\ 0 & \text{otherwise.} \end{cases} \tag{2.5}$$

The matrix form of the Equation (2.5) is as follows.

$$L(M_{C(N,2)}) = \begin{pmatrix} -4 & 1 & 1 & 0 & \cdots & 0 & 0 & 1 & 1 \\ 1 & -4 & 1 & 1 & \cdots & 0 & 0 & 0 & 1 \\ 1 & 1 & -4 & 1 & & 0 & 0 & 0 & 0 \\ & \ddots & & & \ddots & & & \ddots & \\ 0 & 0 & 0 & 0 & & 1 & -4 & 1 & 1 \\ 1 & 0 & 0 & 0 & \cdots & 1 & 1 & -4 & 1 \\ 1 & 1 & 0 & 0 & \cdots & 0 & 1 & 1 & -4 \end{pmatrix}.$$

From the matrices described in this section, which represent the Laplacian system applied to the complete graph, the complete bipartite graph, the cycle graph, and the ring lattice family, it is then possible to define the system of coupled differential equations that corresponds to each type of matrix, as will be seen in later sections.

2.1.2 Linear algebra

A matrix $M \in \mathcal{M}_{N\times N}(\mathbb{R})$, can be interpreted as a linear transformation (because this set is a vector space), such that $M : \mathcal{M}_{N\times N}(\mathbb{R}) \to \mathcal{M}_{N\times N}(\mathbb{R})$ such that for certain $v, w \in \mathbb{R}^N$, $M(v) = w$.

In the case where $v \neq 0$ and $w = \lambda v$, for some $\lambda \in \mathbb{R}$, that is, w is a multiple of v, so it is called λ *eigenvalue* of M and v is its corresponding *eigenvector* (of M). The set of all eigenvalues and eigenvectors of a given matrix M is called the *eigensystem* of M.

On the other hand, a square matrix M is called *diagonalizable*, if there exist $P, D \in \mathcal{M}_{N\times N}(\mathbb{R})$ such that P is *invertible* (that means, there is a $P^{-1} \in \mathcal{M}_{N\times N}(\mathbb{R})$ such that $P^{-1}P = \mathbb{I} = PP^{-1}$, where $\mathbb{I} = Diag(\{1, ..., 1\})$ and $D = Diag(\{\lambda_1, ..., \lambda_N\})$ such that:

$$M = PDP^{-1}.$$

It should be noted that not all square matrices can be diagonalized, but there are

certain subsets that always have this characteristic, an example are the symmetric matrices.

It is important to know that all the elements that appear on the diagonal of D are eigenvalues of M and this set is called the *spectrum* of M denoted as $Spec(M)$. The largest value in the spectrum of M is called the *maximal eigenvalue*. When an eigenvalue does not repeat, it is called a *simple eigenvalue*. On the other hand, the number of times an eigenvalue λ is repeated is called the *algebraic multiplicity* of λ.

Each of the columns of P forms a *eigenbasis* or just *basis* $\mathscr{B}$ of $\mathscr{M}_{N\times N}(\mathbb{R})$, that is, all the elements of $\mathscr{M}_{N\times N}(\mathbb{R})$ can be written as a *linear combination* of the elements of $\mathscr{B}$ (that means, for all $M \in \mathscr{M}_{N\times N}(\mathbb{R})$ there exist $a_1, ..., a_N \in \mathbb{R}$ such that $M = \sum_{i=1}^{N} a_i b_i$, where $b_i \in \mathscr{B}$), in other words we can say that the elements of $\mathscr{B}$ *generate* the space and furthermore, all its elements are *linearly independent* (which means that none of the elements of $\mathscr{B}$ is a linear combination of the other elements of $\mathscr{B}$).

There are several types of bases, in this case will be discussed about the three most used. First of all, the *canonical basis*, in $\mathbb{R}^N$ is formed as the following set, where each of the N vectors has N components (1 equals one and $N-1$ equals zero). It is denoted the i-th element as e^i.

$$\left\{ \begin{pmatrix} 1 \\ 0 \\ \vdots \\ 0 \\ 0 \end{pmatrix}, \begin{pmatrix} 0 \\ 1 \\ \vdots \\ 0 \\ 0 \end{pmatrix}, \cdots, \begin{pmatrix} 0 \\ 0 \\ \vdots \\ 1 \\ 0 \end{pmatrix}, \begin{pmatrix} 0 \\ 0 \\ \vdots \\ 0 \\ 1 \end{pmatrix} \right\}.$$

Secondly, the *orthogonal basis*, is a basis in which each pair of its elements has a scalar product equal to zero. For example, the canonical basis for $\mathbb{R}^2$, $\mathscr{B}^* = \{\binom{1}{0}, \binom{0}{1}\}$ also is an orthogonal basis. Finally, the *orthonormal basis*, which is an orthogonal basis and its elements have *norm* (in this case, if $v = (v_1, .., v_N)$, then $||v|| = \sqrt{\sum_{i=1}^{N} v_i^2}$) equal to one, $\mathscr{B}^*$ is also an example of an orthonormal basis. Now it is taken the opportunity to define the *dominant eigenvector* of a basis, it refers to the eigenvector with the largest norm.

An important property that will be used throughout this thesis is the fact that any symmetric matrix is diagonalizable. As already described, the Laplacian matrix is always symmetric, so it can always be diagonalized. Next it is described the eigensystems of the Laplacian matrices of the three graphs that are the object of study of this thesis, the complete graph K_N, the complete bipartite graph $K_{N,N}$ and the cycle graph C_N, which were calculated in the previous Section 2.1.2.

First, for the Laplacian matrix of the complete graph $L(M_{K_N})$ shown in Equation (2.2), and:

$$Spec(L(M_{K_N})) = \{0, -N\}. \tag{2.6}$$

Where 0 has algebraic multiplicity 1 and $-N$ has algebraic multiplicity $N-1$. On the other hand, the eigenvectors are of the following form:

$$(v_i)_j = \begin{cases} 1 & \text{if } i = N, \text{ for all } 1 \leq j \leq N, \\ & \text{or } i = N+1-j \text{ and } 0 < j \leq N, \\ -1 & \text{if } j = 1, \text{ for all } 1 \leq i < N, \\ 0 & \text{otherwise.} \end{cases} \tag{2.7}$$

Where v_N is the eigenvector corresponding to the eigenvalue 0 and v_i where $1 \leq i < N$ are the eigenvectors corresponding to the eigenvalue $-N$.

In vector form, the vectors of the Equation (2.7) can be written as follows.

$$\left\{ \begin{pmatrix} -1 \\ 0 \\ 0 \\ \vdots \\ 0 \\ 0 \\ 1 \end{pmatrix}, \begin{pmatrix} -1 \\ 0 \\ 0 \\ \vdots \\ 0 \\ 1 \\ 0 \end{pmatrix}, \begin{pmatrix} -1 \\ 0 \\ 0 \\ \\ 1 \\ 0 \\ 0 \end{pmatrix}, \cdots, \begin{pmatrix} -1 \\ 0 \\ 1 \\ \\ 0 \\ 0 \\ 0 \end{pmatrix}, \begin{pmatrix} -1 \\ 1 \\ 0 \\ \vdots \\ 0 \\ 0 \\ 0 \end{pmatrix}, \begin{pmatrix} 1 \\ 1 \\ 1 \\ \vdots \\ 1 \\ 1 \\ 1 \end{pmatrix} \right\}.$$

The norm of these vectors is:

$$\|v_i\| = \begin{cases} \sqrt{2} & \text{if } 1 \leq i < N, \\ \sqrt{N} & \text{if } i = N. \end{cases} \tag{2.8}$$

that means that, when $N > 2$, v_N is the dominant eigenvector of $L(M_{K_n})$.

Secondly, the eigensystem for the Laplacian matrix of the complete bipartite graph $L(M_{K_{N,N}})$ shown in Equation (2.3):

$$Spec(L(M_{K_{N,N}})) = \{0, -N, -2N\}. \tag{2.9}$$

For this spectrum, 0 and $-2N$ have algebraic multiplicity equal to 1 and $-N$ has algebraic multiplicity $2(N-1)$. Now, the respective eigenvectors are defined in the following way:

$$(v_i)_j = \begin{cases} 1 & \text{if } i = 2N, \text{ for all } 1 \leq j \leq 2N, \\ & \text{or } i = 1 \text{ and } N < j \leq 2N, \\ & \text{or } i = N+1-j \text{ and } 0 < j \leq N, \\ & \text{or } i = N+2-j \text{ and } N+1 < j \leq 2N, \\ -1 & \text{if } i = 1, \text{ for all } 1 \leq j \leq N, \\ & \text{or } j = 1 \text{ and } N \leq i < 2N, \\ & \text{or } j = N \text{ and } 1 < i \leq N, \\ 0 & \text{otherwise.} \end{cases} \tag{2.10}$$

Where v_{2N} is the eigenvector corresponding to the eigenvalue 0, v_1 is the eigenvector corresponding to the eigenvalue $-2N$ and v_i where $1 < i < 2N$ are the eigenvectors corresponding to the eigenvalue $-N$.

In vector form, the vectors of the Equation (2.10) can be written as follows.

$$\left\{ \begin{pmatrix} -1 \\ -1 \\ \vdots \\ -1 \\ -1 \\ 1 \\ \vdots \\ 1 \\ 1 \end{pmatrix}, \begin{pmatrix} 0 \\ 0 \\ \vdots \\ 0 \\ -1 \\ 0 \\ \vdots \\ 0 \\ 1 \end{pmatrix}, \begin{pmatrix} 0 \\ 0 \\ \vdots \\ 0 \\ -1 \\ 0 \\ \\ 1 \\ 0 \end{pmatrix}, \cdots, \begin{pmatrix} 0 \\ 0 \\ \vdots \\ 0 \\ -1 \\ 1 \\ \\ 0 \\ 0 \end{pmatrix}, \begin{pmatrix} -1 \\ 0 \\ \\ 1 \\ 0 \\ 0 \\ \vdots \\ 0 \\ 0 \end{pmatrix}, \cdots, \begin{pmatrix} -1 \\ 1 \\ \\ 0 \\ 0 \\ 0 \\ \vdots \\ 0 \\ 0 \end{pmatrix}, \begin{pmatrix} 1 \\ 1 \\ 1 \\ 1 \\ \vdots \\ 1 \\ 1 \\ 1 \\ 1 \end{pmatrix} \right\}.$$

The norm of these vectors is:

$$\|v_i\| = \begin{cases} \sqrt{2N} & \text{if } i = 1, \\ & \text{or } i = 2N, \\ \sqrt{2} & \text{if } 1 < i < 2N. \end{cases} \tag{2.11}$$

In this case there are two eigenvectors corresponding to two different eigenvalues that have the same largest norm.

Then, the eigensystem for the Laplacian matrix of the cycle graph $L(M_{C_N})$ shown in Equation (2.4):

$$Spec\left(L(M_{C_N})\right) = \left\{ 2\left(\cos\left(\frac{2\pi i}{N}\right) - 1\right) : 1 \leq i \leq N \right\}. \tag{2.12}$$

For eachλ_i, by the symmetry of the function $\cos(x)$ and the considered interval $(0, 2\pi)$, $\lambda_i = \lambda_{N-i}$ for $1 \leq i \leq \left\lfloor \frac{N-1}{2} \right\rfloor$, that is, all eigenvalues have algebraic multiplicity equal to 2, except when λ_N, it has algebraic multiplicity equal to 1 and when N is even,

$\lambda_{\frac{N}{2}}$ also has algebraic multiplicity equal to 1.

On the other hand, the eigenvectors of $L(M_{C_n})$ are:

$$(v_i)_j = \cos\left(\frac{2\pi ij}{N}\right), \text{ for } 1 \leq i, j \leq N. \tag{2.13}$$

Where each v_i is the corresponding eigenvector to the eigenvalue λ_i.

In vector form, the vectors of the Equation (2.13) can be written as follows.

$$\left\{ \begin{pmatrix} \cos\left(\frac{2\pi}{N}\right) \\ \cos\left(\frac{4\pi}{N}\right) \\ \vdots \\ \cos\left(\frac{2\pi(N-1)}{N}\right) \\ 1 \end{pmatrix}, \begin{pmatrix} \cos\left(\frac{4\pi}{N}\right) \\ \cos\left(\frac{8\pi}{N}\right) \\ \vdots \\ \cos\left(\frac{2\pi(N-1)}{N}\right) \\ 1 \end{pmatrix}, \cdots, \begin{pmatrix} \cos\left(\frac{2\pi(N-1)}{N}\right) \\ \cos\left(\frac{4\pi(N-1)}{N}\right) \\ \vdots \\ \cos\left(\frac{2\pi(N-1)^2}{N}\right) \\ 1 \end{pmatrix}, \begin{pmatrix} 1 \\ 1 \\ \vdots \\ 1 \\ 1 \end{pmatrix} \right\}.$$

Since $|\cos(x)| \leq 1$ for all $x \in \mathbb{R}$:

$$\|v_i\| \leq \sqrt{N} \tag{2.14}$$

Furthermore, $\|v_i\| = \sqrt{N}$ when each $\cos\left(\frac{2\pi ij}{N}\right) = 1$, it occurs when $i = N$ for all $1 \leq j \leq N$, and when N is even, also if $i = \frac{N}{2}$ which means that v_N is the dominant eigenvector when N is odd, and also $v_{\frac{N}{2}}$ when N is even. This different behavior in the eigensystem depending on the parity of N has repercussions on the dynamic behavior of this matrix as discussed below in Section 3.1.3 where the behavior of the ring lattice family, which is mentioned below, will also be discussed.

The spectrum of the Laplacian matrix associated to the ring lattice family $C(N,k)$ having N vertices and $2k$ neighbors is also known, which is given by:

$$Spec(L(M_{C(N,k)})) = \left\{ 2k - \left(\frac{\sin\left(\frac{\pi}{N}(i-1)(2k+1)\right)}{\sin\left(\frac{\pi}{N}(i-1)\right)} - 1 \right), \quad i = 1, 2, ..., N \right\}.$$

Knowing the behavior of the eigensystems associated with these types of graphs, allows to analytically find the solutions to the associated system of differential equations, which is discussed in the next section.

2.1.3 The Laplacian system

Once the way in which the components of an initial condition will interact and the functions that can be applied to the adjacency matrices associated to the graphs have been defined, it proceeds to define the systems that are considered in this thesis. A graph $G = (V, E)$ is fixed and it is considered a system of coupled differential

equations on $I^{|V|}$, where I is either the set of real numbers $\mathbb{R}$ or the circle, written as S^1. The flow is generated by a system of ordinary differential equations (hereinafter, this phrase is abbreviated as ODEs) coupled according to the interactions defined by E.

As has been anticipated, in this thesis I will focus on the *discrete Laplacian flow* or just *Laplacian flow* on the graph G, which is the linear system defined by:

$$\frac{dx_v}{dt} = (Lx)_v = \sum_{u \in V:(u,v)\in E} (x_u - x_v), \tag{2.15}$$

with $x_v \in \mathbb{R}$ for each $v \in V$. Also, in this equation $L = L(M_G)$ is the Laplacian matrix of the adjacency matrix M_G. In this case, the set that is formed by vectors $x \in I^{|V|}$, such that all its components have the same value, called the *diagonal*:

$$\mathscr{D} = \{x \in I^{|V|} : x_u = x_v \ \forall \ u, v \in V\}, \tag{2.16}$$

is a *global attractor*, i.e., it is such that $\lim_{t\to\infty} dist(x(t), \mathscr{D}) = 0$, for all initial conditions.

For example, in $\mathbb{R}^2$ the set $\mathscr{D}$, is the identity function shown in Figure 2.11, since it is formed by the points whose coordinates (x_1, x_2) are equal, that is $x_1 = x_2$.

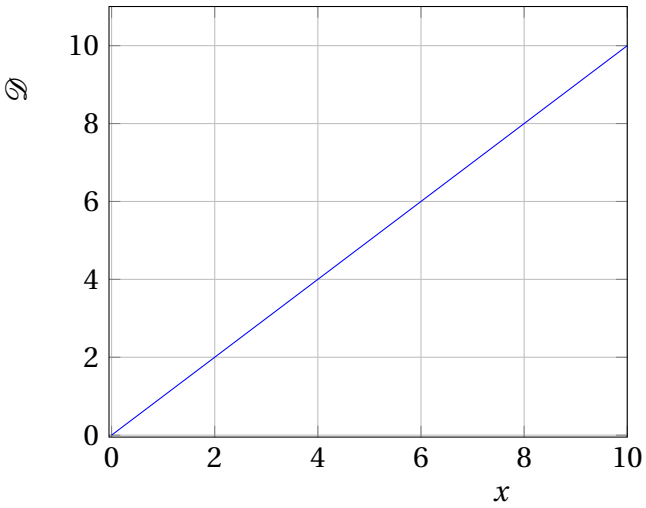

Figure 2.11 – In blue line, the set of the diagonal in dimension 2 is shown for the case of $\mathbb{R}^2$, this particular set has all the points $x = (x_1, x_2)$ whose coordinates are equal $x_1 = x_2$, this is the global attractor of the Laplacian system in dimension 2, analogously it is built for larger dimensions.

The Equation (2.15), is a linear equation with solution $x(t) = e^{tL}x(0)$. Since the Laplacian matrix M_G is symmetric, it can be diagonalized over an orthonormal basis:

$$\mathscr{B}_L := \{v_1, v_2, \ldots, v_N\} \subset \mathbb{R}^N, \tag{2.17}$$

so that:

$$x(t) = \sum_{i=1}^{N} \langle v_i | x(0) \rangle e^{t\lambda_i} v_i, \tag{2.18}$$

where, for each $1 \leq i \leq N$, $\lambda_i \in \mathbb{R}$ is the eigenvalue corresponding to the eigenvector v_i. It is well known, and not so difficult to deduce (see Cvetkovic, Doob, and Sachs 1995 for instance) that, L has a simple maximal eigenvalue $\lambda_N = 0$, and $\lambda_i < 0$ for each $1 \leq i \leq N-1$, that can be verified from the Equations (2.6), (2.9) and (2.12). The dominant eigenvector, v_N is the same as in Equations (2.7), (2.10) and (2.13) but normalized, is precisely the generator of the diagonal, that is $v_N = \frac{1}{\sqrt{N}}(1, ..., 1)$, and in this case:

$$x(t) \to \langle v_N | x(0) \rangle v_N \equiv \left(\frac{1}{N} \sum_{i=1}^{N} x_i(0) \right) v_N \text{ when } t \to \infty.$$

In fact, $dist(x(t), \mathscr{D}) = \sqrt{\sum_{i=2}^{N} |\langle v_i | x(0) \rangle|^2 e^{2\lambda_i t}}$ for each $t \in \mathbb{R}$, as $\lambda_i < 0$, then

$$\lim_{t \to \infty} dist(x(t), \mathscr{D}) = 0.$$

This is the sense in which in this thesis it is considered that the Laplacian system synchronizes, because when time passes, all the coordinates to which the system was applied have the same value.

Consider the complete graph K_N, then, each of its coordinates has a monotonous behavior. Let's consider $L(M_{K_N})$ and either $x \in \mathbb{R}^N$, by Equations (2.6) and (2.7):

$$x(t) = e^{-Nt} \sum_{i=1}^{N-1} x_i v_i + x_N v_N,$$

then, for each coordinate:

$$x_j(t) = e^{-Nt}(x_{N+1-j} - x_1) + x_N,$$

therefore $x_j(t)$ is monotonous. This behavior will be used in Section 4.1 to perform the formal and rigorous analysis of its paths towards synchronization.

2.1.4 The Kuramoto model

Now, the synchronization phenomenon is seen specifically in the case of coupled oscillators. Let's imagine that we have several metronomes, these are artefacts used by beginning musicians that when they are well seated on a table, they can mark the time correctly so that they can trust them to mark the beat, this is done by means

of the sound of a needle that moves from left to right at equal time intervals. This behavior changes when one metronome is influenced by another. This happens when, for example, we put them next to each other on a swing, in this way their mechanical movement flows through the board and thus, that movement is "felt" by the other metronome. We let them interact for a few moments and after time passes, it turns out that, despite the fact that the two metronomes have begun to oscillate at different times with different frequencies, we could see one of the following cases, first, that the influence between them has been so much that they are *synchronized*, that is, that both mark the same beat, when one goes to the right or to the left, the other also, as it is shown in Figure 2.12 (a) represents metronome 1 and (b) represents metronome 2. Secondly, it may be that they both mark the same beat, but when one goes to the left, the other goes to the right and vice versa, which causes some compensation in the oscillation, in other words they are in a *phase locking* state as it is shown in Figure 2.13 (a) represents metronome 1 and (b) represents metronome 2. Finally, if the influence they exerted on each other is too weak, what can happen is that they never get to synchronize and each one marks different and independent beats, that is, they remain in a state of *incoherence* as it is shown in Figure 2.14 (a) represents metronome 1 and (b), represents metronome 2.

Mathematically, according to Kuramoto, asymptotically the dynamics of some systems are almost identical, and he proposed that N coupled oscillators are described by the following coupled system of equations:

$$\frac{dx_i}{dt} = \omega_i + \sum_{j=1}^{N} \Gamma_{i,j}(x_j - x_i), \tag{2.19}$$

for $i = 1,..,N$, where the *interaction function* $\Gamma_{i,j}$ determines the form of coupling between each oscillator i and j, also, ω_i is the *natural frequency*, and x_i is the *phase angle* of each oscillator.

The Equation (2.19) is very general, allowing any type of coupling $\Gamma_{i,j}$, however, this interaction function is very complicated to analyze, which makes the theoretical analysis considerably more difficult. The first and clearest example, is when Γ is equal to the identity function, then, there is a translation of the Laplacian system that depends on the ω_i. This can give an idea that every time that the function Γ is modified, it can be the subject of a large area of study.

Due to this great challenge, Kuramoto assumed that each oscillator affects all other oscillators by calling this kind of interaction *global coupling*. At the same time, he assumed that the interactions between the oscillators are equal and depend only sinusoidally on the phase difference, given by the following function:

$$\Gamma_{i,j}(x_j - x_i) = \frac{K}{N}\sin\big(x_j - x_i\big), \tag{2.20}$$

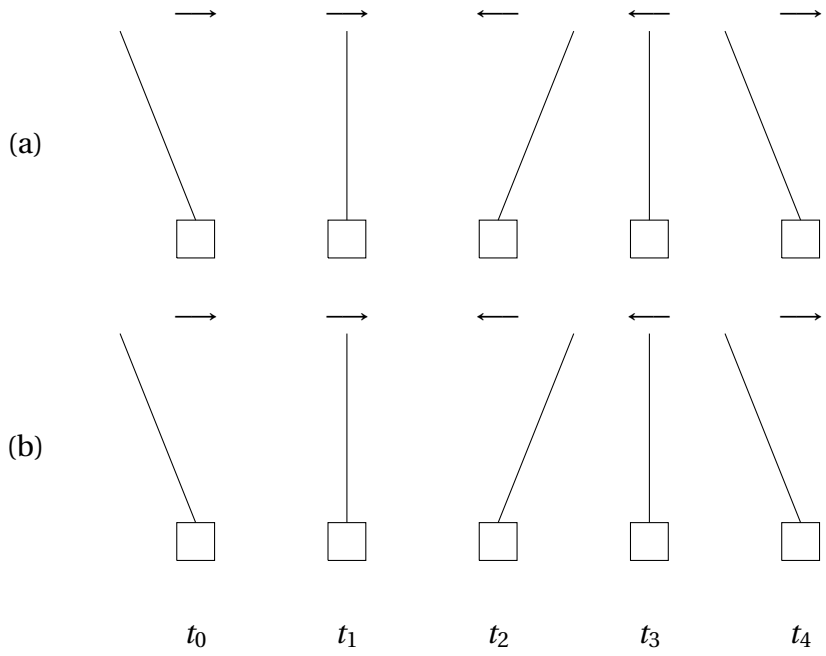

Figure 2.12 – In (a) and (b) two different metronomes are shown, which are photographed at times t_0, t_1, t_2, t_3, t_4, the arrow above each of the photographs shows the direction it has the instant after the photo was taken. In this case, the oscillators at each instant have the same direction, which is called synchronized. The fact that the times t_0 and t_4 are shown is to observe the periodicity of the oscillators.

where the parameter K determines the *coupling strength*.

Substituting the Equation (2.20) in Equation (2.19), it is the so-called *Kuramoto Model*, this is a simple model of N mutually coupled oscillators having different natural frequencies ω_i drawn from some probability density $\omega \mapsto g(\omega)$, with phases x_i, as in the following equation:

$$\frac{dx_i}{dt} = \omega_i + \frac{K}{N}\sum_{j=1}^{N}\sin\big(x_j - x_i\big). \tag{2.21}$$

Because this model describes the synchronization of a system, one of the natural questions has been how to quantify the degree of synchronization (there are a lot of examples, but you can see Fonseca and Abud 2018 for instance), that is why the dynamics of the Equation (2.21) have been analyzed in terms of the *order parameter*, then, the complex *mean field* of the population can be written as follows:

$$Z = X + iY = re^{i\Theta} = \frac{1}{N}\sum_{j=1}^{N} e^{ix_j}. \tag{2.22}$$

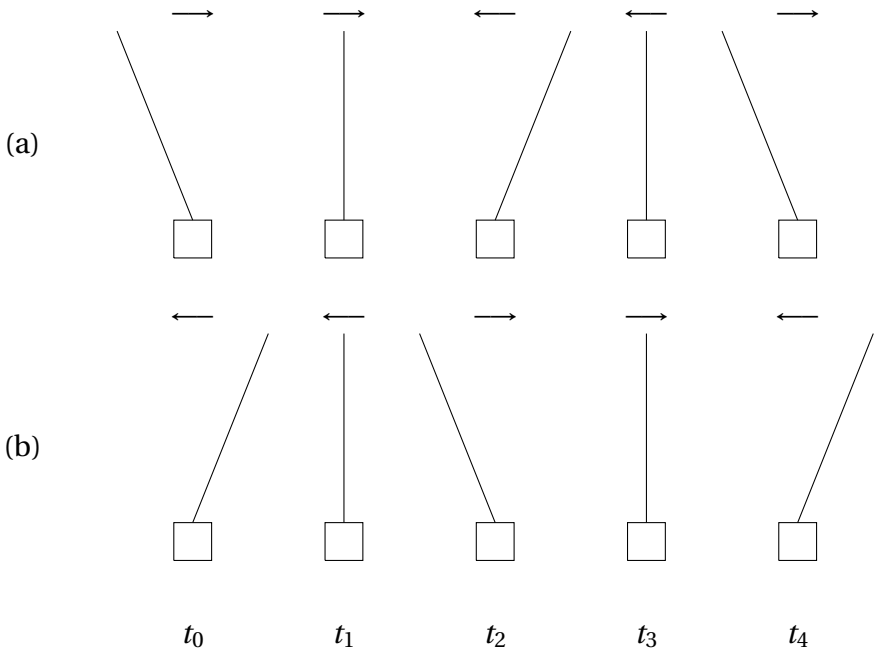

Figure 2.13 – In (a) and (b) two different metronomes are shown, which are photographed at times t_0, t_1, t_2, t_3, t_4, the arrow above each of the photographs shows the direction it has the instant after the photo was taken. In this case, the oscillators at each instant have the opposite direction, which is called phase locking. The fact that the times t_0 and t_4 are shown is to observe the periodicity of the oscillators.

The mean field, has amplitude r and phase Θ, as in the following equation:

$$r\cos(\Theta) = \frac{1}{N}\sum_{j=1}^{N}\cos(x_j), \qquad r\sin(\Theta) = \frac{1}{N}\sum_{j=1}^{N}\sin(x_j) \tag{2.23}$$

Equation (2.22), corresponds to the centroid of all the oscillators when they are represented as points on a circle of radius 1. The magnitude r of the order parameter can also be interpreted as a *measure of synchronization*, in the following sense: if all the oscillators are fully synchronized with identical angles $x_i(t)$, then $r = 1$, and if all the oscillators are distributed around the unit circle, then $r = 0$. It is shown in Figure 2.15 examples of this synchronization measurement for two coupled oscillators, in (a) it is observed that the oscillators are in phase locking state, in (b) it is a state of incoherence and in (c) a synchronization state.

The Kuramoto model, from the Equation (2.21) has been applied to complex networks, in the sense that the involved oscillators will influence each other, depending on the connections that a network has, that is:

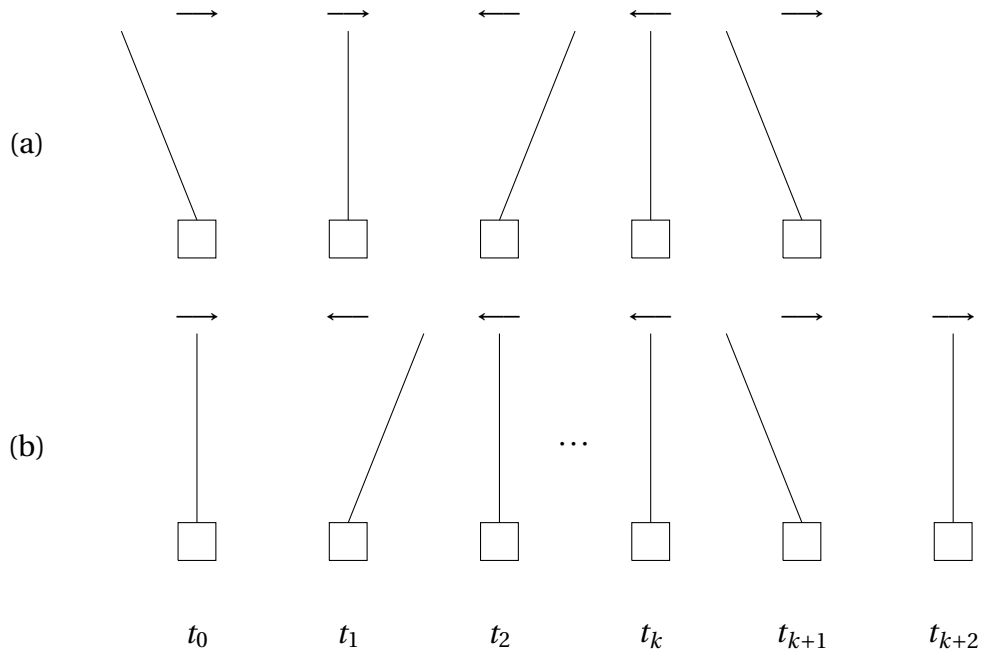

Figure 2.14 – In (a) and (b) two different metronomes are shown, which are photographed at times t_0, t_1, t_2, t_3, t_4, the arrow above each of the photographs shows the direction it has the instant after the photo was taken. In this case, the oscillators have their direction independently of each other, they go at their own pace and it is not possible to make a pattern of their behavior at different times.

$$\frac{dx_i}{dt} = \omega_i + \sigma \sum_{j \in \mathcal{V}(i)} \sin\big(x_j - x_i\big). \tag{2.24}$$

Here, $\mathcal{V}(i)$ represents the *set of closest neighbors* of node i. The natural frequencies are distributed according to a probability density function $\omega \mapsto g(\omega)$, and σ denotes the coupling strength with an appropriate scale to ensure the model exhibits favorable behavior as $N \to \infty$.

It is well known that the Kuramoto model applied to different types of graphs has been widely studied, for example in DeVille and B. Ermentrout 2016; Delabays, Jacquod, and Dörfler 2019; Medvedev and Tang 2017; Moreno and Pacheco 2004; Gómez-Gardeñes, Moreno, and Arenas 2007, both for random and non-random graphs. Whether synchronization occurs depends on two factors: the coupling strength, and the difference between the frequencies of both oscillators. The coupling strength describes how weak or strong the interaction is. In the example of the metronomes on the swing, we can interpret it as a measure of the freedom that the strings allow them to move the board while they oscillate. Conversely, if the strings were rigid, then the movement of the metronomes would not affect the board and

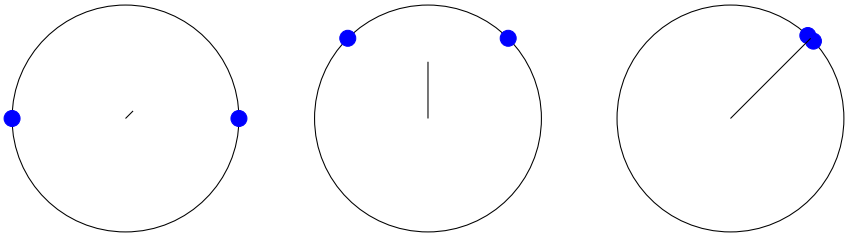

(a) (b) (c)

Figure 2.15 – In (a), (b) and (c) the angles that two oscillators have in three different situations are shown and the line that appears in the center of the circle towards the average of the angles shows the synchronization measure that exists between both oscillators, the first, that is (a), shows that the synchronization measure is zero, because the oscillators are in totally opposite directions, in other words, in phase locking. In (b), at the instant that the synchronization measurement was captured, it is greater than zero, because the angles seem to be close, which will not last long, because it is not an equilibrium state, so each of the angles will follow its path and the synchronization measurement will continue to change without stabilizing. In (c) it is shown that both angles are very close, so the synchronization measure corresponds to the length of the radius, that is, $r = 1$, which means that these oscillators are synchronized.

there would be no way for the two metronomes to interact, so the coupling strength would tend to zero. On the other hand, if the strings are not fixed, but can vibrate or move with some ease, the interaction force would be increased. The other factor that allows synchronization to occur is the difference in natural frequencies between the oscillators describes how different they are. Then, measuring the coupling strength experimentally has some difficulty, but the frequency difference is easy to measure and to vary.

The synchronizing dynamics of the Laplacian flow is preserved in part by the Kuramoto flow neglecting the natural frequencies, written as follows:

$$\frac{dx_v}{dt} = \sigma \sum_{u \in V:\,(u,v)\in E} \sin(x_u - x_v). \tag{2.25}$$

Certainly, the diagonal serves as a global attractor for the Laplacian flow. Moreover, due to the proportionality between the linearization of the Kuramoto flow around the diagonal and the Laplacian flow, a Hartman-Grobman argument Hartman 1960; Grobman 1959 implies that a similar converging dynamics is exhibited in a small neighborhood of the diagonal.

2.1.5 Combinatorics

In this section, basic concepts of combinatorics will be introduced for the previous study of the paths towards the synchronization of the Laplacian system and the Kuramoto model, that are defined in previous sections.

It begins with a very simple concept, but which will be used repeatedly, the *binomial coefficient* is defined from a pair of positive integers N, k such that $k \leq N$. It is written $\binom{N}{k}$, and is given by the formula

$$\binom{N}{k} = \frac{N!}{k!(N-k)!}.$$

Which can be interpreted as the number of ways of k objects can be chosen from a total set of N objects. This concept is widely used and it will help to define more complex concepts as the following, that is the *Narayana number* T_N^k that is defined from a pair of positive integers $N, kin\mathbb{Z}$ such that $k \leq N$. This number is given by the formula:

$$T_N^k = \frac{1}{N}\binom{N}{k}\binom{N}{k-1}. \tag{2.26}$$

In the Table 2.1, the first seven lines of the Narayana numbers are shown, that is when $N = 1, ..., 7$, which generate the *Narayana triangle*.

			1			
		1		1		
	1		3		1	
1		6		6		1
1	10		20		10	1
1	15	50		50	15	1
1	21	105		175	105	21	1

Table 2.1 – The first 7 lines of the Narayana Triangle are shown in this representation which is generated from the Equation (2.26).

The Narayana numbers Narayana 1979 gives a solution to many counting problems in the area of combinatorics as in Stanley and Fomin 1999; Blanco and Petersen 2012 and there is a very complete documentation at Sloane 2021.

In the Equation (2.26), if a sum over all k in each row is done, then, the result is the *Catalan number* denoted as C_N, that is

$$C_N = \sum_{k=1}^{N} T_N^k,$$

which has several expressions as a closed formula, from them, the following is chosen:

$$C_N = \frac{1}{N+1}\binom{2N}{N}. \tag{2.27}$$

The first ten numbers of Catalan are listed below:

$$1, 2, 5, 14, 42, 132, 429, 1430, 4862, 16796.$$

Catalan numbers are the answer to dozens of problems in the area of combinatorics too, there is a very complete documentation at Sloane n.d. For example, this is the number of *Dyck paths* of order N, this is a staircase walk from $(0,0)$ to (N,N) that lies strictly below (or equal) to the diagonal. This case is equivalent to when the staircase walks are above (or equal) the diagonal.

In Figure 2.16 in (a), the Dyck path of dimension $N = 1$ is shown. In (b), the two Dyck paths in $N = 2$ are shown and in (c), the five corresponding to dimension 3. These numbers coincide with the first three digits of the list shown above about the values of the Catalan numbers.

A *parallelo-polyminoe* in the rectangular lattice of size $p \times q$ refers to a connected union of squares that is bounded by two increasing boundary functions L and U. These boundary functions are defined on the set $1, 2, \ldots, p$ and take values in $0, 1, \ldots, q$. The conditions for the boundary functions are as follows: $L(1) = 0$, $U(p) = q$, and $L(n) < U(n-1)$ for every $2 \leq n \leq p$. In Figure 2.17 an example of parallelo-polyminoe in the lattice of size 14×10 is shown. The blue path defines the lower border function $L = (0,0,0,0,0,2,2,2,2,5,5,5,5,5)$, while the red one defines the upper border $U = (1,1,1,3,3,3,5,5,6,6,6,6,7,7)$. The number of parallelo-polyminoes in the lattice $p \times q$ is also related with the Narayana number.

Now, another important concept is presented. A *Golomb ruler* is a set of marks at integer positions along a ruler where no two pairs of marks have the same distance between them. Formally, this rulers are defined as follows, the set $A = \{a_1, a_2, ..., a_N\} \subset \mathbb{Z}$, where $a_1 < a_2 < \cdots < a_N$, is a Golomb ruler if and only if for all $i, j, k, l \in \{1, 2, ..., N\}$ such that $i \neq j$ and $k \neq l$, $a_i - a_j = a_k - a_l \iff i = k$ and $j = l$. In other words, the *difference set* has all its elements distinct. The *order* of this Golomb ruler is N and its length is $a_N - a_1$.

In Figure 2.18 an example of two Golomb rulers is shown. In (a), there is the set $A = \{0,1,3\}$ that satisfies $x_3 - x_1 > x_3 - x_2 > x_2 - x_1$. In (b), there is $A = \{0,2,3\}$ such that

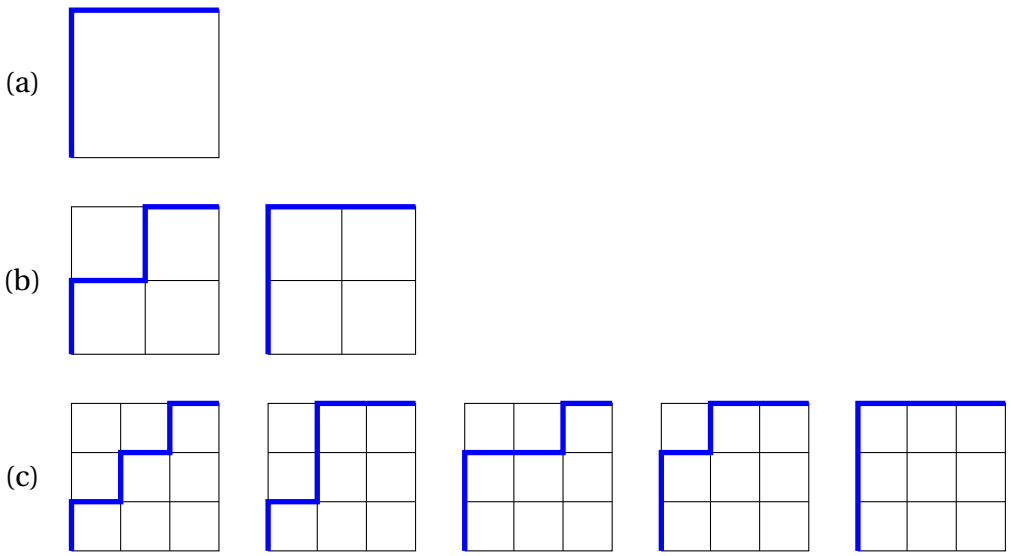

Figure 2.16 – In (a), (b) and (c), the different options of Dyck paths of order 1, 2 and 3, respectively, are shown. As can be seen in (a), the only option to build such a path of order 1 is to take one step up and one step to the right. In (b) there are two different options to build a Dyck path of order 2, the first is to intersperse steps up and to the right, and the second is to go as high as possible and then go as far to the right. Finally, in (c), the 5 options are shown to get from the coordinate $(0,0)$ to the coordinate $(3,3)$ in such a way that it is always above the diagonal, whose options they combine the exposed alternatives in the paths generated in (b).

$x_3 - x_1 > x_2 - x_1 > x_3 - x_2$. In both cases, $|A| = 3$. When the set of differences of two Golomb rules can be ordered in different ways, it is said that these Golomb rules are *combinatorially different*.

Although there is still no closed formula to obtain these numbers, there are previous works as in Johnston 2014a; Beck, Bogart, and Pham 2011, in which they have counted the number of combinatorially different Golomb rulers with N markings which are shown below in Table 2.2. The example shown in Figure 2.18, also illustrates the two possibilities of Golomb rulers with $N = 3$ indicated in the table.

Another concept that is closely related, is the *Sidon set*. The set $A = \{a_1, a_2, ...\} \subset \mathbb{N}$, is a Sidon set in which all pairwise sums $a_i + a_j$ are different for $i \leq j$. The equivalence between the Golomb rulers and the Sidon finite sets has already been studied (see Dimitromanolakis 2002 for instance) and it is easy to prove by contradiction.

Suppose the set $A = \{a_1, a_2, ..., a_N\} \subset \mathbb{N}$ is a finite Sidon set but not a Golomb ruler. Since A is not a Golomb ruler, then there exist $i, j, k, l \in \{1, 2, ..., N\}$ such that

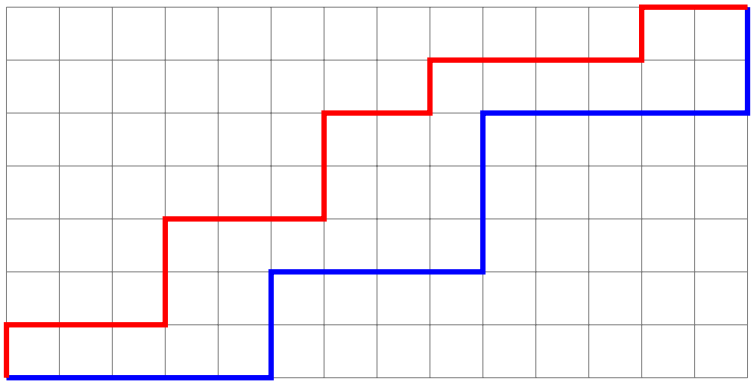

Figure 2.17 – Example of parallelo-polyminoe in the lattice of size 14×10. The blue path defines the lower border function $L = (0,0,0,0,0,2,2,2,2,5,5,5,5,5)$, while the red one defines the upper border $U = (1,1,1,3,3,3,5,5,6,6,6,6,7,7)$, as you can see there are no intersections on the paths, only at the beginning and at the end.

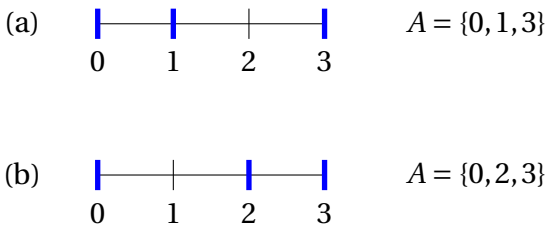

Figure 2.18 – Example of two combinatorially different Golomb rulers of order 3. In (a) and (b) two Golomb rulers are shown, both of order 3. These rules have an associated set that is denoted by the letter A that is written on the right side of each of them. Both rules are combinatorially different, because the differences between each of the elements have a different order. In (a), the set $A = \{0,1,3\}$ is presented, that satisfies $x_3 - x_1 > x_3 - x_2 > x_2 - x_1$. In (b), there is $A = \{0,2,3\}$ such that $x_3 - x_1 > x_2 - x_1 > x_3 - x_2$.

$a_i - a_j = a_k - a_l$ whence it follows that $a_i + a_l = a_k + a_j$ which contradicts the fact that A is a finite Sidon set. In an analogous way it is proved that a Golomb Rule is a finite Sidon set.

With the definitions of these combinatorial objects the section of basic concepts is concluded. Now the methodological framework begins with the methodology proposed and used to build the paths to synchronization, for a system that acts on a fixed graph which it is known that synchronizes.

N	**Number Golomb rulers**
1	1
2	1
3	2
4	10
5	114
6	2608
7	107498
8	7325650
9	771505180

Table 2.2 – Combinatorially different Golomb rulers. This table shows the combinatorially different Golomb rulers from order 1 to order 9 which are the ones that have been calculated so far.

2.2 Path construction

This section will oversee exposing the methodology used to build the paths towards the synchronization of a synchronizing system that acts on a graph. This will be done from the subgraphs that can be generated from the main graph. There are previous works that measure the diffusion distance between networks in the Laplacian system as in Bao, You, and Lin 2018, but the proposal presented here is original.

There is an interest in measuring the degree of synchronization of the system, at a given time t. For this, a precision of $\epsilon > 0$ is set and say that two neighbors are ϵ-*synchronized* if the distance between them is not greater than ϵ. In Figure 2.19 an example of the Laplacian flow as in Equation (2.15) is shown for $N = 2$ in the complete graph. The upper blue curve corresponds to the flow of $x_1(t)$ and the lower one to the flow of $x_2(t)$. Between red lines the ϵ-neighborhood is drawn. From the moment ($t \approx 2$), both flows enter the neighborhood, then they remain ϵ-synchronized.

It is called *active* each connection between neighboring sites which are ϵ-close, and it is defined a subnetwork containing all the active connections. The main objective of the present manuscript is to determine and describe the evolution of these subnetworks.

Therefore, to each fixed threshold $\epsilon > 0$, the graph $G = (V, E)$ and every configuration $x \in \mathbb{R}^{|V|}$, an ϵ-*synchronized subnetwork* $G_x = (V, E_x)$ can be associated, where $E_x \subset E$ is the set of edges:

$$E_x = \{(u, v) \in E : |x_u - x_v| \leq \epsilon\}. \tag{2.28}$$

Due to the phenomenon studied in this thesis is synchronization, the systems under consideration, $G_{x(t)} \to G$ as $t \to +\infty$, when the initial condition is sufficiently close to the diagonal $\mathscr{D}$. This can also be seen in the example presented in Figure 2.19.

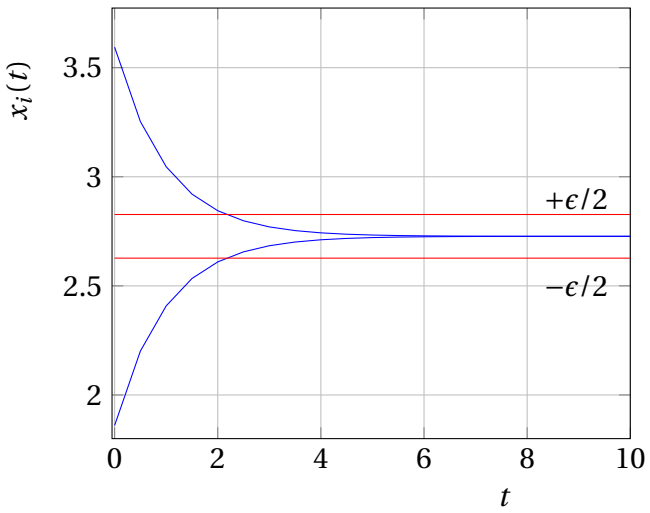

Figure 2.19 – Example of two neighbors ϵ-synchronized. Blue lines show the Laplacian flow of two coordinates from when they begin to interact, until they are synchronized, that is, until both acquire the same value. In red lines, is represented the neighborhood of size $\epsilon/2$ around the average of the values of said coordinates, when the flow enters this neighborhood, which is approximately at $t \approx 2$. These are neighbors ϵ-synchronized.

The graph G has $2^{|E|}$ subgraphs, then for each suitable initial condition $x \in \mathbb{R}^{|V|}$ there exists a finite sequence of switching times $t_0 = 0 < t_1 < t_2 < \cdots < t_\ell$ and a corresponding sequence of ϵ-synchronized subnetworks $(G_x, G_{x(t_1)}, \ldots, G_{x(t_\ell)})$ such that $G_{x(t_\tau)} \neq G_{x(t_{\tau+1})}$, for each $0 \leq \tau < N$, and $G_{x(t)} = G_{x(t_\tau)}$ with $\tau = \max\{0 \leq j \leq \ell : t \geq t_j\}$. In other words, in the sequence of subnetworks, no repeated consecutive subnetworks are found.

In the example that is considered in Figure 2.19, for the Laplacian system for $N = 2$ in the complete graph. For all times before $t_r = 2$, the two-vertex fully disconnected graph $\emptyset_2 = (V, \emptyset)$ shown in (a). After t_r, at any time cut, K_2 appears, as is shown in (b). Resulting in the sequence $\{\emptyset_2, K_2\}$ shown in Figure 2.20.

These sequence of subnetworks of G codify the progression of transient synchronizing patterns. It is important to keep in mind that if $\epsilon > 0$ sufficiently small is taken, all the possible synchronizing sequences can be obtained varying the initial condition $x \in \mathbb{R}$ inside the basin of attraction of the diagonal $\mathscr{D}$.

In Figure 2.21, two paths to synchronization that can be found in the Laplacian system acting on the complete graph K_3 are shown. The path shown in (a) is the same as shown in (b), by making the following label assignment $1 \mapsto 2 \mapsto 3 \mapsto 1$. This occurs

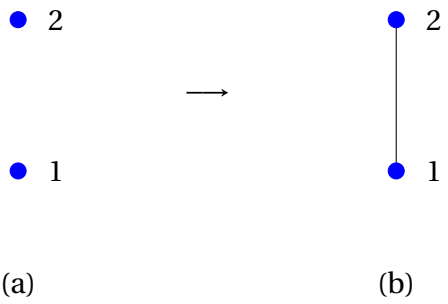

Figure 2.20 – Example path to synchronization. Here, the construction of the graphs represented in Figure 2.19 is shown. Before $t \approx 2$, the coordinates are separated by a length greater than ϵ, then, there is no edge is drawn in (a). From $t \approx 2$, they are already at a distance less than ϵ, then, an edge is drawn connecting vertices 1 and 2.

in systems that act on networks that have some symmetries, such as the complete graph.

In the case of highly symmetric networks, instead of use directly the ϵ-synchronized subnetworks it is convenient to use another combinatorial structure that encodes the subnetwork and respects some of the symmetries that are preserved by the dynamics at the same time. In Figure 2.21, there are paths that could turn out to be redundant (in the sense that they do not provide more information than what is already available and they occupy memory when performing computations). Also, as it will be seen in the Section 4, this facilitates the description of the evolution of the ϵ-synchronized subnetworks.

It is proposed that the whole synchronizing dynamics on G can be compiled in a single combinatorial superstructure. I call this superstructure the *transition diagram*, where to each vertex is associated with a ϵ-synchronized subnetwork (it should be noted that this association is not necessarily injective), this is to ensure that the set of all paths in the transition diagram is equivalent to the set of all observable sequences of ϵ-synchronized subnetworks. In Figure 2.22, the transition diagram for the Laplacian system applied to the complete graph K_3 is shown. Each of its vertices corresponds to a subgraph of K_3. In addition, all the transitions that occur can be observed. Each of the paths that appear in this transition diagram is realized by some initial condition $x \in \mathbb{R}^3$.

To study this dynamic of the paths to synchronization, it is enough to see the transition diagram with other labels that allow to encode the G_x (preferably in a simpler way). In Figure 2.22, it would be easier to analyze if a label to each subgraph is associated. An advantage of it will be taken soon to save information of the corresponding subgraph.

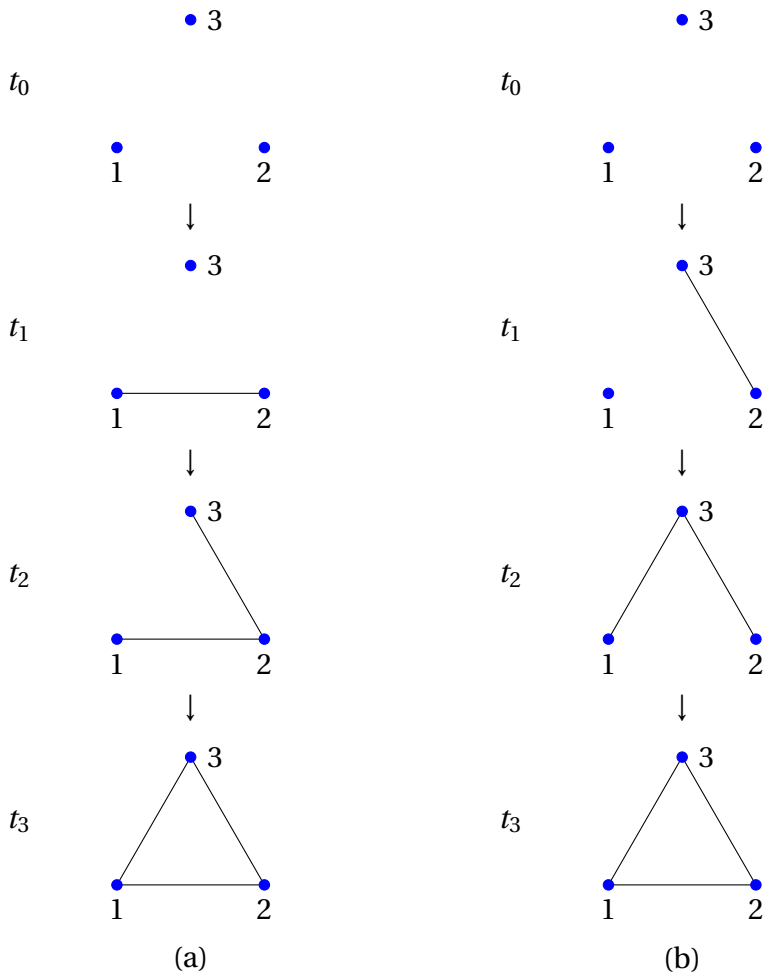

Figure 2.21 – Example of two different but symmetrical paths towards synchronization. In (a) and (b), two paths towards synchronization are shown considering the complete 3-dimensional graph K_3. Both have 4 times t_0, t_1, t_2, t_3 in which the different subgraphs that appear in each of the sequences can be noted whose transitions are represented by an arrow pointing down. In the case of (a), starting with the totally disconnected graph, then add the edge that joins vertices 1 and 2, then the one that joins vertices 2 and 3, and ends with the one that joins vertices 1 and 3. For (b), in the same way, starting with the totally disconnected graph, first the edge that joins vertices 2 and 3 appears, then the one that joins vertices 1 and 3 and ends with the one that joins vertices 1 and 2. One path can be obtained through another by rotating the labels of the graph so that $1 \to 2 \to 3 \to 1$.

Formally, the *transition diagram* is a directed graph which is written as $\mathcal{T}\epsilon = (V_\epsilon, A_\epsilon)$ whose vertices V_ϵ, are combinatorial objects containing all the information it is neces-

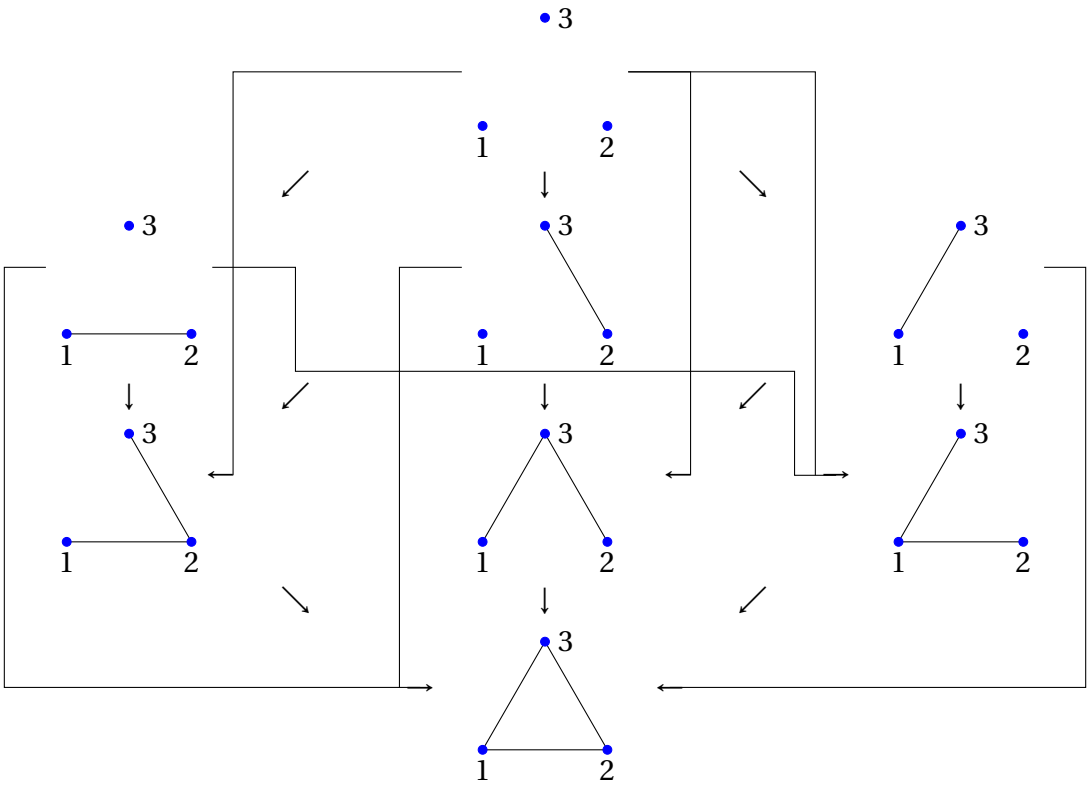

Figure 2.22 – The complete transition diagram of the Laplacian system in K_3 is shown. At the top, is the fully disconnected graph, and at the bottom, is the full 3-dimensional graph K_3. This transition diagram is made up of 8 vertices that are all the subgraphs that can be obtained from K_3, which are arranged by levels, depending on the number of edges that each of them has. Each of the arrows represents the transitions that can be observed. They are steps that jump one or two levels (a jump of three levels leads to a contradiction). Furthermore, this is a very rare case where all the arrows can be constructed following the rule that one graph is a subgraph of the next, with the only exception that the fully disconnected does not go to the fully connected.

sary to determine the ϵ-synchronized subnetworks, and its arrows, A_ϵ, are transitions between those structures, and they need to be consistent with the evolution of each ϵ-synchronized subnetwork. The association of objects in V_ϵ with ϵ-synchronized subnetworks is reached via a mapping:

$$\lambda : V_\epsilon \to \mathscr{E}\epsilon, \tag{2.29}$$

which consists of labeling each vertex in the transition diagram with one ϵ-synchronized subnetwork. The labelling defined by λ is such that the sequence $(G_0, G_1, \ldots, G_\ell)$ is

a *realizable* sequence of ϵ-synchronized subnetworks as long as there exists a path $v_0 \to v_1 \to \cdots \to v_\ell$ in $\mathscr{T}\epsilon$ such that $G_n = \lambda(v_n)$ with $0 \leq n \leq \ell$.

In general, the set $\mathscr{E}_\epsilon$ of all the ϵ-synchronized subnetworks changes with ϵ. Nevertheless, for ϵ sufficiently small, the set of ϵ-synchronized subgraphs defined by initial conditions in a small neighborhood of $\mathscr{D}$ becomes independent of ϵ. For example, in Figure 2.23, when two different values of ϵ are considered, different sequences are generated. For the neighborhood drawn in red, the sequence shown in Figure 2.20 is presented, which is $\{\emptyset_2, K_2\}$. For the neighborhood drawn in green, there is only $\{K_2\}$, because at any time, the flows are close enough to be connected.

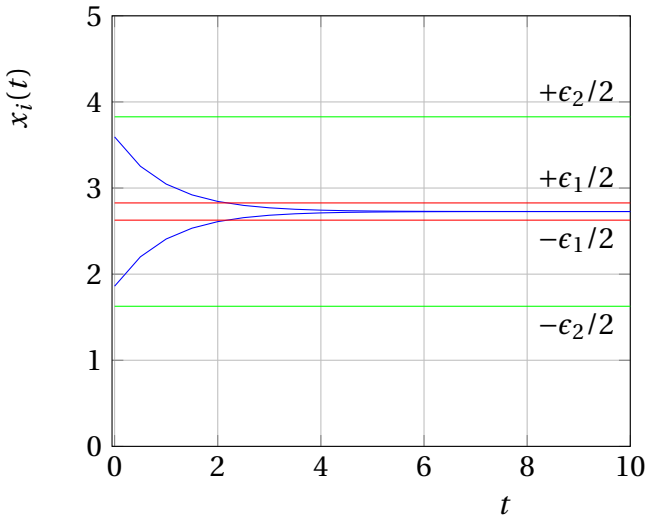

Figure 2.23 – Example when two neighbors ϵ-synchronized with different ϵ. The objective of this image is to show that when one changes the value of the precision $\epsilon > 0$, different sequences can be obtained, then, for some it can be considered a loss of information. For example, for the red neighborhood given by ϵ_1, the change that implies that at first the two coordinates were far apart can be observed, and then, they got close enough to get in synchronization. In the case of the green neighborhood given by ϵ_2, since it is too big, at no time did it notice that there was an approximation between the coordinates, because from the beginning, for this precision, they were already close enough.

In the case of the Laplacian flow, the set $\mathscr{E}_\epsilon$ of all possible ϵ-synchronized subnetworks is independent of ϵ as long as $\epsilon > 0$. It is natural to think that even if $\mathscr{E}_\epsilon$ is independent of ϵ, the corresponding transition diagram may change with ϵ. This, nevertheless, does not happen in the linear case, since for each initial condition $x \in \mathbb{R}^{|V|}$, the corresponding sequence $(G_x, G_{x(t_1)}, \ldots, G_{x(t_\ell)})$ of ϵ-synchronized subnetworks coincides with the sequence $(G_y, G_{y(t_1)}, \ldots, G_{y(t_\ell)})$ of ϵ'-synchronized subnetworks de-

termined by $y = x\epsilon'/\epsilon$. Indeed, by Equation (2.28) and by the linearity of the system, $\{u,v\} \in E_x$ is equivalent to $|x_u - x_v| \leq \epsilon$, hence $|x_u - x_v| = \epsilon/\epsilon'|y_u - y_v| \leq \epsilon$, therefore $|y_u - y_v| \leq \epsilon'$, which is equivalent to $\{u,v\} \in E_y$. From this it follows that the set of ϵ-synchronized sequences does not depend on ϵ in the linear case.

Clearly, each ϵ-synchronized sequence can be realized by an infinite number of initial conditions, due to this number is finite, which could most likely allow to realize some partition of the initial space, that is, the basin of attraction of the final synchronized state.

As it has been anticipated, the study is restricted only to the following families of networks the complete graph K_N, the complete bipartite graph $K_{N,N}$, the cycle graph C_N and the ring lattice family $C(N,k)$.

Considering these families, the following questions are addressed, given the underlying network:

— Which subgraphs are realizable as ϵ-synchronizing subnetworks, how large is this set and how does it grow with the size N of the underlying graph?
— What is the structure of the transition diagram? What is the longest path in this digraph and what is the distribution of path lengths?

2.3 Computational methods

This section will describe the computational methods by which the exploratory studies were carried out to determine the behavior of the Laplacian system and the Kuramoto model in the complete graph, the complete bipartite graph, the cycle graph, and the family of the ring lattices. This thesis will be in the framework of theoretical and numerical physics, for which it is required

— Knowledge in non-linear physics and dynamical systems.
— The mastering of the numerical tools in order to perform numerical simulations (programming language Fortran 90 and C++) and some tools to do post-processing (Wolfram Mathematica) is necessary.

Due to the difficulty that it presents from the beginning to know which are the paths towards the synchronization of a system that has this asymptotic state, computational simulations were initially carried out with the objective of making an exploratory study of the Laplacian system and the Kuramoto model. For this, computations were done, assuming that there are a G graph of dimension N, and considering 10^6, randomly generated initial conditions in $(0,N^2)^N \subset \mathbb{R}^N$ in the case of the Laplacian system and $(0,2\pi)^N \subset \mathbb{R}^N$ in the case of the Kuramoto model, for each $1 \leq N \leq 10$. This will be done for the following types of graphs:

— Complete graph K_N.
— Complete bipartite graph $K_{N,N}$.
— Cycle graph C_N.
— Ring lattice family $C(N,k)$.

From this exploratory study, it can be observed that the dynamics of the initial conditions, in the two systems (the linear system and the non-linear system). That is, how the system behaves under different types of initial conditions, and how are the paths they take until they reach the synchronized state to make a formal characterization. The following concepts were considered from observations and data obtained from random initial conditions:

— Number of feasible and unfeasible subgraphs.
— Depth of the transition diagram.
— Number of realizable paths.
— Path length distribution.

From the observations made and considering the characteristics listed above, the objective was to describe in a general, formal, and rigorous way the behavior of the transient state, through the formulation of theorems. In the cases of the complete graph K_N and the complete bipartite graph $K_{N,N}$, this type of formalization could be carried out in the Laplacian system case and partially in the Kuramoto model. On the other hand, the observations made for the case of the cycle graph and the family of ring lattices will allow us to continue with their general and rigorous study in the future.

Next, in the following chapter, the exploratory study made for the Laplacian system and the Kuramoto system in the complete graph, the complete bipartite graph, the cycle graph and the ring lattice family is shown under the methodology exposed in this section.

3 Exploratory study of the transient state of systems that synchronize

Contents

3.1 Exploring the Laplacian system

This section shows the exploratory studies that were carried out from computational simulations for a set of 10^6 random initial conditions on $(0, N^2)^N$, in the Laplacian system over: the complete graph, the complete bipartite graph, the cycle graph and the family of ring lattices. As was said in Section 2.3, the aim is to find the patterns that meet the initial conditions on their way towards synchronization. In the four graph types that are analyzed, the same initial condition is evaluated to observe the different behavior it has when the topology of the graph changes. In addition, for each of them, the number of feasible subgraphs, the length of the longest path, the number of paths and the distribution of path lengths are explored, all in a set of random initial conditions. These analyzes and exploratory studies were very important for the formulation of theorems and propositions that fulfill the different systems exposed in this thesis in Sections 4.1, 4.2 and 4.3.1.

3.1.1 The Laplacian system of M_{K_N}

To begin, the most important observations, made through computational simulations, regarding the behavior of the Laplacian system on the complete graph of dimension N, $L(M_{K_N})$, will be presented. Specifically, the behavior of this system is investigated when the dimension grows. These calculations were made for a set of 10^6 random initial conditions in $(0, N^2)^N$ as was said in Section 2.3. Now, the trajectory under the Laplacian flow, starting with a fixed initial condition, will be evaluated, it will be used throughout Section 3.1, in order to observe the differences when the graph's topology is changed. Then, the case of the construction of the transition diagram of the Laplacian system applied to the complete two-dimensional graph, K_2, and what are the initial conditions that correspond to each state are exposed. Afterwards, the construction of the transition diagram of the Laplacian system applied to the complete three-dimensional graph, K_3 is also presented, which was found from the evaluation of multiple initial conditions. Next, a calculation of the number of unfeasible subgraphs of K_N and a comparison with the total number of subgraphs of K_N is presented. Then, a formula to calculate the length of the longest path found in $L(M_{K_N})$ is presented. Finally, three path lengths normalized distributions for a set of random initial conditions are shown, with the purpose of observing the length of the paths in the case presented in this section.

Starting from the order defined in the previous paragraph, Figure 3.1 shows the flow of this system in a concrete example, applied to a fixed initial condition in dimension 6:

$$x = (2.64958, 1.9171, 1.86587, -0.861234, -0.41248, 0.5232).$$

In the figure, the flow of each coordinate approaches monotonically (increasingly or decreasingly) to $\bar{x} = 0.947006$, which is the average of the coordinates of x. Moreover, in all dimensions, each coordinate follows its path towards the asymptotic value, without crossing other. This is the most important observation, for its future generalization and writing in a formal version presented in Section 4.1.

Due to this behavior of the Laplacian system in the complete graph, it is immediate to deduce that, in the 2-dimensional case, for any $\epsilon > 0$, there are only 2 cases. Let $x = (x_1, x_2) \in \mathbb{R}^2$, the first case corresponds to $x_1 = x_2$ and the second case corresponds to $x_1 \neq x_2$. If $x_1 = x_2$, then they are already in the synchronized state, if $x_1 \neq x_2$, there are two sub-cases. Without loss of generality, consider that $x_1 < x_2$. First, if $x_1 + \epsilon \leq x_2$, which also corresponds to the synchronized case. The second case, if $x_1 + \epsilon > x_2$, which corresponds to the state of the totally disconnected graph of dimension 2. Due to the monotonic and without crossings behavior, they lead in finite time to the state of synchronization. The transition diagram in this case is explicitly shown in Figure 3.2, composed only of two states and a single way to go from one to the other.

The form that the coordinates must have to know its path towards synchronization

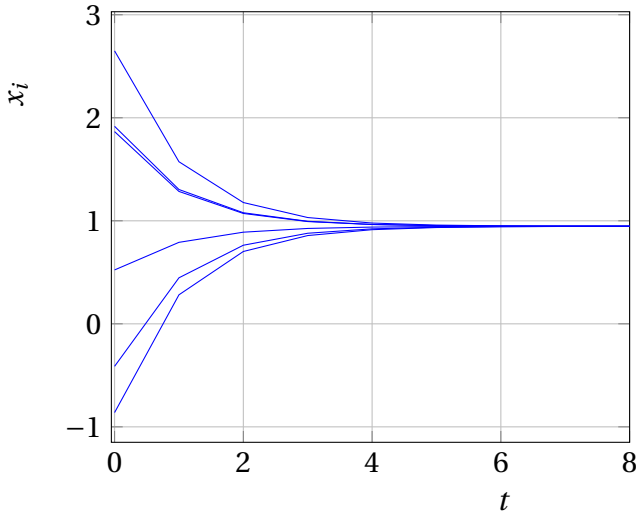

Figure 3.1 – The Laplacian flow in the complete graph of dimension 6 K_6, applied on a fixed initial condition $x \in \mathbb{R}^6$. Each one of the six lines represents the projection of each one of the coordinates x_i of x. It is observed that all of them reach the same value asymptotically, and they do so monotonically without crossings between them.

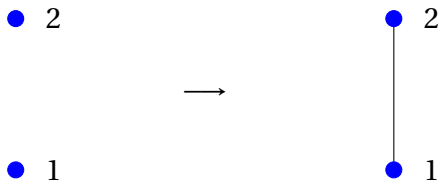

Figure 3.2 – Transition diagram of the Laplacian system applied to the complete graph of dimension 2 K_2. In this case, only two states are observed. The first one corresponds when the initial coordinates are at a distance strictly greater than ϵ. The second, is when its distance is less than this threshold.

was presented in the previous paragraph, then the phase diagram can be drawn as in Figure 3.3. It is interpreted as follows: if an initial condition in the blue zone is taken, it will take one step to arrive to synchronization, otherwise, if a coordinate in the red zone is taken, it is already in the synchronized state. The red zone depends entirely on the magnitude of the ϵ parameter. In the case that $\epsilon = 0$, the red set is equal to the diagonal $\mathscr{D}$ of dimension 2.

Now, the case $N = 3$ is presented, for which a specific set of initial conditions was evaluated to build the associated transition diagram. The specific parameters used

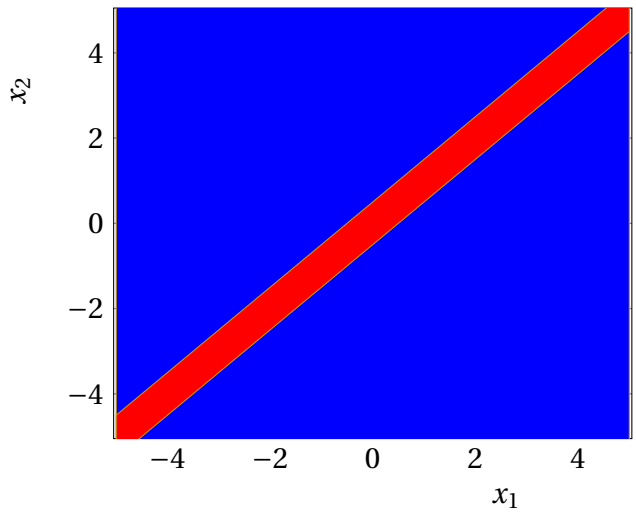

Figure 3.3 – The Laplacian flow applied in the complete graph of dimension 2 K_2 phase diagram. If $\epsilon = 0.5$ is set, each initial condition $x \in \mathbb{R}^2$ selected in the blue area, will take 1 step to reach full synchronization. If it is selected in the red area, it is already in the synchronized state. The red area can be made smaller or larger depending on the threshold ϵ.

are described below. In this case $\epsilon = 0.1$ is considered, and the initial conditions $x = (x_1, x_2, x_3)$ in the set $[-10, 10]^3 \subset \mathbb{Z}^3$, that is, in such a way that points are generated as in a cubic lattice, one arrives at transition diagram shown in Figure 3.4, where each of the vertices is a subgraph of K_3 and all of them appear. In addition, the drawn arrows are equivalent to inclusion, that is, the graph from which an arrow leaves is a subgraph of the graph it enters. To explain the way in which the initial conditions are constructed, the use of a symmetry of the complete graph will be considered: when the coordinates are increasingly ordered. Assume that $x_1 \leq x_2 \leq x_3$. Firstly, the initial conditions already in the synchronized state are such that all their coordinates are equal to or such that $|x_i - x_j| \leq \epsilon$ for all $i, j \in \{1, 2, 3\}$. Those that take one step to reach synchronization, is because two of their coordinates are equal and the distance to the third is greater than ϵ, or they are such that $|x_i - x_j| \leq \epsilon$ and $|x_i - x_k| > \epsilon$ and $|x_j - x_k| > \epsilon$, where i, j, k are any array of the numbers $1, 2, 3$ with no repeats. The initial conditions that take two steps to reach synchronization have the form $(x_1 + a, x_1 - a, x2)$ and any of its permutations, on which it depends if $2a \leq \epsilon$ to know if two edges are connected in the first step or in the second step. Furthermore, the distances between the coordinates that have symmetry and the one that does not, must be greater than ϵ. Finally, the initial conditions that take 3 steps to reach the state of synchronization are that all their pairwise differences are different and greater than ϵ. Then, there are different paths to reach synchronization, in other words, also in this case the partitions that are generated in the phase diagram are inflated subspaces of $\mathbb{R}^3$ that depends on ϵ.

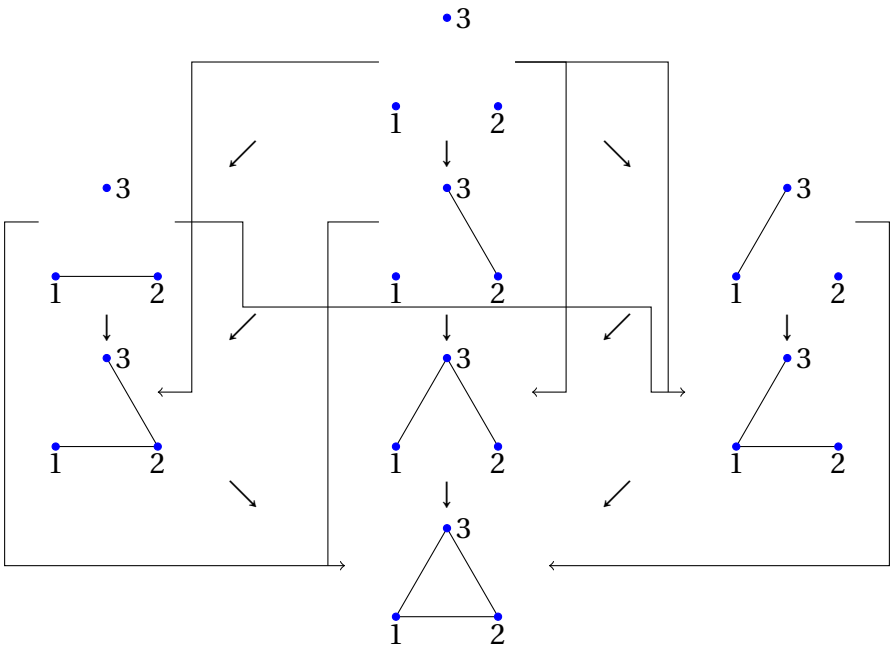

Figure 3.4 – Transition diagram of the Laplacian system applied to the complete graph of dimension 3 K_3. At the top, is the fully disconnected graph and at the bottom, is the full 3-dimensional graph K_3. In this case, all the arrows can be constructed following the rule that one graph is a subgraph of the next, with the only exception that the fully disconnected does not go to the fully connected.

Besides, for cases of dimension larger than 3, the number of vertices in the transition diagram of $L(M_{K_N})$, no longer coincides with the number of subgraphs of K_N, since it is impossible to construct initial conditions that satisfy all the rules of nearness and farness that some subgraphs dictate. These rules will be formally exposed and demonstrated in the Section 4.1.2. Computationally, the number of unfeasible subgraphs was calculated and a comparison was made with respect to the number of subgraphs of K_N, to observe the growth behavior of the feasible subgraphs, shown in Figure 3.5. The red line represents the number of subgraphs of K_N, which is clearly an upper bound for the number of feasibles and unfeasible subgraphs. The blue line represents the number of unfeasible subgraphs of K_N. There is a very little difference between the lines, which represents the number of feasibles subgraphs.

Through the computational simulations that were carried out, considering randomly generated initial conditions in a subset of $\mathbb{R}^N$, it was found that the longest path that an initial condition can follow towards synchronization, coincides with the

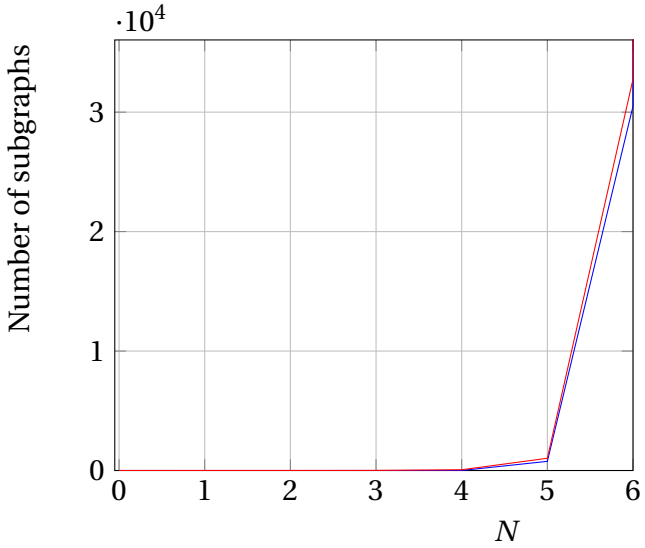

Figure 3.5 – Number of unfeasible subgraphs by initial conditions in K_N and number of subgraphs of K_N. The blue line represents the number of unfeasibles subgraphs of K_N. The red line represents the number of subgraphs of K_N. The difference between these lines is the number of feasible subgraphs of K_N.

number of edges that K_N has, that is

$$\text{Depth of } L(M_{K_N}) \text{ transition diagram} = \frac{N(N-1)}{2}.$$

Under the same conditions of randomness, the path towards synchronization of 10^6 different initial conditions were calculated and then all those that were different from each other were counted. The result of this process is shown in Figure 3.6. Note that although the number of feasibles subgraphs is very small, the number of paths towards synchronization grows very fast, which allows, from little information and through a fixed function, to create a large number of possibilities, for its future exploitation and use.

Now, for the set of random initial conditions and considering $\epsilon = 0.1$, the path length distribution was calculated in each dimension N, in order to observe the behavior of a typical path towards synchronization, to have an idea of what to expect about the length of a path to synchronization associated with a random initial condition. Moreover, it can also be seen how likely it is to find an initial condition with maximum length, and similarly, an initial condition that reaches synchronization in very few steps. In Figure 3.7, this behavior is shown for the dimensions $N = 8, 9, 10$ in blue, red and green lines respectively (normalized by the total number of initial conditions evaluated). As can be seen, these distributions have a Gaussian shape, whose average

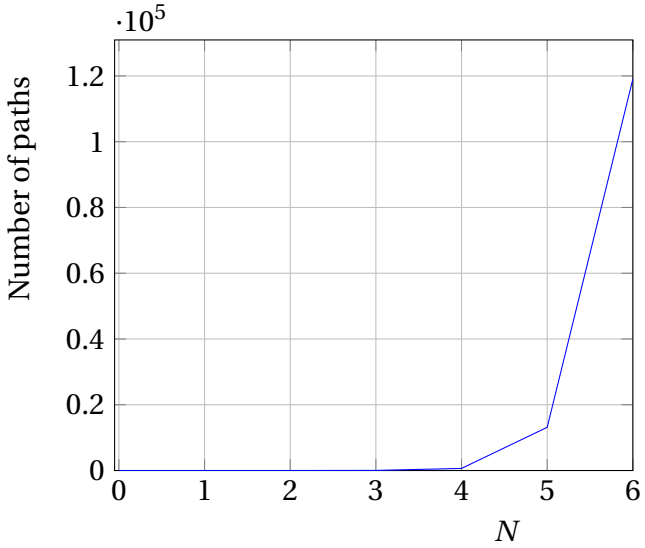

Figure 3.6 – Number of paths towards synchronization in $L(M_{K_N})$. The blue line represents the number of paths towards synchronization in the Laplacian system of the complete graph of dimension N.

moves to the right as the dimension N grows. The distributions show that it is not easy to find initial conditions that synchronize neither in a few nor in many steps, rather the behavior oscillates in intermediate values.

As a conclusion of this section, due to the monotonicity of the Laplacian flow applied to the complete graph of dimension N, there is an upper bound for the maximum length of the paths to synchronization in its transition diagram. In addition, the symmetry of the graph being analyzed is inherited by the transition diagram, which makes some paths redundant. Hence, a simplification of the paths will be considered in the formal analyses. Besides, due to the diversity of subgraphs, it is not possible for all of them to be feasible by initial conditions, which means that the number of states in the transition diagram is less than the number of subgraphs of K_N. Finally, the path length distributions provide an idea of what to expect from the behavior of a random initial condition, which should be treated carefully when ϵ is varied, because by making this threshold smaller, then the average of the typical length grows. The observations made in this section are the basis for the future formalization of the results presented in Section 4.1 with respect to the transient state behavior of the Laplacian system over the complete graph of dimension N.

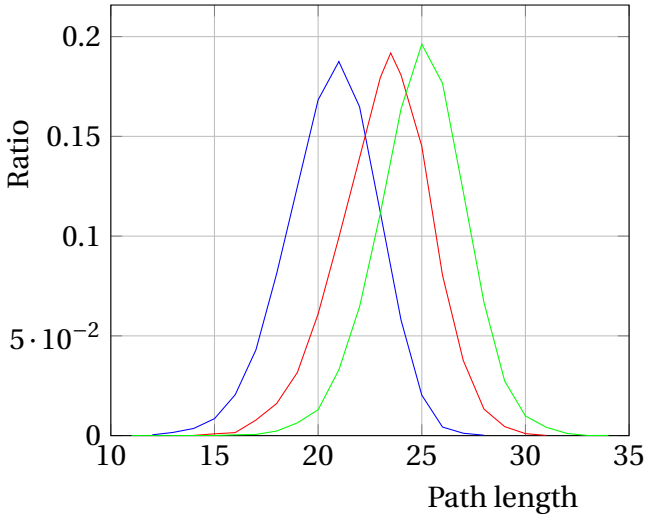

Figure 3.7 – Path length distribution of $L(M_{K_N})$. The blue line represents the normalized path length distribution of Laplacian system of the complete graph of dimension $N = 8$, the red line in dimension $N = 9$ and green line in dimension $N = 10$, for a set of random initial conditions.

3.1.2 The Laplacian system of $M_{K_{N,N}}$

Now, the most important observations, made through computational simulations, regarding the behavior of the Laplacian system on the complete bipartite graph of dimension $2N$, $L(M_{K_{N,N}})$, will be presented. Specifically, the behavior of this system is investigated when the dimension grows. These calculations were made for a set of 10^6 random initial conditions in $(0, N^2)^N$ as was said in Section 2.3. To begin with, the trajectory under the Laplacian flow starting with a fixed initial condition will be evaluated, that will be used throughout Section 3.1, in order to observe the differences when the topology of the graph is changed. Then, a comparison of the longest path to synchronization found from computational calculations and the number of subgraphs that $K_{N,N}$ has is shown. Next, a calculation of the number of unfeasible subgraphs of $K_{N,N}$ is presented. Then, the behavior of the number of different paths to synchronization that were found is depicted. Finally, three path lengths normalized distributions for a set of random initial conditions are shown, with the purpose of observing the length of typical paths.

As mentioned in the previous paragraph, the same initial condition that was evaluated in Section 3.1.1 is evaluated, to observe its behavior when the interactions are given by the complete bipartite graph $K_{3,3}$, which is,

$$x = (2.64958, 1.9171, 1.86587, -0.861234, -0.41248, 0.5232).$$

In Figure 3.8 it can be seen that not all of its coordinates approach monotonically

(increasingly or decreasingly) to $\bar{x} = 0.947006$, which is the average of the coordinates of x. In addition, each coordinate follows its path towards the asymptotic value, crossing each other, which does not happen for all the initial conditions. In Section 4.2, a subset of $\mathbb{R}^{2N}$ in which the initial conditions are monotone and there are no crossings between them will be presented.

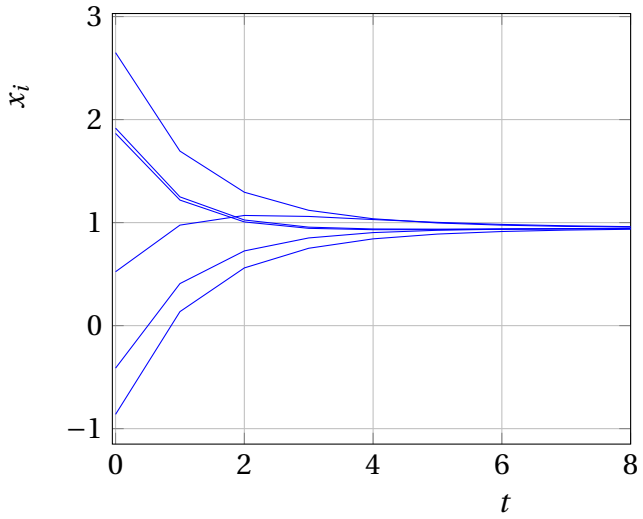

Figure 3.8 – The Laplacian flow in the complete bipartite graph of dimension 6 $K_{3,3}$ applied on a fixed initial condition $x \in \mathbb{R}^6$. Each one of the six lines represents the projection of each one of the coordinates x_i of x. It is observed that all of them reach the same value asymptotically non monotonically, and they cross each other.

Since there are crossings between the lines depicted in Figure 3.8, according to the way of quantifying the synchronization exposed in Section 2.2, there will be connections and disconnections between the edges formed in each one of the subgraphs that composes the sequence of ϵ-synchronized subnetworks. Then, given that the complete bipartite graph $K_{N,N}$ has N^2 edges, and the fact that there can be disconnects, therefore, the length of the longest path in the transition graph of the Laplacian system of $M_{K_{N,N}}$ will exceed N^2. In Figure 3.9, the results of the computational calculations that were made for the case of $L(M_{K_{N,N}})$ are shown. On the one hand, the blue line represents the maximum number of steps towards synchronization $L(M_{K_{N,N}})$. On the other hand, the red line represents the number of edges that $K_{N,N}$ has. As can be seen, the maximum number of steps that an initial condition takes, exceeds the number of edges of the graph in which it is located. Of course, in the monotonic case, which will be shown in Section 4.2, due to the absence of crossings between the coordinates, the length of the longest path will be less than that shown in this section.

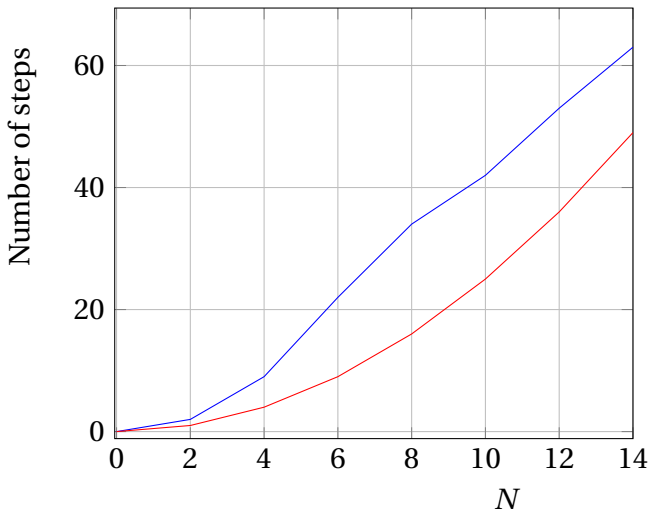

Figure 3.9 – Depth of $L(M_{K_{N,N}})$ transition diagram. The blue line represents the maximum number of steps towards synchronization in the Laplacian system of the complete bipartite graph of dimension $2N$. The red line represents the number of edges that the complete bipartite graph of dimension $2N$ has.

Now, computational simulations were carried out to see if there are subgraphs of $K_{N,N}$ that cannot be realized by some initial condition in $\mathbb{R}^{2N}$, obtaining the following results shown in the Table 3.1. As can be seen, for small dimensions, all the subgraphs of $K_{N,N}$ are feasible, but once the dimension grows, subgraphs that are no longer feasible appear. In the particular case of $K_{3,3}$, the six unfeasible subgraphs correspond to the hole of size 6 (and all possible permutations of their vertex labels), with which it can be affirmed that not all the subgraphs of the complete bipartite graph are feasible. The formal proof of this result will be done in Section 4.2.

	Complete bipartite graph $K_{N,N}$		
N	1	2	3
Unfeasible subgraphs	0	0	6

Table 3.1 – Number of unfeasible subgraphs of $K_{N,N}$.

Considering a set of random initial conditions in $(0, N^2)^{2N} \subset \mathbb{R}^{2N}$, the path towards synchronization of these 10^6 initial conditions was calculated, all those that were different from each other were counted. The result of this process is shown in Figure 3.10, from which it can be seen that the growth of the number of paths towards synchronization, despite there being only a few vertices in the transition diagram,

seems to be greater than exponential.

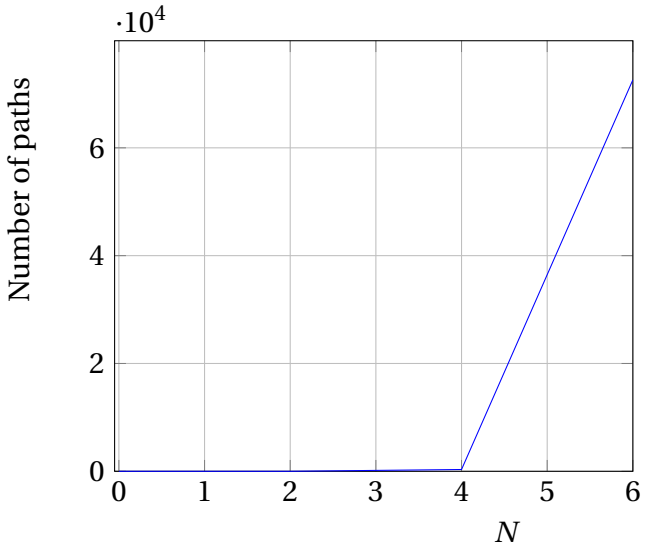

Figure 3.10 – Number of paths towards synchronization in $L(M_{K_{N,N}})$. The blue line represents the number of paths towards synchronization in the Laplacian system of the complete bipartite graph of dimension $2N$.

To conclude this computational analysis, for the set of random initial conditions, the path length distribution was calculated in each dimension $2N$, in order to observe the behavior of a typical path towards synchronization, to give an idea of what to expect about the length of a path to synchronization associated with a random initial condition. In addition, it can also be seen how likely it is to find an initial condition with maximum length, and similarly, an initial condition that reaches synchronization in very few steps. In Figure 3.11, this behavior is shown for the dimensions $N = 10, 12, 14$ in blue, red and green lines respectively (normalized by the total number of initial conditions evaluated). As can be seen, these distributions have a Gaussian shape, whose average moves to the right as the dimension $2N$ grows. This behavior means that it is not easy to find initial conditions that synchronize neither in a few nor in many steps, rather the behavior oscillates in intermediate values.

As a conclusion of this section, due to the non-monotonicity of the Laplacian flow applied to the complete bipartite graph of dimension $2N$, there is a lower bound for the maximum length of the paths to synchronization in its transition diagram, which is the number of edges that $K_{N,N}$ has, and computer simulations suggest that the longest path triples it. Due to the diversity of subgraphs, it is not possible for all of them to be feasible by initial conditions, which means that the number of states in the transition diagram is less than the number of subgraphs of $K_{N,N}$, which begins to be seen from dimension 6. Also, it was observed that the growth of the number of

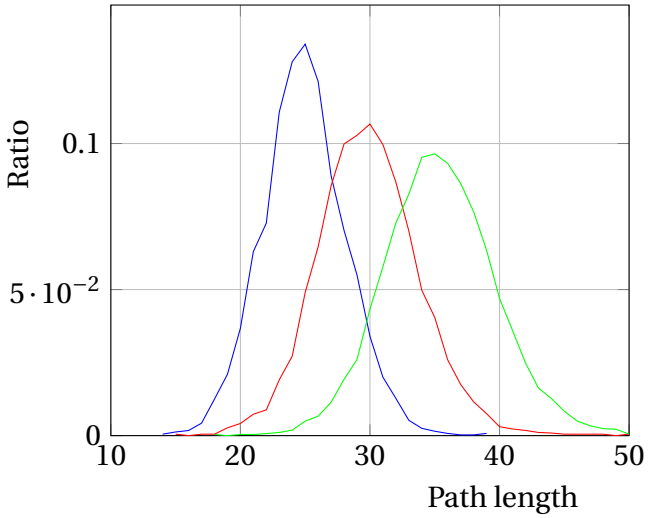

Figure 3.11 – Path length distribution of $L(M_{K_{N,N}})$. The blue line represents the normalized path length distribution of Laplacian system of the complete graph of dimension 10, the red line in dimension 12 and green line in dimension 14, for a set of random initial conditions.

different paths that can be found in this transition diagram, grows by means of a rule that seems greater than exponential. Finally, the path length distributions provide an idea of what to expect from the behavior of a random initial condition, which should be treated carefully when ϵ is varied, because by making this threshold smaller, then the average of the typical length grows. Moreover, the observations made in this section are the basis for the future formalization of the results presented in Section 4.2 with respect to the transient state behavior of the Laplacian system over the complete bipartite graph of dimension $2N$.

3.1.3 The Laplacian system of M_{C_N}

In this section the quantitative properties of the Laplacian system on the cycle graph of dimension N are seen, which were calculated computationally. Specifically, the behavior of this system is investigated when the dimension grows. These calculations were made for a set of 10^6 random initial conditions in $(0, N^2)^N$ as was said in Section 2.3. To begin with, the trajectory under the Laplacian flow, starting with a fixed initial condition, will be evaluated, that will be used throughout Section 3.1 in order to observe the differences when the topology of the graph is changed. Then, a comparison of the longest path to synchronization found from computational calculations and the number of subgraphs that C_N has is presented. Next, a formula of the number of feasible subgraphs of C_N is presented. In addition, a case in dimension 6 in which a subgraph does not belong to any path starting from the totally disconnected

graph despite being feasible. Also, the transition diagram of the Laplacian system applied to the cycle graph of dimension 6 is shown. Then, the behavior of the number of different paths to synchronization that were found is presented. Finally, two path lengths normalized distributions each separated by parity of path lengths, for a set of random initial conditions are shown, with the purpose of observing the length of typical paths.

Just as it was presented in the two previous sections, the behavior of the initial condition

$$x = (2.64958, 1.9171, 1.86587, -0.861234, -0.41248, 0.5232),$$

in the cycle graph C_6 is shown in Figure 3.12. It can be seen that all of its coordinates approaches monotonically (increasingly or decreasingly) to $\bar{x} = 0.947006$, which is the average of the coordinates of x. Furthermore, in this case, it is observed that the convergence time is longer than for when x is considered over the complete graph and the complete bipartite graph (it can be seen that the convergence time is more than double than in the other cases).

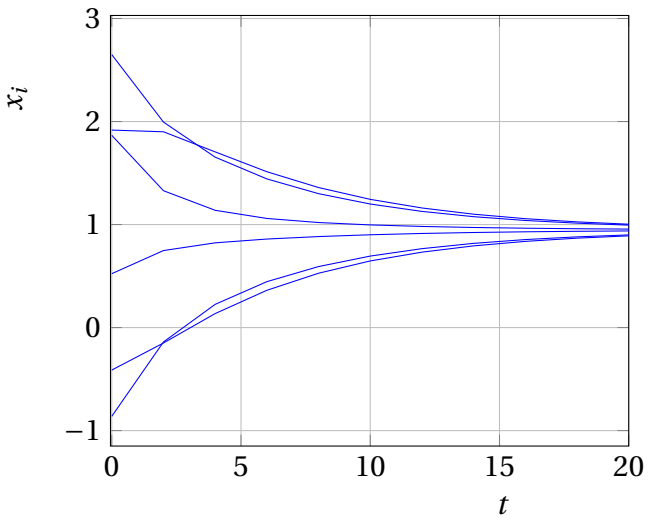

Figure 3.12 – The Laplacian flow in the cycle graph of dimension 6 C_6 applied on a fixed initial condition $x \in \mathbb{R}^6$. Each one of the six lines represents the projection of each one of the coordinates x_i of x. It is observed that all of them reach the same value asymptotically monotonically, and they cross each other.

Besides, as in the case presented in Section 3.1.2, due to the crossings that occur in the flow of the coordinates that we observe in Figure 3.12, it can be thought that the maximum number of steps to reach the synchronization exceed the number of

edges of the cycle graph of dimension N (which is $N-1$). Thereby, computational calculations were performed to observe the behavior of the longest path in the Laplacian system applied to M_{C_N}, as is shown in Figure 3.13. The blue line represents the maximum number of steps towards synchronization in the Laplacian system in the cycle graph C_N. The red line represents the number of edges that C_N has. It is observed that the maximum number of steps to reach the synchronization, approximately triples the dimension in which it is found.

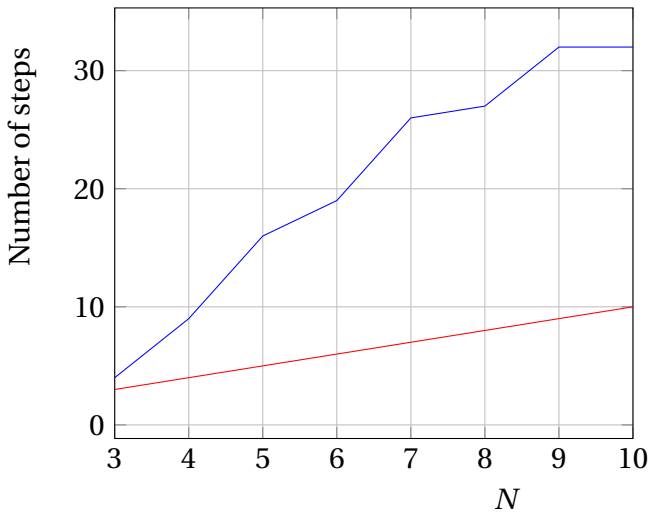

Figure 3.13 – Depth of $L(M_{C_N})$ transition diagram. The blue line represents the maximum number of steps towards synchronization in the Laplacian system of the cycle graph of dimension N. The red line represents the number of edges that the cycle graph of dimension N has.

On the side of the feasible subgraphs of the cycle graph of dimension N, according to the simulations carried out, it was found that all of them are feasible. Here, the number of possible states in the transition diagram of de Laplacian system applied to M_{C_N} was exactly found. In Section 4.3.1 there is a way to construct an initial condition for each subgraph of C_N. Below is the formula with which the number of possible states in the transition diagram of the Laplacian system applied to the cycle graph is obtained.

$$\text{Number of vertices of } L(M_{C_N}) \text{ transition diagram} = 2^N.$$

As an observation, the corresponding cases of C_2 and C_3, coincides with the complete graphs K_2 and K_3 respectively. The behaviors that are strictly corresponding to the cycle graph can be observed for dimensions larger than 4. That's why, evaluating initial conditions in a 4-dimensional hypercube of sides $(0,23)$, the trajectory that an initial condition takes, only a maximum of two turns remain in the directed cycles

(that is, there are no periodic points in this dynamics).

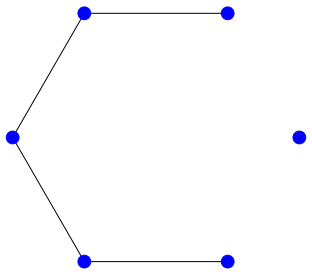

Figure 3.14 – Subgraph of C_6 that, despite being feasible due to an initial condition, cannot be reached from the totally disconnected graph, due to the symmetries presented by the Laplacian spectrum applied to the cycle of dimension 6.

Focusing on the behavior of the path step by step, that is, when at each step it is only added one edge to a subgraph, in the specific case of dimension 6, the transition diagram is shown in Figure 3.15. Vertex 1 represents the totally disconnected graph with 6 vertices and vertex number 64 represents C_6. When the initial conditions start at vertex 1, it is possible that they oscillate at the first and second levels, but eventually they reach vertex 1 and follow a path to vertex 64. Specifically, the subgraphs that do not pass from vertex 1 to some vertices in level 5 in the transition diagram of $M(L_{C_6})$ are all the symmetries of Figure 3.14. This is because the behavior of the flow coordinates inherits the symmetry of the cycle graph, so this configuration cannot be reached from vertex 1.

Next, in the Figure 3.16, some computational calculations for random initial conditions in $(0,N^2)^N \subset \mathbb{R}^N$ of the number of different paths towards synchronization in the Laplacian of the cycle graph are shown. It is observed that although the number of possible states in the transition diagram of M_{C_N} is small, the number of paths they generate grows considerably faster.

The path length distribution of the Laplacian system of the cycle graph was also analyzed for a set of random initial conditions. It was noted that there was a different behavior, depending on whether the dimension N considered is even or odd. Furthermore, it came to light that there is also a difference in paths having even or odd lengths.

On the one hand, in Figure 3.17, an example for the behavior of path length distributions when the dimension is odd is depicted, particularly when $N = 9$. Represented with a blue line, the behavior of paths with odd length is shown, and represented with a red line, the behavior of paths with even length. It is observed that there is a not so biased tendency of the paths to prefer even lengths, because the area associated with this curve is notably larger than that associated with the blue curve. On the other

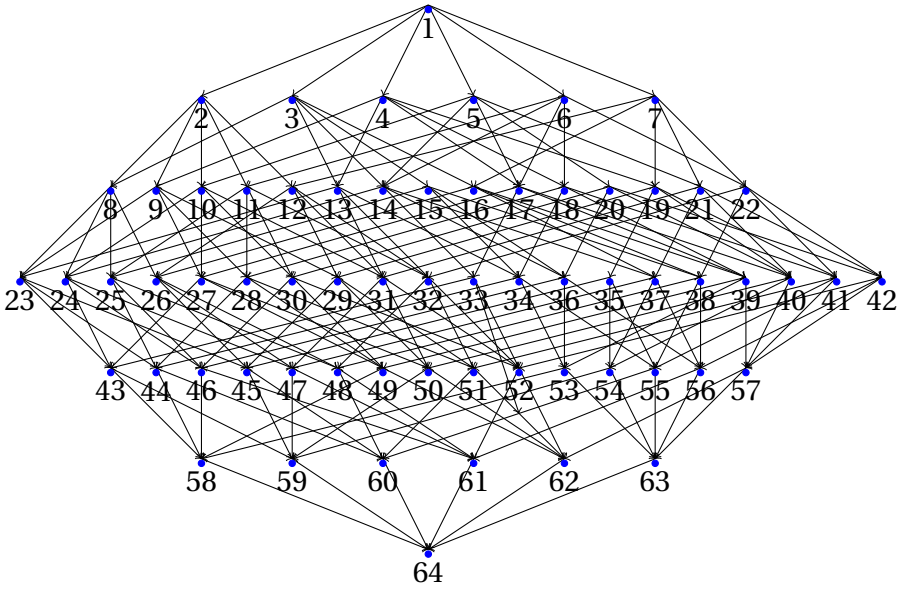

Figure 3.15 – Transition diagram of $L(M_{C_6})$ with labels assigned by the number of the subgraph that lexicographically corresponds to it, is shown. This is composed of 64 vertices and 192 edges. At the top, the vertex 1 corresponds to the totally disconnected graph of dimension 6, and at the bottom, the vertex 64 corresponds to the cycle graph of dimension 6, C_6.

hand, in Figure 3.18, an example of the behavior of these path length distributions is presented when the dimension is even, in particular when $N = 10$. In the figure, the blue line represents the behavior paths with odd length and the red line the paths with even length. In this case, it is observed that it is more likely that the paths have odd length, because the associated curve has a larger area.

To end, as a conclusion of this section, due to the non-monotonicity of differences in the Laplacian flow applied to the cycle graph of dimension N, there is a lower bound for the maximum length of the paths to synchronization in its transition diagram, which is the number of edges that C_N has, and computer simulations suggest that the longest path triples it. On the other hand, due to the non-diversity of subgraphs, it is possible for all of them to be feasible by initial conditions, which means that the number of states in the transition diagram is equal to the number of subgraphs of C_N. Despite this, it is not possible to get from the fully disconnected graph to all other subgraphs by a realizable path, and an example is presented. On the other hand, it was observed that the growth of the number of different paths that can be found in this transition diagram grows by means of a rule that seems greater than exponential. Finally, the path length distributions provide an idea of what to expect from the behavior of a random initial condition, which should be treated carefully when ϵ is varied, because by making this threshold smaller, then the average of the typical length grows.

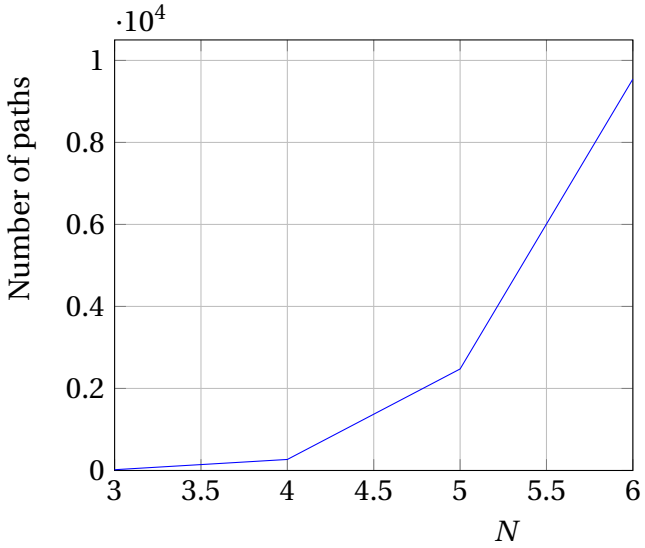

Figure 3.16 – Number of paths towards synchronization in $L(M_{C_N})$. The blue line represents the number of paths towards synchronization in the Laplacian system of the cycle graph of dimension N.

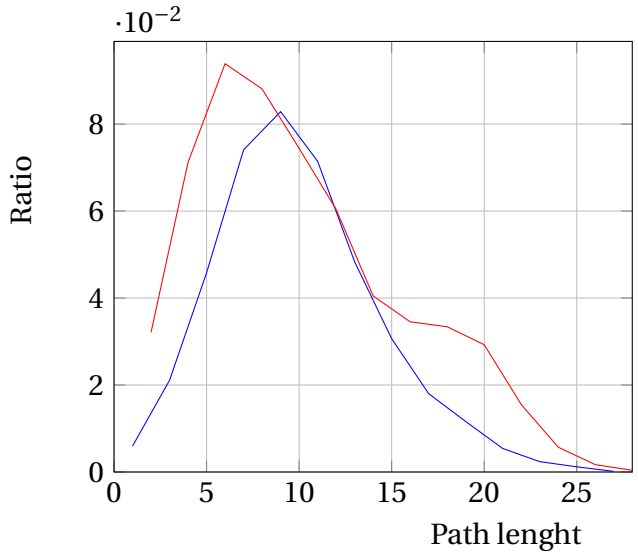

Figure 3.17 – Path length distribution of $L(M_{C_N})$, odd dimension. The blue line represents the normalized path odd length distribution of Laplacian system of the cycle graph of dimension $N = 9$ and red line the normalized path even length distribution in the same dimension, for a set of random initial conditions.

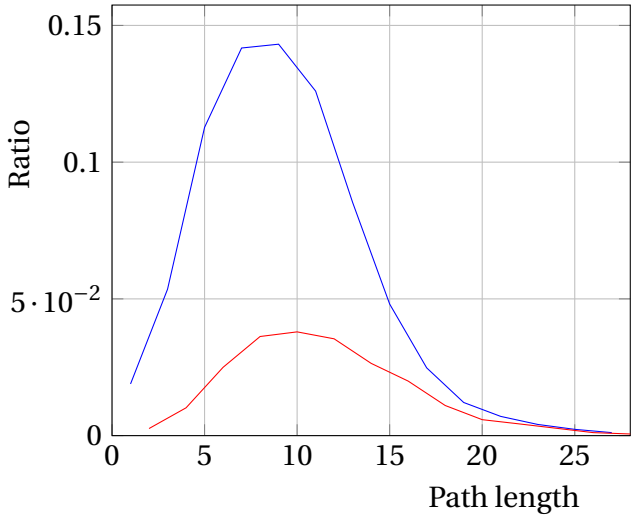

Figure 3.18 – Path length distribution of $L(M_{C_N})$, even dimension. The blue line represents the normalized path odd length distribution of Laplacian system of the cycle graph of dimension $N = 10$ and red line the normalized path even length distribution in the same dimension, for a set of random initial conditions.

In this case, it was found that there is a difference in the distributions depending on the parity of the dimension and the parity of the length of the paths. The observations made in this section are the basis for the future formalization of the results presented in Section 4.3.1 with respect to the transient state behavior of the Laplacian system over the cycle graph of dimension N.

3.1.4 The Laplacian system of $M_{C(N,k)}$

In this section the quantitative properties of the Laplacian system on the ring lattice family $C(N,k)$ are seen, which were calculated computationally. Specifically, the behavior of this system is investigated when the dimension grows. These calculations were made for a set of 10^6 random initial conditions in $(0,N^2)^N$ as was said in Section 2.3. To begin with, the trajectory under the Laplacian flow, starting with a fixed initial condition, will be evaluated, to observe the differences when the topology of the graph is changed. An estimate of the number of unfeasible subgraphs when $k = 2$ is then presented and a comparison with the subgraphs of $C(N,2)$. Then, a comparison of the longest path to synchronization found from computational calculations when $k = 2$ and $k = 3$ is presented. Finally, four path lengths normalized distributions, separated by path lengths parity and dimensions parity when $k = 2$, and four path lengths normalized distributions when $k = 3$ are shown, for a set of random initial conditions, with the purpose of observing the length of typical paths.

Now, the behavior of the initial condition

$$x = (2.64958, 1.9171, 1.86587, -0.861234, -0.41248, 0.5232),$$

that has been analyzed throughout this chapter is observed in the ring lattice $C(6,2)$. In Figure 3.19, it can be seen that all of its coordinates approach monotonically (increasingly or decreasingly) to $\bar{x} = 0.947006$, which is the average of the coordinates of x. Furthermore, no crossings in the trajectories towards the asymptotic are observed. It seems that the more connected the principal graph is, the fewer crossings are found in the flow of coordinates and also, its convergence is faster.

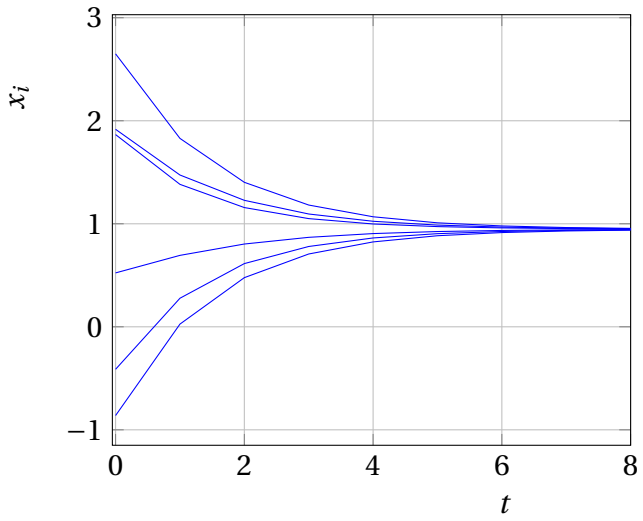

Figure 3.19 – The Laplacian flow in the ring lattice of dimension 6 $C(6,2)$ applied on a fixed initial condition $x \in \mathbb{R}^6$. Each one of the six lines represents the projection of each one of the coordinates x_i of x. It is observed that all of them reach the same value asymptotically monotonically, and they do not cross each other.

This case is interesting because it said how the family of ring lattices behaves and what happens when the connectivity between the vertices increases, that is, how is the transition from being in a graph with a very low density of edges (as is C_N) to be in a graph with the maximum edge density (that is, K_N).

Below is an estimate of the number of unfeasible subgraphs of the ring lattice when $k = 2$, based on the presence of fork graphs. Note that for each vertex of the ring lattice $C(N,2)$, there are 4 different ways to make forks. Enlisting the edges of the outer cycle of the ring from 1 to N, clockwise, and the inner ones of $N+1$ to $2N$, clockwise forming the triangle $1 \to 2 \to N+1$, for $N > 6$, the 4 forks that are formed in each vertex are:

$$i, i+N, Mod[i-1,N,1], \quad Mod[i+1,N,1], Mod[i-1,N,1]+N$$

$$i, Mod[i+N-2,N,1]+N, Mod[i-1,N,1], \quad Mod[i+N-2,N,1], Mod[i-1,N,1]+N$$

$$i, i+N, Mod[i+N-2,N,1]+N, \quad Mod[i+1,N,1]$$

$$i+N, Mod[i+N-2,N,1]+N, Mod[i-1,N,1], \quad Mod[i+N-2,N,1]$$

for $1 \leq i \leq N$. Where on the left side, the edges that make up the fork are written, and on the right side, the edges that should not appear in the subgraph are written. The $Mod[m,n,d]$ gives the remainder on division of m by n uses an offset d. As already stated, when a subgraph does not contain a fork (or a hole), then it is feasible by an initial condition, then, calculating this number allows to give an upper bound on the number of unfeasible graphs. In Figure 3.20, a representation of the number of unfeasible subgraphs of $C(N,2)$ is presented with a blue line, which was estimated using fork containment, and in a red line, the total number of subgraphs of $C(N,2)$, the difference between these two lines would be the total of feasible subgraphs.

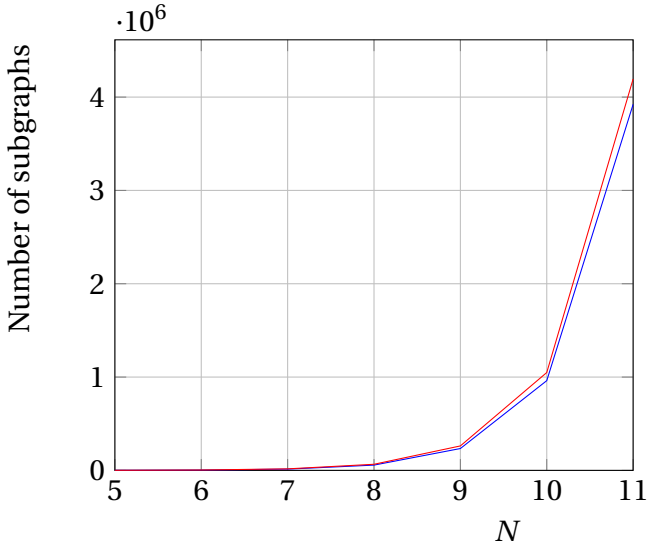

Figure 3.20 – Number of unfeasible subgraphs by initial conditions in $C(N,2)$ and number of subgraphs of $C(N,2)$. The blue line represents the number of unfeasibles subgraphs of $C(N,2)$ and the red line represents the number of subgraphs of $C(N,2)$, the difference between them is the number of feasible subgraphs.

Regarding the length of the longest path found in the ring lattice family $C(N,k)$, computational calculations were made for $k=2$ and $k=3$, which are presented in Figure 3.21. The blue line represents the maximum number of steps towards synchronization when $k=2$, and the red line when $k=3$. Since $C(N,3)$ has more edges than $C(N,2)$, then it is natural to think that its paths towards synchronization will be longer. But, when $N=7$, it can be observed which is less. Note that $C(7,3)=K_7$, then, its longest path is exactly 21, and $C(7,2)$ is a sufficiently disconnected graph that there are internal cycles in its transition diagram. Then, at that $N=7$ a difference is observed.

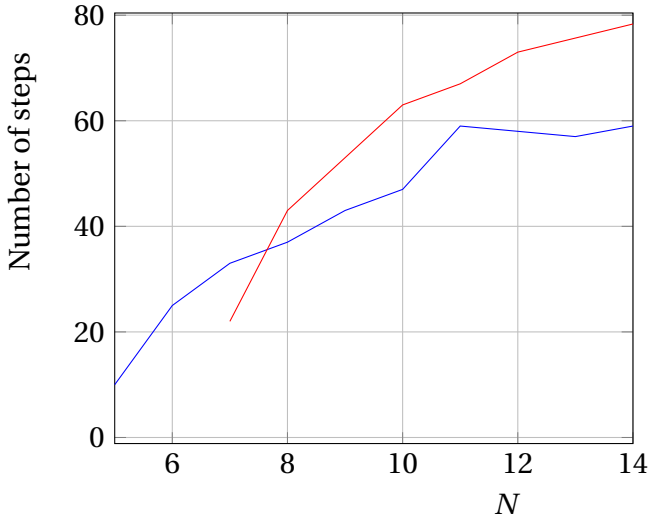

Figure 3.21 – Depth of $L(M_{C(N,k)})$ transition diagram. The blue line represents the maximum number of steps towards synchronization in the transition diagram over the Laplacian system of the ring lattice $C(N,2)$ and the red line represents the maximum number of steps towards synchronization in the transition diagram over the Laplacian system of the ring lattice $C(N,3)$.

Then, the path length distribution of the transition diagram over the Laplacian system of the ring lattice $C(N,2)$ and $C(N,3)$ were also analyzed for a set of random initial conditions. It was noted that there was a different behavior, depending on whether the dimension N considered is even or odd. For the first case, for the dimensions N that were analyzed, as the behavior in C_N, there is a difference when the paths have even and odd lengths. In the second case, for the analyzed dimensions N, no difference that depends on the path length parity is seen. This behavior is associated with the fact that the density of edges in $C(N,3)$ (for the analyzed dimensions), is large enough to resemble the behavior of K_N or $K_{N,N}$. Contrary to $C(N,2)$, whose behavior (for the analyzed dimensions), is more similar to C_N.

On the one hand, in Figure 3.22, two examples for the behavior of path length distributions when the dimension is odd are depicted. Particularly when $N = 9$, they are represented with blue lines. When $N = 11$, they represented with red lines. In both cases, one line represents the paths that have an even length, and the other the paths that have an odd length. In addition, the curves with the most area in each case are those associated with odd lengths of the paths.

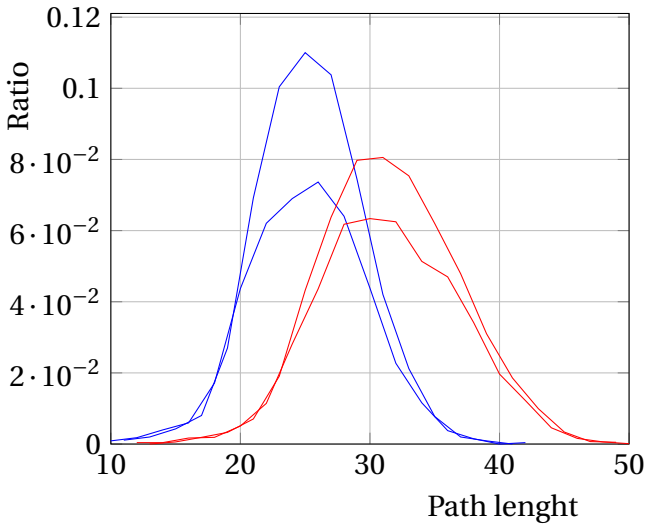

Figure 3.22 – Path length distribution of $L(M_{C(N,2)})$, odd dimensions. The blue line represents the normalized path odd and even length distribution of Laplacian system of the ring lattice $C(9,2)$ and red line is for $C(11,2)$, for a set of random initial conditions.

On the other hand, in Figure 3.23, two examples of the behavior of path length distributions when the dimension is even are depicted. When $N = 10$, they are represented with blue lines. When $N = 12$, they are represented with red lines. In both cases, one line represents the paths that have an even length and the other the paths that have an odd length. In addition, the curves with the most area in each case are those associated with even lengths of the paths.

In contrast, the distributions presented for odd dimensions in Figure 3.22 are more symmetric than those presented for even dimensions in Figure 3.23, which has a bias to the left. That is why they were presented in different figures.

Now, for the case of the ring lattice $C(N,3)$, its path length distributions were obtained for a set of random initial conditions, with the aim of give an idea of the behavior of the conditions initials when they are evaluated in the Laplacian system on this type of graph. Specifically, they are shown in Figure 3.24 for $N = 8,9,10,11$. The blue line

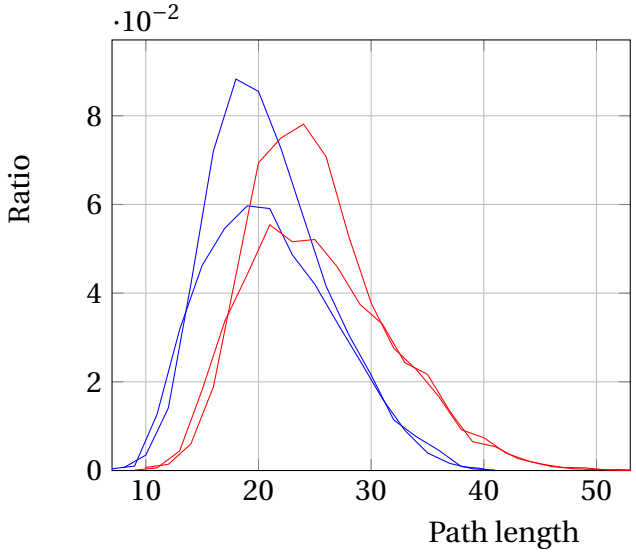

Figure 3.23 – Path length distribution of $L(M_{C(N,2)})$, even dimensions. The blue line represents the normalized path odd and even length distribution of Laplacian system of the ring lattice $C(10,2)$, and red line is for $C(12,2)$, for a set of random initial conditions.

represents the normalized path length distribution of Laplacian system of the ring lattice $C(8,3)$, red line is for $C(9,3)$, green line is for $C(10,3)$ and yellow line is for $C(11,3)$. In the four cases, no change in the distributions is observed depending on the parity of the length of the paths, that is why for each distribution, only a single line is assigned. For the dimensions analyzed in this case, the density of the edges for each of the four ring lattices is very high, then, a radically different behavior is not observed depending on the dimension parity, then they are shown in the same figure. This behavior is more similar to that of the complete graph K_N, or that of the bipartite complete graph $K_{N,N}$.

Then, to conclude, the computational calculations that were made to study the behavior of the family of ring lattices $C(N,k)$, allows to relate and understand the behavior of the different types of graphs studied in this thesis, which range from the complete graph K_N that has all its vertices connected (so the edge density is 1), to the behavior of the cycle graph C_N (whose edge density is small $\frac{2}{N-1}$ for $N \geq 3$), when the dimension N grows. This is because $K_N = C(N, \lfloor N/2 \rfloor)$, when N is odd and when N is even it is only necessary to remove the duplicate edge. Besides, the other extreme case, is when $k = 1$, that means $C_N = C(N,1)$. The observations made from the analyzes presented in this section suggest that when the density of edges is small, the behavior will be like that of the cycle graph C_N, and when the density is large, it will resemble the complete graph K_N. The formal results of these observations will be presented as perspectives of this thesis.

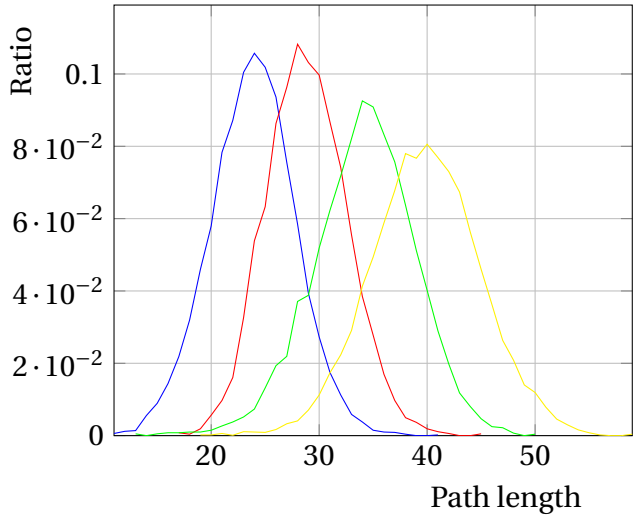

Figure 3.24 – Path length distribution of $L(M_{C(N,3)})$. The blue line represents the normalized path length distribution of Laplacian system of the ring lattice $C(8,3)$, red line is for $C(9,3)$, green line is for $C(10,3)$ and yellow line is for $C(11,3)$, for a set of random initial conditions.

3.1.5 Discussion

In this section, an exploratory study of the transitory state of the Laplacian system was carried out, applied to the complete graph, the bipartite complete graph, the cycle graph, and the ring lattice family, to open the panorama and understand the behavior of the system before reaching the synchronization. The behavior of a randomly generated and fixed initial condition in the four types of graphs was studied. The number of vertices contained in each of the transition diagrams was estimated. The length of the longest path in each diagram was calculated. In addition, the number of realizable paths towards synchronization was calculated, and the section is concluded with the presentation of the normalized distributions of path lengths for each case.

Analyzing the same initial condition in the four types of graphs, allow to see the differences between the dynamics when the Laplacian flow is applied. It is recalled that the cases analyzed were in dimension six. It was observed in the complete graph, in the cycle graph and in the ring lattice that the way to approach the asymptotic value is monotonically, either with increasing or decreasing values. On the other hand, in the case of the complete bipartite graph one of coordinates do not have monotonic behavior. Also, the differences between the coordinates are monotonically reduced in the case of the complete graph and the ring lattice, in contrast to the cases of the complete bipartite graph and the cycle graph. In addition, the times in which syn-

chronization is reached for the complete graph, the complete bipartite graph and the ring lattice are very similar, and always smaller than 8-time units. In the case of the cycle graph, the convergence time appears to be $t > 20$, which may be due to poor connectivity of the graph.

The number of realizable states for each of the four different types of transition diagrams was analyzed, this refers to the number of subgraphs of the complete graph, the complete bipartite graph, the cycle graph, and the ring lattice family that are feasible for some initial condition. Only for the case of the cycle graph, each of its subgraphs are feasibles, then, from computational calculations, it was possible to give an exact formula for the number of states in their respective transition diagram. For the other three cases, the types of unfeasible subgraphs were found, and an estimate was made of how many subgraphs there are of each of them.

Regarding the length of the longest path found in the transition diagram of the Laplacian system applied to the four different types of graphs, the following results were obtained. In the case of the complete graph, due to the monotony it presents, the longest length found corresponds to the number of edges that K_N has, and the same thing happens in small dimensions of the families of ring lattices when $k = 2$ and $k = 3$, because there is a coincidence between the two type of graphs, but when the dimension increases, then the presence of directed cycles in the transition diagrams is observed, therefore, its depth increases, until it triples the number of edges they have. This behavior is observed in the cycle graph, in the complete bipartite graph and in the families of ring lattices when $k = 2$ and $k = 3$ when the dimension is relatively large, then, the edge density decreases and is comparable to the density of the cycle graph.

About the number of different paths towards synchronization in the four different types of transition diagrams, it was observed that although the number of realizable states is much less than the number of possible states (referring to the number of subgraphs that the complete graph, the complete bipartite graph and the ring lattice family has), the number of paths towards synchronization in all cases seems to grow at least exponentially. Therefore, it can be concluded that with little information, the number of possibilities to build new information is large enough, then, that it can be exploited in the future, making use of applications, for example, in information storage and classification.

To end this discussion section, the behavior of a set of 10^6 random initial conditions in $(0, N^2)^N$ was analyzed, and whose sequence of ϵ-synchronized subnetworks was calculated, the length of each of them was measured and the normalized distribution of the length of these paths was constructed. For cases with a high density of edges, such as the complete graph, the complete bipartite graph, and the ring lattice when $k = 3$ (for the dimensions analyzed), unimodal distributions like the Gaussian distribution were observed, which the average increases when the dimension increases. In the case where the density of edges is small, as in the cases of the cycle graph and

the ring lattice when $k = 2$, then a case-by-case behavior is observed, which separates the parity of the dimension and the parity of the path's length, these distributions are also unimodal, and appear to be slightly skewed to the left. Knowing how these distributions behave for a set of random initial conditions, gives an idea of what to expect about the length of a path to synchronization for a random initial condition. In all cases, it is observed that there is very little possibility of choosing randomly an initial condition that has a path that reaches synchronization in a few or many steps, rather the behavior would be intermediate. In addition, this behavior depends on the threshold ϵ that is chosen to make the computational calculations, when the threshold is lower, the average length of the paths will increase.

3.2 Exploring the Kuramoto model

This section shows the exploratory studies that were carried out from computational simulations for a set of 10^6 random initial conditions on $(0,2\pi)^N$ in the Kuramoto model the complete graph, the complete bipartite graph, the cycle graph and the family of ring lattices, as was said in Section 2.3, with the aim of finding the patterns that meet the initial conditions on their way to finding the synchronization. In the four types of subgraphs that are analyzed, the same initial condition is evaluated to observe the different behavior it has when the topology of the graph changes. In addition, for each of them, the number of feasible subgraphs, the length of the longest path, the number of paths and the distribution of path lengths are explored, for a set of random initial conditions. These analyzes and exploratory studies are very important for the elaboration of theorems and propositions that fulfill the different systems exposed in this thesis in Section 4.3.2.

3.2.1 The Kuramoto model of M_{K_N}

To begin, the most important observations, made through computational simulations, regarding the behavior of the Kuramoto model on the complete graph of dimension N, $K(M_{K_N})$, will be presented. Specifically, the behavior of this system is investigated when the dimension grows. These calculations were made for a set of 10^6 random initial conditions in $(0,2\pi)^N$ as was said in Section 2.3. The trajectory under the Kuramoto flow, starting with a fixed initial condition, will be evaluated, this will be used throughout Section 3.2 in order to observe the differences when the topology of the graph is changed. Then, a summary with the probability that when generating a random initial condition is shown, evaluating it with the Kuramoto model, its behavior is not monotonous. Below a comment about the number of unfeasible subgraphs of K_N is presented. Then, a computational calculation about the length of the longest path found in the transition diagram of the Kuramoto model applied to the complete graph K_N is shown. Moreover, a calculation of the number of distinct paths found in

the transition diagram discussed in this section is shown. Finally, three path lengths normalized distributions for a set of random initial conditions are shown, with the purpose of observing the length of typical paths in the Kuramoto model applied to the complete graph K_N.

Starting from the order defined in the previous paragraph, Figure 3.25 shows the flow of this model in a concrete example, applied to a fixed initial condition in dimension 6:

$$x = (3.69253, 1.95285, 2.48317, 0.984696, 3.39029, 4.82533).$$

It meets that $x \in (0, 2\pi)^6$, and each of its coordinates approaches monotonically (increasingly or decreasingly) to $\bar{x} = 2.88815$, which is the average of the coordinates of x. Moreover, each of the coordinates follows its path towards the asymptotic value, without crossing each other. In this case, the differences between the coordinates do not decrease monotonically. This is the first and most important difference between the Laplacian system and the Kuramoto model in this type of graph.

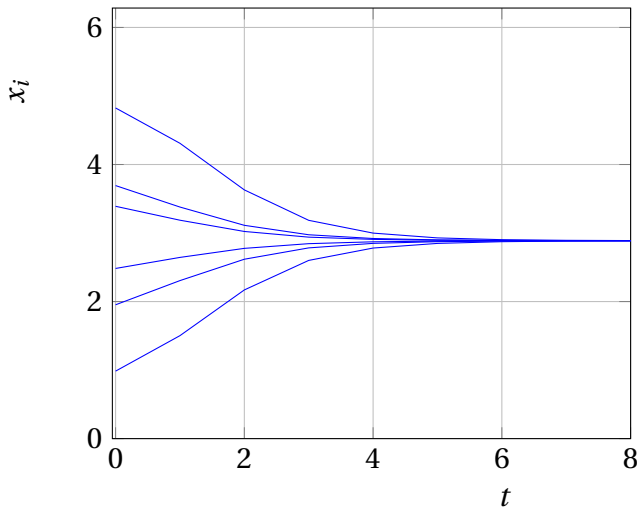

Figure 3.25 – The Kuramoto flow in the complete graph of dimension 6, K_6, applied on a fixed initial condition $x \in (0, 2\pi)^6$. Each one of the six lines represents the projection of each one of the coordinates x_i of x. It is observed that all of them reach the same value asymptotically and that they do so monotonically, without crossings between them, but the differences between the coordinates do not decrease monotonically.

Simulations to see if the differences between the coordinates are monotonic in different dimensions were performed. That means, to find the probability that an initial condition, when applying the Kuramoto flow, its components are monotone. A total

of 10000 random ordered initial conditions in $(0,2\pi)$ showed the behavior described by Table 3.2. It can be seen that as the dimension increases, the probability of finding an initial condition in which its differences remain monotonic tends to zero.

N	% not monotonous
2	0
3	2.53
4	12.57
5	31.28
6	47.30
7	61.34
8	72.81
9	81.70

Table 3.2 – Percentage of non-monotonic initial conditions. For different dimensions $N = 2,3,...,9$, the percentage of initial conditions over the Kuramoto flow, such that the behavior of the differences between the coordinates are not monotonous, was evaluated.

Simulations to see the behavior of the differences of the coordinates when we limit the interval of the initial conditions were made. In dimension 15, it was observed that for $(-\pi/8,\pi/8)$, $(-\pi/6,\pi/6)$ and $(-3\pi/8,3\pi/8)$, 0% of the initial conditions are non-monotonic, that is, all the differences are monotonic. This means that when an interval close to the diagonal is considered, it has the same behavior as for the Laplacian system.

It is important to point out that, the possible states in the Kuramoto flow transition diagram applied to the complete graph are the same as for the Laplacian flow over the complete graph, since an initial condition can have a given configuration is a matter of the graph that it is found, and not of the system that is applied.

Regarding the length of the longest path found for the Kuramoto flow over the complete graph, Figure 3.26 shows the result of the computational calculations that were carried out for a set of random initial conditions on $(0,2\pi)^N$. In this case, contrary to what happens when the Laplacian system is applied, the size of ϵ is important, because, since the way in which the differences of the coordinates decrease is not monotonic, then, for certain values of ϵ connections and disconnections between edges could be detected. In the case shown in Figure 3.26, ϵ was taken small enough to not detect the non-monotony of the differences. Then, the longest path length in the transition diagram coincides with the number of edges of K_N.

The number of different paths to synchronization was calculated in the Kuramoto model applied to the complete graph K_N, for the set of random initial conditions, and

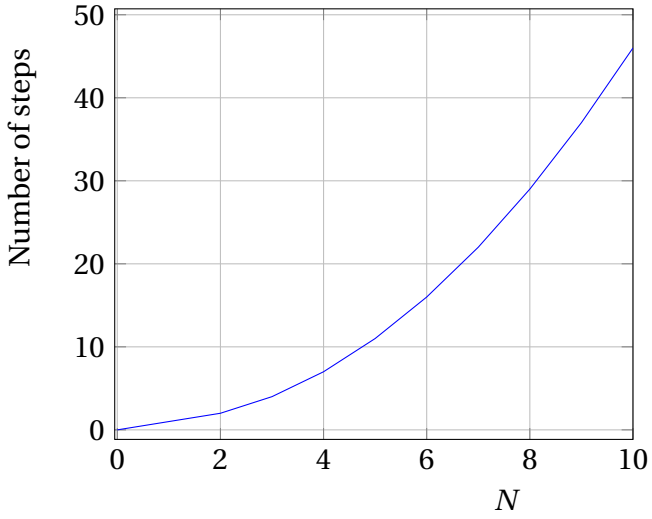

Figure 3.26 – Depth of $K(M_{K_N})$ transition diagram. The blue line represents the maximum number of steps towards synchronization in the Kuramoto model of the complete graph of dimension N.

is presented in Figure 3.27. As well as for the case in which the Laplacian system was applied, the number of paths generated grows at least exponential.

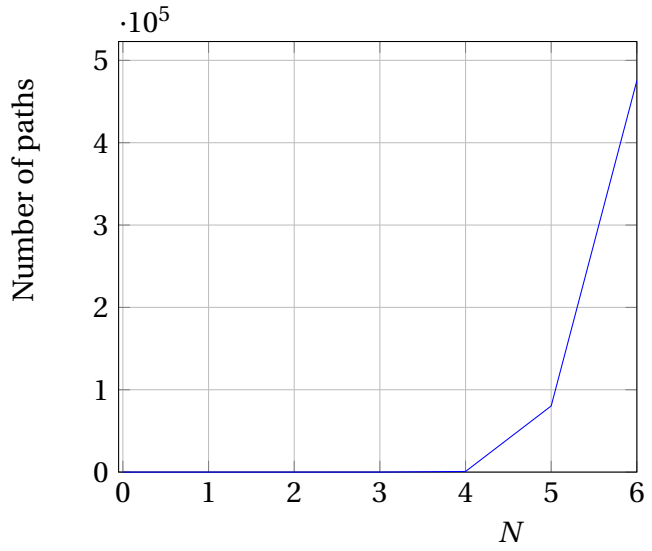

Figure 3.27 – Number of paths towards synchronization in $K(M_{K_N})$. The blue line represents the number of paths towards synchronization in the Kuramoto model of the complete graph of dimension N.

For a set of random initial conditions in $(0,2\pi)^N$, specifically in the dimensions $N = 8,9,10$, the number of steps they must take to reach full synchronization was counted. In Figure 3.28 the normalized numerical results by the number of initial conditions evaluated (10^6) are shown. In which a blue line is presented to represent the behavior when $N = 8$, in red color when $N = 9$ and in green color when $N = 10$, which are unimodal and symmetric. Unlike when the initial conditions were applied to the Laplacian system, these functions have a larger variance.

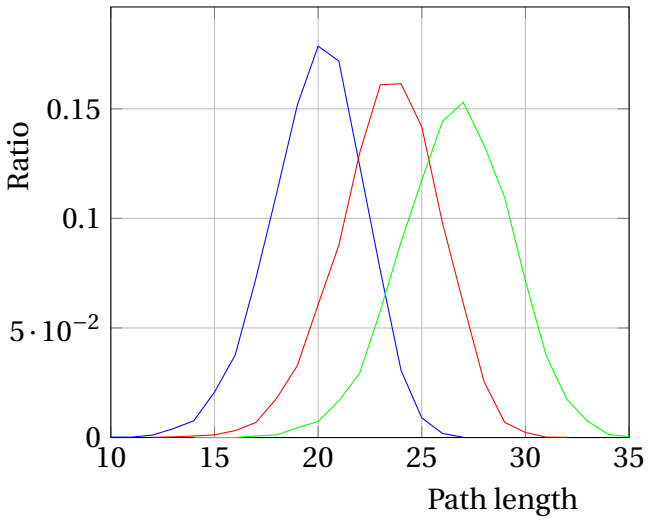

Figure 3.28 – Path length distribution of $K(M_{K_N})$. The blue line represents the normalized path length distribution of Kuramoto model of the complete graph of dimension $N = 8$, the red line in dimension $N = 9$ and green line in dimension $N = 10$, for a set of random initial conditions.

As a conclusion of this section, due to the monotonicity of the Kuramoto flow applied to the complete graph of dimension N, considering a very small ϵ threshold, first, there is an upper bound for the maximum length of the paths to synchronization in its transition diagram. In addition, as in the case of the Laplacian system, the number of feasible subgraphs is the same, since it is not a property that depends on the system that is applied, but on the topology of the graph. On the other hand, the number of different paths to synchronization generated by Kurimoto's model in the complete graph seems to be growing at least exponentially. Finally, the path length distributions provide an idea of what to expect from the behavior of a random initial condition, which should be treated carefully when ϵ is varied, because by making this threshold smaller, then the average of the typical length grows. The observations made in this section are the basis for the future formalization of the results presented in Section 4.3.2, with respect to the transient state behavior of the Kuramoto model over the complete graph of dimension N.

3.2.2 The Kuramoto model of $M_{K_{N,N}}$

Now, the most important observations, made through computational simulations, regarding the behavior of the Kuramoto model on the complete bipartite graph of dimension $2N$, $K(M_{K_{N,N}})$, will be presented. Specifically, the behavior of this system is investigated when the dimension grows. These calculations were made for a set of 10^6 random initial conditions in $(0,2\pi)^N$ as was said in Section 2.3. The trajectory under the Kuramoto flow, starting with a fixed initial condition, will be evaluated, this will be used throughout Section 3.2 in order to observe the differences when the topology of the graph is changed. Then, a comparison of the longest path to synchronization found from computational calculations and the number of subgraphs that $K_{N,N}$ has is presented. Next, a comment about the number of unfeasible subgraphs of $K_{N,N}$ is presented. Then, the behavior of the number of different paths to synchronization that were found is presented. Finally, three path lengths normalized distributions are shown for a set of random initial conditions, with the purpose of observing the length of typical paths in the case presented in this section.

As mentioned in the previous paragraph, the same initial condition that was studied in Section 3.2.1 is evaluated, to observe its behavior when the interactions are given by the complete bipartite graph $K_{3,3}$, which is,

$$x = (3.69253, 1.95285, 2.48317, 0.984696, 3.39029, 4.82533).$$

It can be seen that not all of its coordinates approach non monotonically (increasingly or decreasingly) to $\bar{x} = 2.88815$, which is the average of the coordinates of x. In addition, each of the coordinates follows its path towards the asymptotic value, without crossing each other, but the differences between the coordinate values do not decrease monotonically.

Due to the non-monotonic behavior of the differences of the coordinates towards the asymptotic value, in this case, there are also crossings between them, then, the maximum length of a path towards synchronization exceeds the number of edges of the complete bipartite graph $K_{N,N}$ which is N^2. In Figure 3.30, the results of the computational calculations for the case of $K(M_{K_{N,N}})$ are shown. On the one hand, the blue line represents the maximum number of steps towards synchronization in the Kuramoto model of the complete bipartite graph of dimension $2N$. On the other hand, the red line represents the number of edges that the complete bipartite graph of dimension $2N$ has. As can be seen, the maximum number of steps exceeds the number of edges of the graph in which it is located. Recall that this behavior also appears in the case of the Laplacian system applied to the same graph.

Regarding the number of unfeasible subgraphs in $K_{N,N}$ over the Kuramoto model, as mentioned for the complete graph K_N case, they are the same as for the Laplacian system, because it is not a characteristic associated to the system that is applied, but

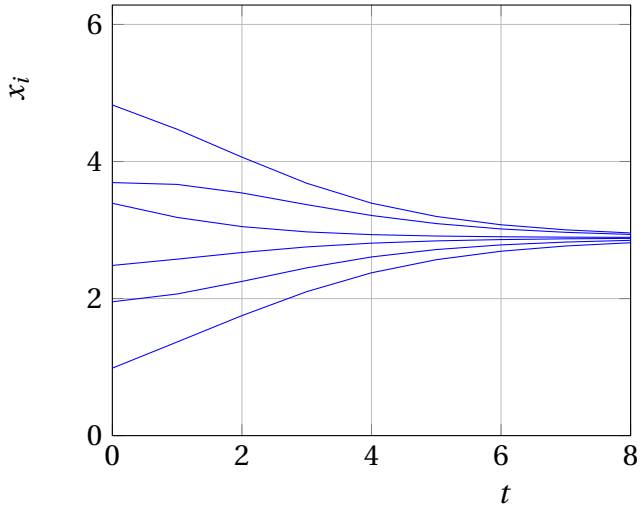

Figure 3.29 – The Kuramoto flow in the complete bipartite graph of dimension 6 $K_{3,3}$ applied on a fixed initial condition $x \in \mathbb{R}^6$. Each one of the six lines represents the projection of each one of the coordinates x_i of x. It is observed that all of them reach the same value asymptotically non monotonically.

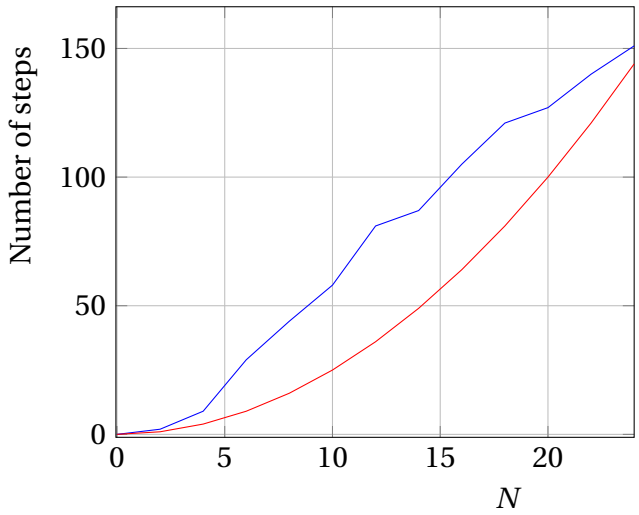

Figure 3.30 – Depth of $K(M_{K_{N,N}})$ transition diagram. The blue line represents the maximum number of steps towards synchronization in the Kuramoto model of the complete bipartite graph of dimension $2N$. The red line represents the number of edges that the complete bipartite graph of dimension $2N$ has.

to the topology of the graph.

Considering a set of random initial conditions in $(0,2\pi)^{2N} \subset \mathbb{R}^{2N}$. The path towards synchronization of these 10^6 initial conditions was calculated, then all those that were different from each other were counted. The result of this process is shown in Figure 3.31. The growth of the number of paths towards synchronization, despite there being only a few vertices in the transition diagram, seems to follow a rule, at least of exponential growth.

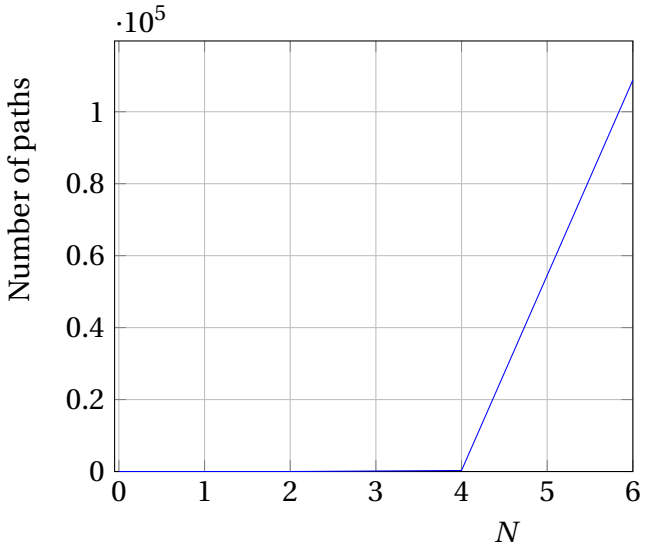

Figure 3.31 – Number of paths towards synchronization in $K(M_{K_{N,N}})$. The blue line represents the number of paths towards synchronization in the Kuramoto model of the complete bipartite graph of dimension $2N$.

To finish the computational analysis, for the set of random initial conditions, the path length distribution in each dimension $2N$ was calculated, to observe the behavior of a typical path towards synchronization. To give an idea of what to expect about the length of a path to synchronization associated with a random initial condition. In addition, it can also be seen how likely it is to find an initial condition with maximum length, and similarly, an initial condition that reaches synchronization in very few steps. In Figure 3.32, this behavior for the dimensions $N = 10, 12, 14$ is shown, in blue, red and green lines respectively (normalized by the total number of initial conditions evaluated) in the Kuramoto model. As can be seen, these distributions seem to follow a Gaussian behavior, and are not as smooth as those found for the case of the Laplacian system applied to the same graph. In addition, the paths found are considerably longer.

As a conclusion of this section, due to the non-monotonicity of the differences of the coordinates in the Kuramoto flow applied to the complete bipartite graph of

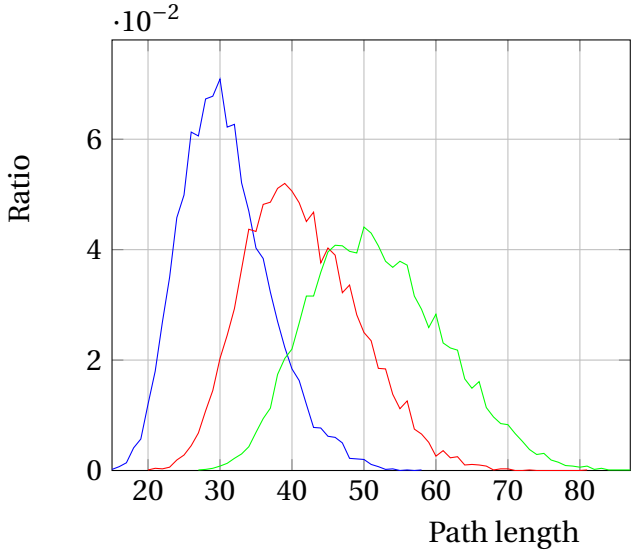

Figure 3.32 – Path length distribution of $K(M_{K_{N,N}})$. The blue line represents the normalized path length distribution of Kuramoto model of the complete graph of dimension 10, the red line in dimension 12 and green line in dimension 14, for a set of random initial conditions.

dimension $2N$, there is a lower bound for the maximum length of the paths to synchronization in its transition diagram, which is the number of edges that $K_{N,N}$ has, and computer simulations suggest that the longest path triples it. As in the case of the complete graph, the number of states in the complete bipartite graph is the same as in the case of the Laplacian flow, since it is a property that depends on the topology of the graph and not on the system that is applied to it. On the other hand, it was observed that the growth of the number of different paths that can be found in this transition diagram grows by means of a rule that seems at least exponential. Finally, the path length distributions provide an idea of what to expect from the behavior of a random initial condition, which should be treated carefully when ϵ is varied, because by making this threshold smaller, then the average of the typical length grows.

3.2.3 The Kuramoto model of M_{C_N} and $M_{C(N,k)}$

In this section the quantitative properties of the Kuramoto model on the cycle graph of dimension N and the ring lattice family $C(N,k)$ are seen, which were calculated computationally. Specifically, the behavior of this model when the dimension grows is investigated. The trajectory under the Kuramoto flow, starting with a fixed initial condition, will be evaluated, this will be used throughout Section 3.2, to observe the differences when the topology of the graph is changed. The objective of this section is to observe the transient behavior of the Kuramoto model in the space $\mathbb{R}^N$, before

reaching synchronization, that is, all its coordinates have the same value after a certain period. Sections 3.1 and 3.2 have focused on the behavior when the dimension of spaces N increases, and the problem presented in these cases is exposed.

Just as it was presented in the two previous sections, the behavior of the initial condition

$$x = (3.69253, 1.95285, 2.48317, 0.984696, 3.39029, 4.82533),$$

in the cycle graph C_6 is presented. In Figure 3.33 it can be seen that all of its coordinates approaches monotonically (increasingly or decreasingly) to $\bar{x} = 0.947006$, which is the average of the coordinates of x. Furthermore, in this case, it is observed that the convergence time is longer than for when this initial condition is considered over the complete graph and the complete bipartite graph (the convergence time is more than double than in the other cases). In addition, this behavior occurs when the Laplacian system is considered.

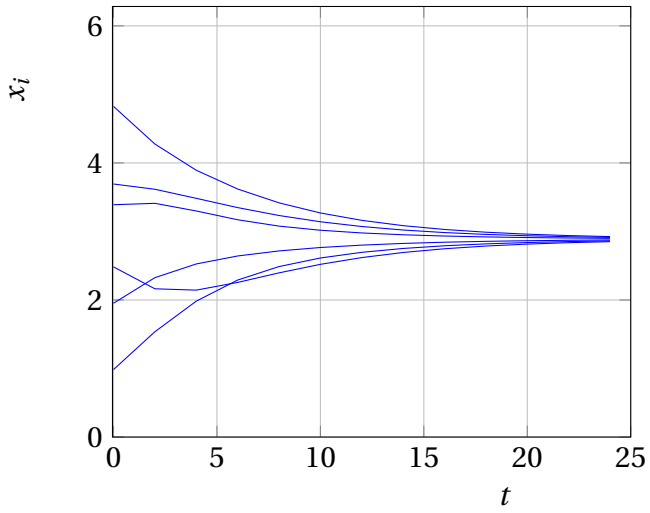

Figure 3.33 – The Kuramoto flow in the cycle graph of dimension 6, C_6, applied on a fixed initial condition $x \in \mathbb{R}^6$. Each one of the six lines represents the projection of each one of the coordinates x_i of x. It is observed that all of them reach the same value asymptotically monotonically, and they cross each other.

Once again, as was said for the case of the Laplacian system applied to these graphs, C_N and $C(N,k)$, the same subgraphs are feasible in the case of the Kuramoto model.

In Figure 3.34, a comparison of the proportion of initial conditions that synchronize in the Kuramoto system in the cycle graph C_N, and in three types of ring lattices

($C(N,2)$, $C(N,3)$ and $C(N,4)$), which depends on the dimension are shown. They are represented with a blue, red, green, and yellow line respectively. As can be seen, as the dimension increases, the probability of finding synchronizing initial conditions decreases, therefore, it is not possible to provide an analysis like that of the other cases presented, in which what is of interest is to know the behavior of the transient state when the dimension N increases.

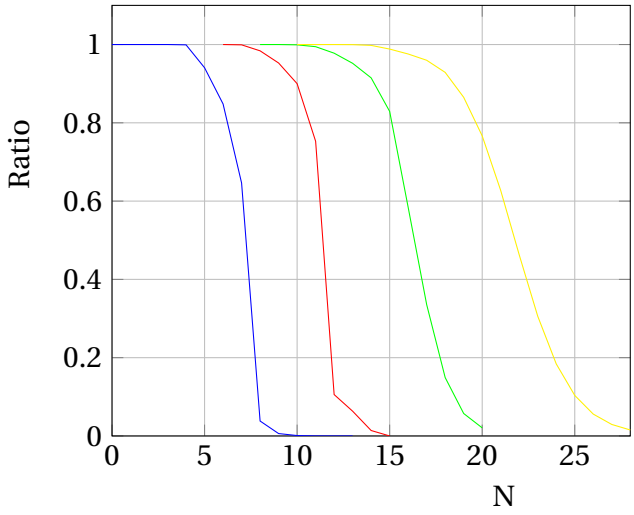

Figure 3.34 – Proportion of initial conditions that synchronize in the Kuramoto model in the rind lattice family $C(N,k)$ for $k = 1,2,3$ and 4.

To end, as a conclusion of this section, regarding the number of possible states in the transition diagrams associated with these graphs, it is observed that they are the same quantity as in the Laplacian system, because it is a property that depends on the topology of the graph and not on the system that is applied. On the other hand, it is not possible to give an analysis of the behavior of the transition diagram when N grows, because the probability of finding synchronizing initial conditions tends to zero from very small dimensions. Despite this, the asymptotic state reached by the initial conditions corresponds to phase locking, that is, to a state where the angles of each of the initial conditions are equally distributed in the interval $(0,2\pi)$. The analysis of this state will remain as a perspective of the thesis.

3.2.4 Discussion

In this section, an exploratory study of the transitory state of the Kuramoto model was carried out, applied to the complete graph, the bipartite complete graph, the cycle graph, and the ring lattice family, to open the panorama and understand the behavior

of the model before reaching the synchronization. The behavior of a randomly generated and fixed initial condition in the four types of graphs was studied. The number of vertices contained in each of the transition diagrams was estimated. The length of the longest path in each diagram was calculated. In addition, the number of realizable paths towards synchronization was calculated and concluded with the presentation of the normalized distributions of path lengths for each case.

Analyzing the same initial condition in the four types of possible graphs allow to see the differences between the dynamics when the Kuramoto flow is applied. It is recalled that the cases analyzed were in dimension six. It was observed in the complete graph that the way to approach the asymptotic value is monotonically, either with increasing or decreasing values. On the other hand, in the case of the complete bipartite graph and the cycle graph some coordinates do not have monotonic behavior. Also, the differences between the coordinates are monotonically reduced in no case. In addition, the times in which synchronization is reached for the complete graph and the complete bipartite graph are very similar, and always smaller than 8-time units. In the case of the cycle graph, the convergence time appears to be $t > 20$, which may be due to poor connectivity of the graph.

The number of realizable states was analyzed for each of the four different types of transition diagrams studied. This refers to the number of subgraphs of the complete graph, the complete bipartite graph, the cycle graph, and the ring lattice family that are feasible for some initial condition. Only for the case of the cycle graph, each of its subgraphs are feasible, from computational calculations, it was possible to give an exact formula for the number of states in their respective transition diagram. For the other three cases, the types of unfeasible subgraphs were found, and an estimate of how many subgraphs there are of each of them was made.

Regarding the length of the longest path found in the transition diagram of the Kuramoto model applied to the complete graph and the complete bipartite graph, the following results were obtained. In the case of the complete graph, due to the monotony it presents when ϵ is small enough, the longest length found corresponds to the number of edges that K_N has. When the presence of directed cycles in the transition diagrams is observed, therefore, its depth increases, until it triples the number of edges they have, that is the case of the complete bipartite graph.

Regarding the number of different paths to synchronization that are observed in the complete graph and the complete bipartite graph transition diagrams, it was observed that although the number of realizable states is much less than the number of possible states (referring to the number of subgraphs that the complete graph and the complete bipartite graph has), the number of paths towards synchronization in all cases seems to grow at least exponentially. Therefore, it can be concluded that with little information, the number of possibilities to build new information is large enough so that it can be exploited in the future, making use of applications, for example, in

information storage and classification.

To end this discussion section of the behavior of the transition diagrams associated with the Kuramoto model in the complete graph and the complete bipartite graph, computational calculations for a set of 10^6 random initial conditions in $(0,2\pi)^N$, whose sequence of ϵ-synchronized subnetworks was calculated. The length of each of them was measured and the normalized distribution of the length of these paths was constructed. For case of the complete graph, unimodal distribution like the Gaussian distribution was observed, which the average increases when the dimension increases. In the case of the complete bipartite graph a case-by-case behavior is observed, which separates the parity of the path's length, these distributions are also unimodal, and appear to be slightly skewed to the left. Knowing how these distributions behave for a set of random initial conditions, gives an idea of what to expect about the length of a path to synchronization for a random initial condition. In all cases, it is observed that there is very little possibility of choosing randomly an initial condition that has a path that reaches synchronization in a few or many steps, rather the behavior would be intermediate. In addition, this behavior depends on the threshold ϵ that is chosen to make the computational calculations, when the threshold is lower, the average length of the paths will increase.

4 Results

Contents

4.1 The transition diagram of $L(M_{K_N})$

In this section it is formally and rigorously analyzed the behavior of the transition diagram of the Laplacian system applied to the complete graph of dimension N. This study is organized as follows: to begin with, the coding used to describe the states, and the paths towards synchronization are presented, which respects all the dynamics of the system. Then, the unfeasible subgraphs that the complete graph has been shown, which imply the states that cannot have the initial conditions in the transition diagram. Finally, the way to generate the paths to synchronization in the Laplacian flow over the complete graph, an estimation of the diversity of paths and their distribution are exposed.

4.1.1 Coding

The coding of the subgraphs of the complete graph and the dynamics that follow on their path to synchronization was carried out taking advantage of the fact that the differences of the flow of the coordinates monotonically tend to zero. The following shows how this process occurs. Due to the Laplacian matrix for K_N, as it is shown in Equation (2.2) is symmetrical, it can be diagonalized, and the basis $\{u^1, u^2, \ldots, u^N\}$ can

be chosen, where $u^1 := \sum_{n=1}^{N} \mathsf{e}^n$ and, for each $n \geq 1$, $u^n := \mathsf{e}^n - \mathsf{e}^1$. Let's remind that e^n denotes the n-th vector of the canonical basis of $\mathbb{R}^N$.

In this section, L will denote the Laplacian system over the adjacency matrix of the complete graph $L(M_{K_N})$. Writing some simple calculations, first:

$$\begin{aligned} Lu^1 &= L\left(\sum_{n=1}^{N} \mathsf{e}^n\right), \\ &= \sum_{n=1}^{N} L\mathsf{e}^n, \\ &= \overline{0}. \end{aligned}$$

and for each $n \geq 2$:

$$\begin{aligned} Lu^n &= L\left(\mathsf{e}^n - \mathsf{e}^1\right), \\ &= L\mathsf{e}^n - L\mathsf{e}^1, \\ &= -N\left(\mathsf{e}^n - \mathsf{e}^1\right), \\ &= -Nu^n. \end{aligned}$$

Now an arbitrary initial condition $x \in \mathbb{R}^N$ is considered and it can be decomposed as:

$$x = \bar{x}\, u^1 + \sum_{n=1}^{N-1} (x_{n+1} - \bar{x})\, u^n,$$

where $\bar{x} := \left(\sum_{n=1}^{N} x_n(0)\right)/N$. Therefore, its Laplacian flow can be written as:

$$\begin{aligned} x(t) &= \bar{x}\, u^1 + e^{-Nt} \sum_{n=1}^{N-1} (x_{n+1} - \bar{x})\, u^n, \\ &= \sum_{n=1}^{N} \left(\bar{x}\left(1 - e^{-Nt}\right) + e^{-Nt} x_n\right) \mathsf{e}^n, \end{aligned}$$

for all $t \in \mathbb{R}$.

From this, it follows that the behavior of the differences between each of its coordinates is as in the following expression:

$$x_n(t) - x_m(t) = e^{-Nt}(x_n - x_m), \tag{4.1}$$

for all $t \in \mathbb{R}$ and each $1 \leq m, n \leq N$. In other words, the behavior of coordinate differences is *monotone*. Hence, the edge $\{n, m\}$ belongs to the ϵ-synchronized subnetwork $G_{x(t)}$, for all times exceeding:

$$t_{n,m} = \frac{\log|x_n - x_m| - \log(\epsilon)}{N}.$$

In other words, once an edge appears on a path in the transition diagram, it never disappears.

As explained in Section 3.1.1, when considering the paths generated in the transition diagram of the complete graph, due to the symmetries that K_N has, there are paths that turn out to be redundant and that can be described more simply by considering some symmetry. Then without loss of generality, I will focus on considering ordered initial conditions, that is, I will assume that $x_1(0) \leq x_2(0) \leq \cdots \leq x_N(0)$ which, by Equation (4.1), ensures that $x_1(t) \leq x_2(t) \leq \cdots \leq x_N(t)$ for all t.

Now, it will be defined the transition diagram not over the ϵ-synchronized subnetworks but over another combinatorial object that encodes both the ϵ-synchronized subnetworks, and at the same time, it recognizes the order of the coordinates. By employing this methodology, the depiction of transition diagrams becomes more convenient. The coding scheme employed here enables the straightforward identification of the sequential emergence of new edges in the synchronized sequence. This coding approach is not only advantageous but also essential for preserving the order of coordinates while constructing new edges.

The ϵ-synchronized subnetwork G_x, determined by the ordered configuration $x_1 \leq x_2 \leq \cdots \leq x_N$ is coded by the *increasing function* $\phi_x : \{1, 2, \ldots, N\} \to \{1, 2, \ldots, N\}$ given by:

$$\phi_x(m) = \max\{n \geq m : x_n \leq x_m + \epsilon\}. \tag{4.2}$$

The function ϕ_x is clearly increasing and such that $\phi_x(n) \geq n$ for each $1 \leq n \leq N$, in other words, this function goes above the diagonal $\phi_x \geq \mathrm{Id}$. Here and below Id denotes the identity function in $\{1, 2, \ldots, N\}$. Now, an example of the construction of the increasing function from a given initial condition is presented in Figure 4.1. In the first line (a), an example of the values of $x = (x_1, x_2, x_3, x_4)$ are illustrated with black dots on a fixed axis. To construct the corresponding subgraph G_x based on Equation (2.28), we can observe that x_1 and x_2 lie within one ϵ-neighborhood (depicted as a rectangle with side length ϵ), while x_3 and x_4 are within another neighborhood. This implies that in scenario (b), there are links connecting vertices 1 and 2, as well as vertices 3 and 4. In the final line (c), the increasing function ϕ_x associated with x is shown. The information conveyed by ϕ_x can be interpreted as follows: the furthest vertex connected to vertex 1 is vertex 2, vertex 2 does not have a connection to vertex 3, and

vertex 3 is connected to vertex 4, which is the last one.

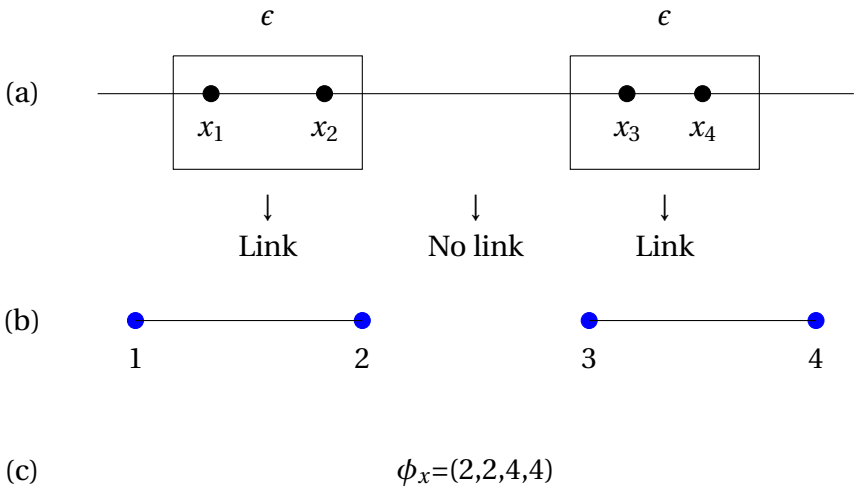

Figure 4.1 – Construction of an increasing function from a given network. In (a), a graphic representation of the values of the four coordinates of an initial condition is shown, in boxes, the pairs of coordinates that are ϵ-neighbors are shown, which implies that a link will be added to build the subgraph between the vertices that represent each coordinate. With this idea in (b), the graph that connects vertex 1 with vertex 2 and vertex 3 with vertex 4 is shown. Finally, in (c), the increasing function ϕ_x is shown, which is associated with the initial condition $x = (x_1, x_2, x_3, x_4)$ that appears in (a). In this case, the first component is written the vertex number with the largest label that is connected to vertex 1, and so on. The vertices 2 and 4 meet this condition with themselves, and vertices 1 and 3 meet it with their consecutive.

It should also be noted that if for certain $t > 0$: $x_j(t) - x_i(t) < \varepsilon$, then: $x_j(t) - x_k(t) < \varepsilon, \forall\ \ 0 < i < k < j \leq N$. In the following Figure 4.2, an example of the behavior of the closeness of the vertices under the previous proposition is shown. Since vertex 2 and vertex 5 are connected, it implies that $|x_5 - x_2| < \epsilon$, since there are considering ordered initial conditions, then all interior differences will be less than ϵ as well, which for this example, having the longest edge implies having 5 more edges. To avoid tiring the eyes, will be restricted in the future, it will only draw the longest edge, if all the inner edges still exist.

The collection:

$$\Phi_N := \{\phi : \{1, \ldots, N\} \to \{1, \ldots, N\} \text{ increasing and s. t. } \phi \geq \text{Id}\}, \tag{4.3}$$

is in a one-to-one correspondence with the set of all ϵ-synchronized subnetworks

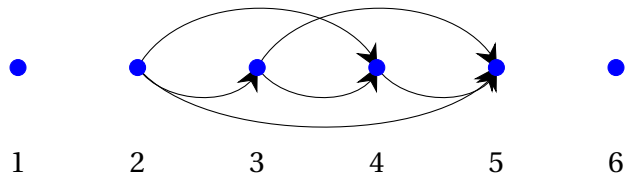

Figure 4.2 – Example of the closeness of the vertices. This figure shows a graph with 6 vertices associated with an ordered initial condition, that is, it satisfies $x_1 < x_2 < x_3 < x_4 < x_5 < x_6$. Since 2 is connected to 5, it implies that all the internal links are also found, that is, 2 with 3, 3 with 4, 4 with 5, 2 with 4 and 3 with 5. To avoid writing so many arrows, only the largest one will be drawn, with the understanding that the inner arrows also exist.

of K_N defined by ordered initial conditions, that is $x_1 \leq x_2 \leq \cdots \leq x_N$. The correspondence is given by:

$$\phi \mapsto (\{1,2,\ldots,N\}, E_\phi) \text{ where } E_\phi = \{\{m,n\} : \min(m,n) \leq \phi(\max(n,m))\}. \tag{4.4}$$

In this case, the coding in Equation (2.29) which associates increasing functions to synchronized subnetworks is given by Equation (4.4). The proof is outlined below.

Firstly, it is possible to establish a correspondence between each increasing function $\phi : 1,2,\ldots,N \to 1,2,\ldots,N$, satisfying $\phi \geq \mathrm{Id}$, and an ordered initial condition $x \in \mathbb{R}^N$ such that $\phi = \phi_x$. This correspondence is achieved by representing ϕ as a collection of disjoint directed trees, according to the following method. Let $\mathrm{Fix}(\phi) := \{1 \leq n \leq N : \phi(n) = n\}$. To each $n \in \mathrm{Fix}(\phi)$ a directed tree T_n, rooted at n, with vertex set:

$$V_n := \bigcup_{l=0}^{h(n)} \phi^{-l}(\{n\}),$$

is associated and directed edges in:

$$A_n := \{(k, \phi(k)) : k \in V_n \setminus \{n\}\}.$$

The vertex set V_n splits into $h(n)+1$ disjoint levels, $V_n^l := \phi^{-l}(\{n\})$, $0 \leq l \leq h(n)$. The number $h(n)$ is the high of T_n.

The maximal paths in T_n are completely determined by their starting vertices, which must be leaves. Let $\ell_n^1 < \ell_n^2 < \cdots < \ell_n^{w(n)}$ be the leaves of T_n. Its number, $w(n)$, is the width of the tree T_n.

Since ϕ is increasing and such that $\phi \geq \mathrm{Id}$, then every element in the l-th level, V_n^l, is greater than all the elements in the l'-th level, $V_n^{l'}$ whenever $l < l'$. This implies

that the length $l(m)$ of the path starting at m and ending at the root is a decreasing function of m.

In the tree T_n, every maximal path starts at a leaf, and the longest of these paths have a length of $h(n)$ and begin at leaves in the highest level. Additionally, all vertices in T_n are part of a maximal path, indicating that they are reachable from a leaf.

Now, consider an increasing function $\phi : 1,2,\ldots,N \to 1,2,\ldots,N$ such that $\phi \geq \mathrm{Id}$. Let $T_{n_k} : 1 \leq k \leq R$ be the associated collection of directed trees, and let $n_1 < n_2 < \cdots < n_R$ be the corresponding roots in $\mathrm{Fix}(\phi)$. Choose $x \in \mathbb{R}^N$ such that $x_{n_1} = \epsilon \cdot h(n_1)$, and for each $1 \leq k < R$, proceed as follows:

$$x_{n_{k+1}} = x_{n_k} + (h(n_k) + 2)\,\epsilon. \tag{4.5}$$

Using this approach, the value of x_n is determined for each $n \in \mathrm{Fix}(\phi)$ in such a way that $x_{n_k} + \epsilon < x_{n_{k+1}} - h(n_{k+1})\epsilon$ for every $1 \leq k < R$.

Next, for each $n \in \mathrm{Fix}(\phi)$, let $\ell_n^1 < \ell_n^2 < \cdots < \ell_n^{w(n)}$ represent the leaves of T_n. For every $1 \leq j \leq w(n)$ and $0 \leq k \leq l(n_j)$, where $x_{\phi^k(\ell_n^j)}$ has not yet been defined, we define it as follows:

$$x_{\phi^k(\ell_n^j)} = x_n - (l(n_j) - k)\,\epsilon + (j-1)\frac{\epsilon}{w(n)}. \tag{4.6}$$

It is recalled that $l(n_j)$ is the length of the maximal path starting at ℓ_n^j. It is not difficult to verify that Equations (4.5) and (4.6). Define an ordered initial condition $0 = x_1 < x_2 < \cdots < x_N = \sum_{k=1}^{R}(h(n_k)+2)$, such that $\phi_x = \phi$.

By establishing the equivalence of these objects, it is then possible to search for properties of one that may be useful in the study of the other. In this case, the collection Φ_N is equivalent to a well-studied combinatorial set, the set of *D*yck paths of order N that have length $2N$. Let's remember that this combinatorial set has a cardinality given by the Catalan numbers Stanley and Fomin 1999 as said in Section 2.1.5. The formula shown below is one of the most important relationships found in this thesis.

$$|\Phi_N| = C_N = \frac{1}{N+1}\binom{2N}{N}. \tag{4.7}$$

In this way, the ϵ-synchronized subnetworks or the increasing functions can be used interchangeably and better yet, at the convenience of the problem that is addressed.

In Figure 4.3, a concrete example of the encoding of all the increasing functions in the subgraphs of K_3 is shown. For each row from (a) to (e). In the first column, an increasing function of dimension 3 is shown, then to its right, its representation as a linear graph is shown, as was done in Figures 4.1 and 4.2. Further to the right, its associated subgraph in the form of a subgraph of K_3 is shown, with the aim of using

whatever is preferably for the reader. In this way, in future sections it will be possible to have more clarity when passing from the transition diagram with vertices representing subgraphs, to when the transition diagram undergoes a relabeling in terms of increasing functions. Through this code it will be possible to do the translation step by step. As a last observation, note that in Equation (4.7), making a substitution, then $|\Phi_3| = \frac{1}{4}\binom{6}{3} = 5$, which corresponds precisely to the number of rows observed in Figure 4.3.

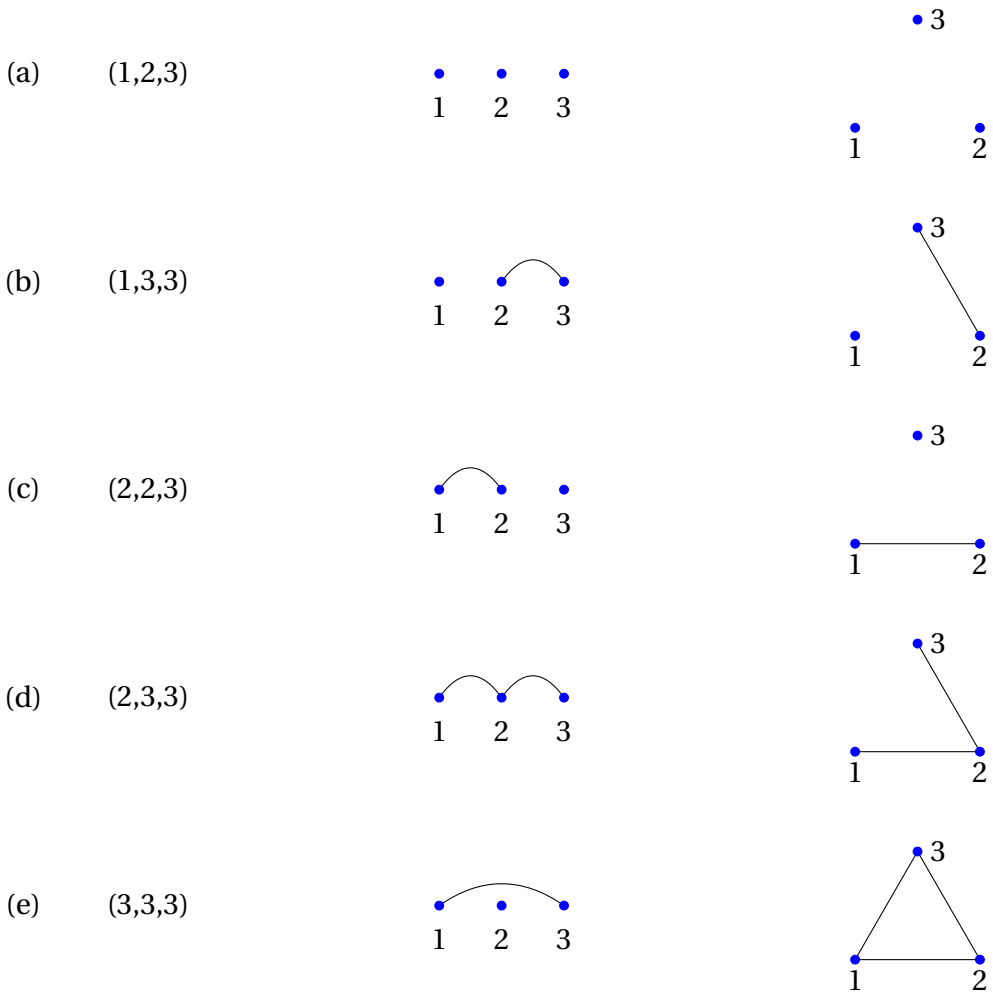

Figure 4.3 – Correspondence between graphs and increasing functions when $N = 3$. List of increasing functions for typical initial conditions in dimension 3, to its right the representation as a graph in a line and to its right the representation in the complete graph array.

Furthermore, in Figure 4.4, the list of increasing functions in dimension 4 is shown and to its right, the associated graph in its linear version is shown. Note that in Equa-

tion (4.7), making a substitution, then $|\Phi_4| = \frac{1}{5}\binom{8}{4} = 14$, which corresponds precisely to the number of increasing functions depicted in the figure.

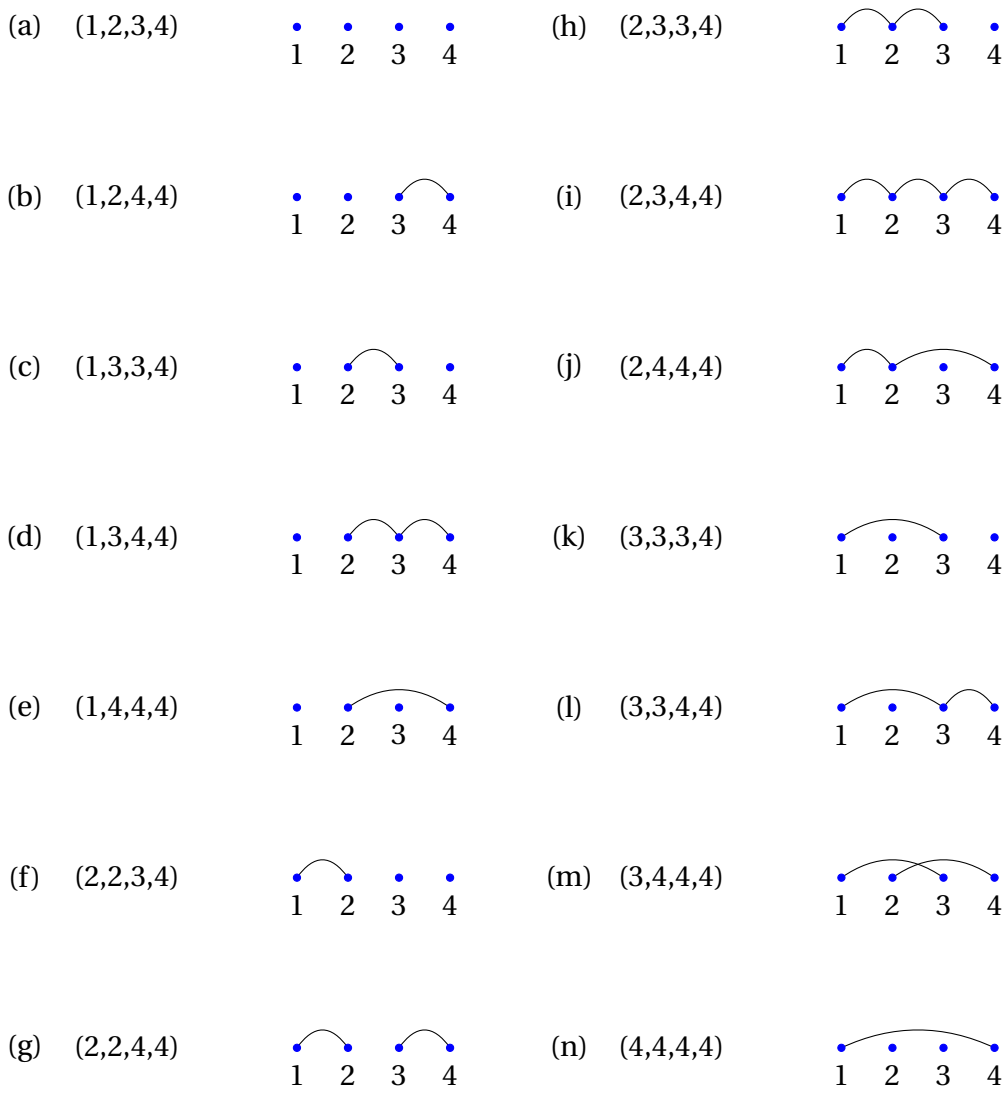

Figure 4.4 – Correspondence between graphs and increasing functions when $N = 4$. List of increasing functions for typical initial conditions in dimension 4 and to its right the representation as a graph in a line.

To end, as a conclusion of this section, when making a simplification of the initial conditions in $\mathbb{R}^N$, through one of the symmetries that the complete graph K_N has (considering its coordinates in strictly increasing order), which describe the entire space except for a set of Lebesgue measure zero, allows to establish a coding of the ϵ-synchronized subnetworks through increasing functions. Concepts already established in the literature can describe one of the most important properties of the

transition diagram of $L(M_{K_N})$, that is: the number of increasing functions corresponds to the number of possible states in the transition diagram.

4.1.2 Unfeasible subgraphs of K_N

Given the characteristics of increasing functions and the way they consistently encode initial conditions in the sense of ϵ-synchronized subnetworks, it turns out that some subgraphs of K_N remain uncoded, precisely because they are not feasible by no initial condition. Initially, it can be thought that all the subgraphs of K_N are feasible by initial conditions, which unfortunately is not true. Below are described these types of subgraphs.

As noted in the Section 3.1.1, all subgraphs of K_3 are feasible, therefore, this analysis starts for $N = 4$. In this dimension, there are two clear examples shown in Figure 4.5. Both the subgraphs in (a) and (b), including all their symmetries, cannot be performed by any initial condition on $\mathbb{R}^4$ and the reasons are given below.

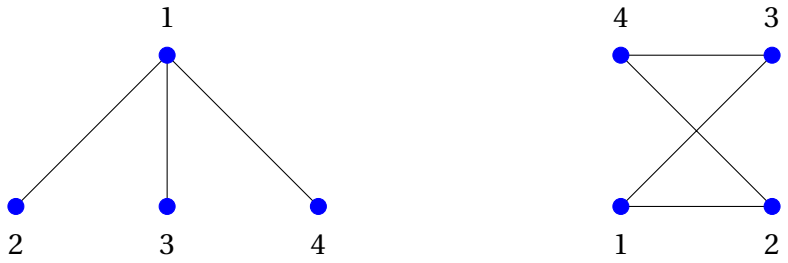

Figure 4.5 – Unfeasible subgraphs of K_4. In (a) and (b) subgraphs of K_4 which are not feasible for any initial condition in $\mathbb{R}^4$ are shown. The subgraph in (a) is named fork, and the subgraph shown in (b) is named hole.

Firstly, consider the case of Figure 4.5 (a), by construction of the subgraph, at time t the following inequalities in Equations (4.8-4.13) must be met.

$$|x_1(t) - x_2(t)| \leq \epsilon, \tag{4.8}$$
$$|x_1(t) - x_3(t)| \leq \epsilon, \tag{4.9}$$
$$|x_1(t) - x_4(t)| \leq \epsilon, \tag{4.10}$$
$$|x_2(t) - x_3(t)| > \epsilon, \tag{4.11}$$
$$|x_2(t) - x_4(t)| > \epsilon, \tag{4.12}$$
$$|x_3(t) - x_4(t)| > \epsilon. \tag{4.13}$$

By Equations (4.8) and (4.9), and the condition of the Equation (4.11) $x_2(t) < x_1(t) < x_3(t)$ or $x_3(t) < x_1(t) < x_2(t)$. Suppose the first is true, then:

$$x_2(t) = x_1(t) - \delta_2, \quad \delta_2 < \epsilon, \tag{4.14}$$
$$x_3(t) = x_1(t) + \delta_3, \quad \delta_3 < \epsilon. \tag{4.15}$$

Where $\delta_2 + \delta_3 > \epsilon$. By the condition of the Equation (4.10), there are two cases:

$$x_4(t) = x_1(t) + \delta_4, \quad \delta_4 < \epsilon, \tag{4.16}$$
$$x_4(t) = x_1(t) - \delta_4, \quad \delta_4 < \epsilon. \tag{4.17}$$

By the conditions of Equations (4.17) and (4.16):

$$\begin{aligned} |x_4(t) - x_3(t)| &< |x_1(t) + \delta_4 - x_1(t) - \delta_3|, \\ &< |\delta_4 - \delta_3|, \\ &< \epsilon. \end{aligned}$$

What contradicts the condition of the Equation (4.13). And by the conditions of Equations (4.16) and (4.17):

$$\begin{aligned} |x_4(t) - x_2(t)| &< |x_1(t) + \delta_4 - x_1(t) - \delta_2|, \\ &< |\delta_4 - \delta_2|, \\ &< \epsilon. \end{aligned}$$

What contradicts the condition of the Equation (4.12). Therefore, no initial condition meets all the requirements of the Equations (4.8-4.13).

Lastly, consider the case of Figure 4.5 (b), by construction of the subgraph, at time t the following inequalities in Equations (4.18-4.23) must be met.

$$|x_1(t) - x_2(t)| \leq \epsilon, \tag{4.18}$$
$$|x_1(t) - x_3(t)| \leq \epsilon, \tag{4.19}$$
$$|x_2(t) - x_4(t)| \leq \epsilon, \tag{4.20}$$
$$|x_3(t) - x_4(t)| \leq \epsilon, \tag{4.21}$$
$$|x_1(t) - x_4(t)| > \epsilon, \tag{4.22}$$
$$|x_2(t) - x_3(t)| > \epsilon. \tag{4.23}$$

By Equations (4.18) and (4.18), and the condition of the Equation (4.23), $x_2(t) < x_1(t) < x_3(t)$ or $x_3(t) < x_1(t) < x_2(t)$. Suppose the first is true, then:

$$x_2(t) = x_1(t) - \delta_2, \quad \delta_2 < \epsilon, \tag{4.24}$$
$$x_3(t) = x_1(t) + \delta_3, \quad \delta_3 < \epsilon. \tag{4.25}$$

Where $\delta_2 + \delta_3 > \epsilon$. By the condition of the Equation (4.21), there are two cases:

$$x_4(t) = x_3(t) + \delta_4, \quad \delta_4 < \epsilon, \tag{4.26}$$
$$x_4(t) = x_3(t) - \delta_4, \quad \delta_4 < \epsilon. \tag{4.27}$$

If the condition of the Equation (4.27) is met, then by Equation (4.25):

$$\begin{aligned} |x_3(t) - x_4(t)| &= |x_1(t) + \delta_3 - x_4(t)|, \\ &= |x_1(t) - x_4(t) + \delta_{3,}|, \\ &< \epsilon. \end{aligned}$$

What contradicts the Equation (4.22). And if Equation (4.26) is true, then:

$$\begin{aligned} |x_4(t) - x_2(t)| &= |x_3(t) + \delta_4 - x_1(t) + \delta_2|, \\ &= |x_1(t) + \delta_3 + \delta_4 - x_1(t) + \delta_2|, \\ &= |\delta_3 + \delta_4 + \delta_2|, \\ &> \epsilon. \end{aligned}$$

What contradicts Equation (4.20). Therefore, there is no initial condition that meets all the requirements of the Equations (4.18-4.23).

On the other hand, considering dimension $N > 4$, all subgraphs containing the graphs in Figure 4.5 as induced subgraphs cannot be obtained from an initial condition. For this reason, the number of vertices in the transition diagram does not coincide with the number of subgraphs of the initial graph. The coding that is presented in this thesis, as well as the rules for constructing edges between them, respects this fact.

Formally, in order for a subgraph $S \subseteq K_N$ to appear in the transition diagram of $L(M_{K_N})$, it must meet with the following:

1. If S contains a *fork* (3-star) (denoted by F^N the set of forks in a set of N vertices), that is, it have 4 vertices v_1, v_2, v_3, v_4, such that there is an edge $e_{i,j}$ that connects v_i with v_j as follows: $\{e_{1,2}, e_{1,3}, e_{1,4}\}$, then $e_{2,3}$ or $e_{2,4}$ or $e_{3,4}$ is also an edge of S.
2. If S contains a k-hole H_k (denoted by H_k^N the set of k-holes in a set of N vertices, such that $k \leq N$), where $k > 3$, that is $v_1, v_2, ..., v_k$, such that $e_{i,i+1}$ if $i < k$ and $e_{k,1}$,

are the edges of H_k, then $e_{i,j}$ is also an edge of S where $j \neq i+1$ and this is for all $3 < k < N$ that must meet the previous condition.

From the above, it can be inferred that the number of subgraphs that do not appear in the transition diagrams increases with the dimension N which is done next. On the one hand, by construction, the complete graph K_N has the following number of forks in dimension N:

$$\begin{aligned} |F^4| &= \binom{4}{1}, \\ |F^N| &= |F^{N-1}|\binom{N}{4}2^{(N-4)(N-1)-\sharp E(K_{N-4})}, \end{aligned}$$

where $N > 4$.

On the other hand, by construction too, the complete graph K_N has the following number of m-holes in dimension N:

$$\begin{aligned} |H_m^N| &= |H_m^m|\binom{N}{m}2^{(N-m)(N-1)-\sharp E(K_{N-m})}, \\ |H_N^N| &= \frac{(N-1)!}{2}, \end{aligned}$$

where $3 < m \leq N$.

The set of the forks F^N and the set of the holes H_m^N are not disjoint, then, for the number of feasible graphs in dimension N (without considering any symmetry), $\mathscr{G}_N$, there is an upper bound:

$$|\mathscr{G}_N| \geq 2^{\sharp E(K_N)} - \left(\sum_{i=4}^{N}\left(|F^N| + |H_i^N|\right)\right).$$

The important fact to highlight in this section is that not all the subgraphs of the complete graph K_N, when the dimension is greater than 3, are feasible for some initial condition, therefore, establish how many states its transition diagram has is not a trivial problem, which could be calculated exactly in Section 4.1.1, when a symmetry is considered, but which can be extended to the whole graph.

4.1.3 Paths towards synchronization

In this section, the paths towards synchronization of the Laplacian system applied to the complete graph of dimension N are studied, from the coding established in

Section 4.1.1. To begin with, a simplification of the initial conditions in $\mathbb{R}^N$ to a set that faithfully represents the behavior of the space is made. Then, the conditions that the increasing functions must fulfill, so they can be consecutive to form a path towards synchronization are mentioned. Two concepts are conceived: an admissible path and a realizable path, the differences between them are mentioned and the conditions that an admissible path must meet to become a realizable one. In addition, concrete examples for dimensions three and four are presented. In general, bounds and computational calculations for the first nine dimensions of the number of paths towards synchronization $L(M_{K_N})$ transition diagram are presented. Finally, two types of distributions associated to path lengths and the degrees in the transition diagram of are shown.

As mentioned above in Section 4.1.1, the switching times $t_1 < t_2 < \cdots < t_\ell$ are completely determined by the increments $x_n - x_m$, with $m < n$. A path associated with an initial condition that satisfies that all those increments are different from zero and pairwise different is called *typical*. Clearly, the non-typical paths correspond to initial conditions in a set of zero Lebesgue measure in $\mathbb{R}^N$.

By this assumption, from the example shown in Figure 2.22 (which shows the transition diagram of the Laplacian system over the complete graph K_3 with all its symmetries and steps), can be replaced considering the diagram shown in Figure 4.6. If all increments are different, then there are no jumps larger than one level in the transition diagram of $L(M_{K_3})$. This is an easier diagram to read and that continues to represent all the dynamics of space, except in a set of zero Lebesgue measure (which considers for example, the initial conditions that have one or several equal coordinates).

To recapitulate, a path to synchronization will be, in this context, a succession of increasing functions. For typical paths, below how are two consecutive functions in the sequence is presented.

The sequence:

$$(\phi_0, \phi_1, \ldots, \phi_\ell) := (\phi_x, \phi_{x(t_1)}, \ldots, \phi_{x(t_\ell)}),$$

is such that ϕ_i and ϕ_{i+1} for all $i = 0, ..., \ell - 1$, differ at a single point. If it is denoted by $\delta_n \in \{0, 1\}$ the *characteristic function* of the singleton $\{n\}$, hence $\phi_{\tau+1} = \phi_\tau + \delta_{n_\tau}$ for some $n_\tau \in \{1, 2, \ldots, N\}$ satisfying the condition $\phi_\tau(n_\tau) < \phi_\tau(n_\tau + 1)$.

Therefore, an *admissible sequence* $(\phi_0, \phi_1, \ldots, \phi_\ell)$, can be obtained by choosing a valid initial function $\phi_0 \in \Phi_N$, then for each $\tau \geq 0$, a point $n_\tau \in \{1, 2, \ldots, N-1\}$ such that:

$$\phi_\tau(n_\tau) < \phi_\tau(n_\tau + 1),$$

to update:

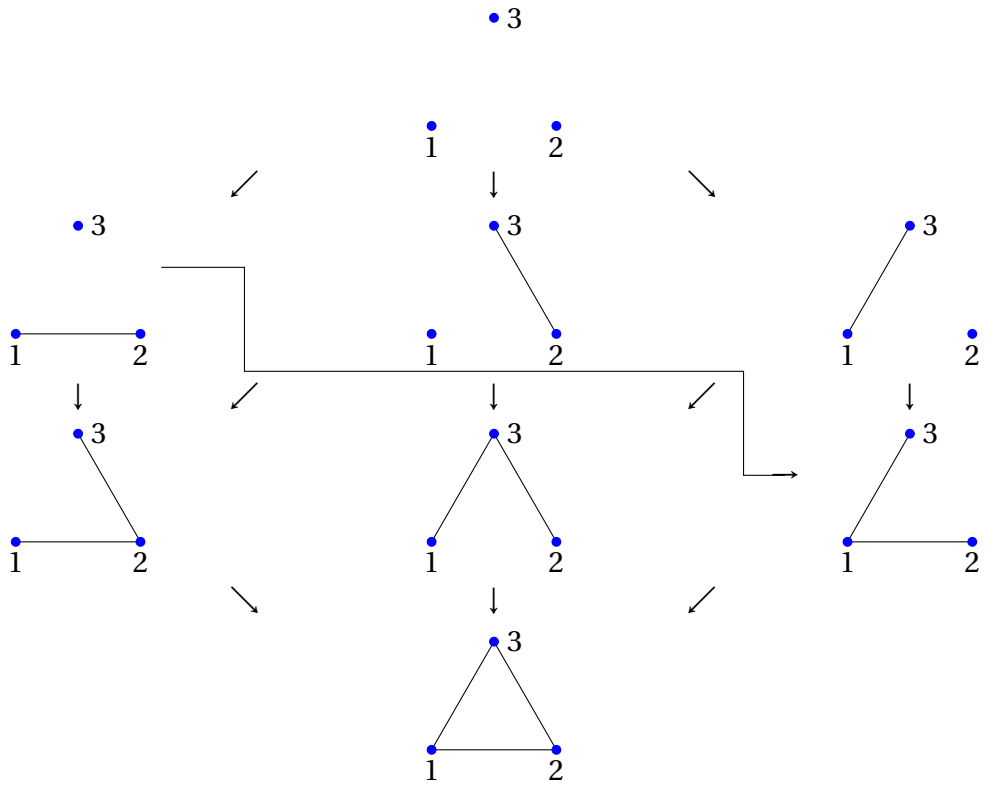

Figure 4.6 – Transition diagram of the Laplacian system in K_3 for typical initial conditions. When considering typical three-dimensional initial conditions, that is, all its coordinates are different and the differences between them are also not repeated. Under Laplacian flow the transition diagram shown here is generated.

$$\phi_{\tau+1} = \phi_\tau + \delta_{n_\tau}.$$

Nevertheless, not all the sequences obtained in this way are realizable as synchronizing sequences. The sequence $(n_\tau)_{0\leq\tau<\ell}$ of jump sites is determined based on the ordering of the increments:

$$\Delta := \{\Delta_{n,k} := x_{n+k} - x_n : 1 \leq n < n+k \leq N\},$$

such that the τ-th smallest increment in Δ corresponds to $\Delta_{n_\tau,k}$.

On the other hand, continuing with the example of the Laplacian system in the complete graph of dimension 3, considering the initial conditions $x = (x_1, x_2, x_3) \in \mathbb{R}^3$ such that $x_1 < x_2 < x_3$, and all the differences $|x_i - x_j|$ for all i, j and $i \neq j$, are different from zero and pairwise different. Also, considering the coding in Figure 4.3 (where the assignment of increasing functions to subgraphs of K_N is presented), then, in Fig-

ure 4.7 the transition diagram with the corresponding vertices labeled with increasing functions is depicted. This diagram converts Figure 4.6, into a simpler one, which preserves its properties (for example, the length of the longest path and the diversity of paths is given by the geometry of K_N).

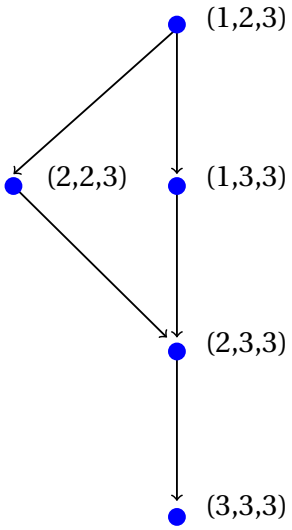

Figure 4.7 – Transition diagram of $L(M_{K_3})$ with labels assigned by the corresponding increasing functions is shown. This is composed of 5 vertices and 5 edges. At the top the vertex $(1,2,3)$, corresponds to the totally disconnected graph of dimension 3. At the bottom, the vertex $(3,3,3)$, corresponds to the complete graph of dimension 3 K_3. This transition diagram corresponds to the typical ordered initial conditions $x = (x_1, x_2, x_3) \in \mathbb{R}^3$ such that $x_1 < x_2 < x_3$. The symmetries in Figure 4.6, no longer appear.

When $L(M_{K_3})$ is considered over typical initial conditions, there are only 2 possible orders, which are the following:

$$\Delta_{1,1} < \Delta_{1,2} < \Delta_{2,1},$$
$$\Delta_{1,2} < \Delta_{1,1} < \Delta_{2,1}.$$

These two possible orders correspond to the following paths in terms of increasing functions shown in Figure 4.7, which start with the increasing function $(1,2,3)$ which corresponds to the fully disconnected graph of dimension 3, and end with $(3,3,3)$ which corresponds to the complete graph of dimension 3.

(1,2,3,4)	(1,2,3,4)
(2,2,3,4)	(2,2,3,4)
(2,3,3,4)	(2,3,3,4)
(2,3,4,4)	(2,3,4,4)
(2,4,4,4)	(3,3,4,4)
(3,4,4,4)	(3,4,4,4)
(4,4,4,4)	(4,4,4,4)

Table 4.1 – Example of an admissible path and a realizable path in the $L(M_{K_4})$ transition diagram as increasing functions. In each line, the increasing function associated to each subgraph in Figure 4.8 are shown. In the first column for (a) and in the second column for (b).

$$(1,2,3) \to (2,2,3) \to (2,3,3) \to (3,3,3),$$
$$(1,2,3) \to (1,3,3) \to (2,3,3) \to (3,3,3).$$

Therefore, it is observed that to each valid strict ordering in Δ corresponds a unique realizable path towards synchronization.

It should be noted that for the construction of the paths towards synchronization, it is not only required that one graph be a subgraph of another for there to be an edge in the transition diagram (as one might think from Figure 2.22). The following example which illustrates the differences between an *admissible path* and a *realizable path* in the $L(M_{K_4})$ transition diagram is shown. In Figure 4.8, each row represents a subgraph of K_4 in their linear form (which are not numbered, but the labels from left to right from 1 to 4 for each of them are considered) and each blue arrow represents an edge in the transition diagram of $L(M_{K_4})$, which satisfy that the graph from which the arrow leaves is a subgraph of the one it enters. The problem in (b) is step 4, because when the sequence of the first three steps is followed, the last 3 are already determined, and it does not coincide with those described in the figure. Step 4 should join (from left to right) the first vertex with the third and the third with the fourth as in Figure 4.8. In this way, there are a realizable path as in (a). Moreover, in the Table 4.1 the increasing functions associated to the subgraphs that are showed in Figure 4.8 are written and these two successions of increasing functions are the paths to synchronization.

On the one hand, the total number of admissible paths towards synchronization for $L(M_{K_4})$ is sixteen, and all of them are shown below, each letter in parentheses is the one assigned in Figure 4.4.

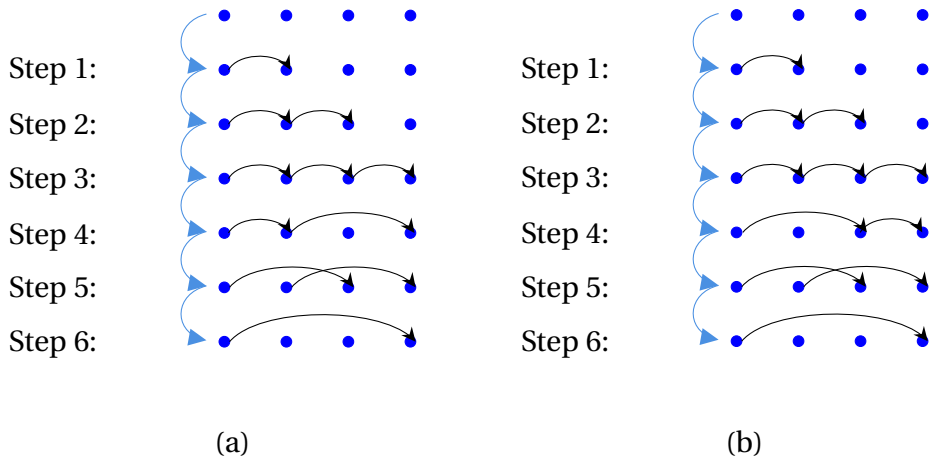

Figure 4.8 – Example of an admissible path and a realizable path in the $L(M_{K_4})$ transition diagram. In (a) and (b) two paths towards synchronization in a set of four elements over the Laplacian of the complete graph are shown. In (a), the path shown is admissible because it is a sequence of feasible subgraphs of K_4. On the other hand, in (b), a realizable path is shown, in addition to being an admissible path, the succession of the edges that are presented follow a coherent logic to an initial condition that exists. The problem in (b) is step 4, because when the sequence of the first three steps is followed, the last 3 are already determined, and it does not coincide with those described in the figure. Step 4 should join (from left to right) the first vertex with the third and the third with the fourth.

$((a),(f),(h),(k),(l),(m),(n))$	$((a),(f),(h),(i),(l),(m),(n))$
$((a),(f),(h),(i),(j),(m),(n))$	$((a),(f),(g),(i),(l),(m),(n))$
$((a),(f),(g),(i),(j),(m),(n))$	$((a),(c),(h),(k),(l),(m),(n))$
$((a),(c),(h),(i),(l),(m),(n))$	$((a),(c),(h),(i),(j),(m),(n))$
$((a),(c),(d),(i),(l),(m),(n))$	$((a),(c),(d),(i),(j),(m),(n))$
$((a),(c),(d),(e),(j),(m),(n))$	$((a),(b),(g),(i),(l),(m),(n))$
$((a),(b),(g),(i),(j),(m),(n))$	$((a),(b),(d),(i),(l),(m),(n))$
$((a),(b),(d),(i),(j),(m),(n))$	$((a),(b),(d),(e),(j),(m),(n))$

On the other hand, the total number of admissible paths towards synchronization for $L(M_{K_N})$ is ten and the associated valid strict orderings are shown in Table 4.2.

Each ordering uniquely determines an observable path towards synchronization in the transition diagram of $L(M_{K_4})$, and all of them are organized in a transition

$\Delta_{1,1} < \Delta_{2,1} < \Delta_{3,1} < \Delta_{1,2} < \Delta_{2,2} < \Delta_{1,3}$	$\Delta_{1,1} < \Delta_{2,1} < \Delta_{1,2} < \Delta_{3,1} < \Delta_{2,2} < \Delta_{1,3}$
$\Delta_{1,1} < \Delta_{3,1} < \Delta_{2,1} < \Delta_{1,2} < \Delta_{2,2} < \Delta_{1,3}$	$\Delta_{2,1} < \Delta_{1,1} < \Delta_{3,1} < \Delta_{1,2} < \Delta_{2,2} < \Delta_{1,3}$
$\Delta_{2,1} < \Delta_{1,1} < \Delta_{1,2} < \Delta_{3,1} < \Delta_{2,2} < \Delta_{1,3}$	$\Delta_{2,1} < \Delta_{3,1} < \Delta_{1,1} < \Delta_{2,2} < \Delta_{1,2} < \Delta_{1,3}$
$\Delta_{2,1} < \Delta_{3,1} < \Delta_{2,2} < \Delta_{1,1} < \Delta_{1,2} < \Delta_{1,3}$	$\Delta_{3,1} < \Delta_{1,1} < \Delta_{2,1} < \Delta_{2,2} < \Delta_{1,2} < \Delta_{1,3}$
$\Delta_{3,1} < \Delta_{2,1} < \Delta_{1,1} < \Delta_{2,2} < \Delta_{1,2} < \Delta_{1,3}$	$\Delta_{3,1} < \Delta_{2,1} < \Delta_{2,2} < \Delta_{1,1} < \Delta_{1,2} < \Delta_{1,3}$

Table 4.2 – The ten different orderings of the increments for the typical initial conditions in $\mathbb{R}^4$.

diagram depicted in Figure 4.9. As has been said before, the ϵ-synchronized subnetworks are encoded by increasing functions as defined by Equation (4.4) and depicted in Figure 4.4. At the top is placed the identity function $(1,2,3,4)$ which codifies the completely disconnected graph. All the paths towards synchronization end at the constant function $(4,4,4,4)$ which codifies the globally synchronized state.

In a general way, the path towards synchronization for the initial condition $x \in \mathbb{R}^N$ is given by the sequence $(G_x, G_{x(t_1)}, \ldots, G_{x(t_\ell)})$ of ϵ-synchronizing subnetwork, which is equivalent to a sequence of increasing functions:

$$(\phi_x, \phi_{x(t_1)}, \ldots, \phi_{x(t_\ell)}) \subset \Phi_N.$$

This sequence $(\phi_x, \phi_{x(t_1)}, \ldots, \phi_{x(t_\ell)})$ is completely determined by the order of the increments Δ. Each ordering of increments determines the sequence $(n_\tau)_{0\leq\tau<\ell}$ of sites where consecutive increasing functions differ, that is, the sites n_τ such that $\phi_{x(t_{\tau+1})} - \phi_{x(t_\tau)} = \delta_{n_\tau}$ for each $0 \leq \tau < \ell$. Therefore, each valid ordering in Δ corresponds to a unique realizable path towards synchronization.

As a result, the total number of paths towards synchronization is determined by the number of distinct orderings of Δ that can be obtained from an ordered initial condition $x \in \mathbb{R}^N$. Interestingly, this combinatorial problem is closely related to the concept of "Golomb rulers" in mathematics Golomb 1972. Counting the number of valid orders is equivalent to counting the combinatorially distinct Golomb rulers. Now, let's explain how this equivalence is established.

As mentioned in Section 2.1.5, A Golomb ruler with N marks is defined as a vector $a \in \mathbb{Z}^N$ with $a_1 < a_2 < \cdots < a_N$, where no two increments $a_{n+k} - a_n$, with $1 \leq n < N$ and $1 \leq k \leq N-n$, are equal. In essence, a Golomb ruler represents a specific type of initial condition characterized by integer entries which we call: *typical*. Interestingly, a Golomb ruler can be associated with each typical initial condition $x \in \mathbb{R}^N$ using the following procedure. Since x is typical, then both $\epsilon_1 = \min\{\Delta_{n,k} : 1 \leq n < N, 1 \leq k < N-n\}$ and $\epsilon_2 = \min\{|\Delta_{n,k} - \Delta_{m,\ell}| : (m,k) \neq (n,\ell) : 1 \leq n < N, 1 \leq k < N-n, 1 \leq m < N, 1 \leq \ell < N-m\}$ are strictly positive. Let $p \in \mathbb{N}$ be such that $p \cdot \min(\epsilon_1, \epsilon_2/4) > 1$, and for each $1 \leq n \leq N$ let $q_n := \max\{q \in \mathbb{Z} : q/p \leq x_n\}$. The vector $q = (q_1, q_2, \ldots, q_N) \in \mathbb{Z}^N$ represents the desired Golomb ruler. Indeed, since $p\epsilon_1 > 1$, then for each $1 \leq n < N$,

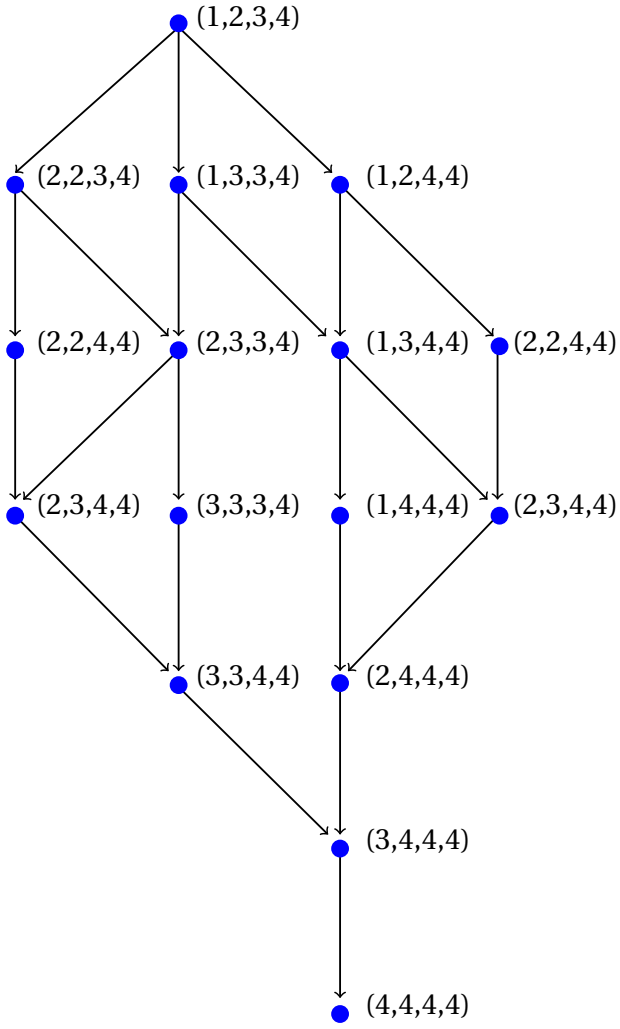

Figure 4.9 – Transition diagram of $L(M_{K_4})$ with labels assigned by the corresponding increasing functions is shown. This is composed of 16 vertices and 22 edges. At the top, the vertex $(1,2,3,4)$ corresponds to the totally disconnected graph of dimension 4, and at the bottom, the vertex $(4,4,4,4)$ corresponds to the complete graph of dimension 4 K_4. This transition diagram corresponds to the ordered initial conditions $x = (x_1, x_2, x_3, x_4) \in \mathbb{R}^4$ such that $x_1 < x_2 < x_3 < x_4$, then, the other symmetries no longer appear.

then

$$q_n \leq p\, x_n \leq p\,(x_{n+1} - \epsilon_1) \leq q_{n+1} + 1 - p\,\epsilon_1 < q_{n+1}.$$

On the other hand, if $\Delta_{n,k} > \Delta_{m,\ell}$, then the following condition holds:

$$(q_{n+k} - q_n) - (q_{m+\ell} - q_m) \geq p(\Delta_{n,k} - \Delta_{m,\ell} - 4/p) > p(\epsilon_2 - 4/p) > 0.$$

Furthermore, two Golomb rulers are considered combinatorially equivalent if they yield the same ordering in their differences. In other words, for $a, b \in \mathbb{R}^N$, the rulers are equivalent if and only if the inequality $((a_{n+k} - a_n) - (a_{m+\ell} - a_m))((b_{n+k} - b_n) - (b_{m+\ell} - b_m)) > 0$ holds for every $1 \leq m, n < N$ and $1 \leq k < n, , 1 \leq \ell < m$. Consequently, the number Golomb(N) of equivalence classes of Golomb rulers with N marks corresponds to the number of paths towards synchronization. Therefore, the following relationship is established:

$$\text{Number of paths towards synchronization for } K_N = \text{Golomb}(N). \tag{4.28}$$

The growth of the number of paths towards synchronization with the dimension N grows, can be seen as a measure of complexity like the topological complexity Farber 2003 of discrete-time dynamical systems. In this scenario, the topological complexity measures the increase in the number of distinguishable trajectories over time. However, in the case of Golomb(N), it counts the number of distinguishable paths towards synchronization as a function of the system's dimension rather than time.

Additionally, a Golomb ruler $a \in \mathbb{Z}$ is characterized by the property that all the sums $a_m + a_n$ are distinct. This can be observed from the fact that:

$$\text{sign}((a_{n+k} - a_n) - (a_{m+\ell} - a_m)) = \text{sign}((a_{n+k} + a_m) - (a_{m+\ell} + a_n)),$$

the number of combinatorially different Golomb rules can be determined by counting the different orderings of the set $S = a_m + a_n : 1 \leq m < n \leq N$. Interestingly, this is equivalent to counting the different orderings of the set $P = a_m, a_n : 1 \leq m < n \leq N$.Now count the number of possible orders of all pairwise sums $\{a_i + a_j\}_{1 \leq i \leq j \leq n}$ such that the ordered set $A = \{a_1, a_2, ..., a_n\} \subset \mathbb{N}$ is a finite Sidon set, as an adaptation of Johnston 2014b upper bound.

Let's generate a matrix $M_N \in \mathscr{M}(\mathbb{N})_{N \times N}$ such that each (i, j)-element is $a_i + a_j$. For instance, when $N = 5$, there is the following symmetric matrix:

$$M_5 = \begin{pmatrix} 2a_1 & a_1 + a_2 & a_1 + a_3 & a_1 + a_4 & a_1 + a_5 \\ a_2 + a_1 & 2a_2 & a_2 + a_3 & a_2 + a_4 & a_2 + a_5 \\ a_3 + a_1 & a_3 + a_2 & 2a_3 & a_3 + a_4 & a_3 + a_5 \\ a_4 + a_1 & a_4 + a_2 & a_4 + a_3 & 2a_4 & a_4 + a_5 \\ a_5 + a_1 & a_5 + a_2 & a_5 + a_3 & a_5 + a_4 & 2a_5 \end{pmatrix}.$$

As $a_1 < a_2 < \cdots < a_N$, then the rows and columns of the upper-triangular part of M_5 are increasing. And in this way, an upper bound can be given by counting the number of ways that the numbers $1, 2, ..., N(N+1)/2$, can be accommodated in $N(N+1)/2$ places in the upper-triangular part of a matrix such that the rows and columns of that upper-triangular part are increasing by Thrall bound in Thrall 1952,

$$\sharp\text{Paths towards sync in } L(M_{K_N}) \leq \left(\frac{N(N+1)}{2}\right)! \frac{\prod_{i=1}^{N-1} i!}{\prod_{i=1}^{N}(2i-1)!}, \tag{4.29}$$

which furnishes an upper bound for the number of paths towards synchronization as well.

Since the finite Sidon sets and the Golomb rulers are related, then this bound also works for the number of paths to synchronization. The number Golomb(N) holds significance in the study of quantum entanglement Hildebrand 2007. It is listed in the On-line Encyclopedia of Integer Sequences (OEIS) under the entry A237749 Johnston 2014a, where the first nine terms are explicitly computed and presented in Table 1 (see Table 4.3). For dimensions 3 and 4, they coincide with the number of paths that are presented previously.

N	Golomb(N)
1	1
2	1
3	2
4	10
5	114
6	2608
7	107498
8	7325650
9	771505180

Table 4.3 – Number of classes of Golomb rulers.

On the other hand, finding a closed formula for Golomb(N) remains an unsolved problem. However, we can establish quick and demonstrable bounds for this number, as shown in Equation (4.30). The lower bound can be obtained by considering all possible orderings of the first differences $x_{i+1} - x_i$ for $1 \leq i \leq N-1$, while the upper bound arises from considering all possible orderings of the differences $x_i - x_k$ for $1 \leq k < i \leq N$. Thus, we obtain:

$$(N-1)! < \text{Golomb}(N) < \binom{N}{2}!. \tag{4.30}$$

Based on the established concepts, various characteristics can be calculated, including the number of ϵ-synchronized sequences with a fixed length ℓ and the distribution of path lengths in the synchronization process. These calculations enable us to determine the mean length and the most common length of the paths. Furthermore, by examining the behavior of these quantities as the dimension increases, we can extrapolate their trends for larger dimensions.

In all the examples, the transition diagram for $L(M_{K_N})$ exhibits a hierarchical structure. At the top of the hierarchy, there is a disconnected subnetwork represented by the identity function $\mathrm{Id} = (1,2,...,N) \in \Phi_N$. At the bottom of the hierarchy, there is a complete graph represented by the constant function $\mathbf{N}(n) = N$ for $1 \leq n \leq N$. Only typical initial conditions are considered, and at each step, only one new edge appears in the ϵ-synchronized subnetwork.

Each level of the hierarchy, starting from the top and counting down, represents the subnetworks that can be reached from the disconnected subnetwork after exactly ℓ steps. These subnetworks have precisely ℓ edges and are encoded by increasing functions $\phi \in \Phi_N$ that satisfy the following condition:

$$\sum_{n=1}^{N} (\phi(n) - n) = \ell.$$

In particular, the maximal length of a synchronizing sequence is given by:

$$\begin{aligned} l_{\max} &= \sum_{n=1}^{N} (N-n), \\ &= N(N-1)/2. \end{aligned}$$

From the previous observations, it follows that the number $F_N(\ell)$ of synchronized sequences of length ℓ is given by the number of Dyck paths of order N with length $2N$ and area $N^2 - \ell$. In other words, we have:

$$F_N(\ell) := \left| \left\{ \phi \in \Phi_N : \sum_{n=1}^{N} \phi(n) = N^2 - \ell \right\} \right|. \tag{4.31}$$

These quantities can be computed from the following generating polynomials:

$$\begin{aligned} P_N(t) &:= \sum_{\phi \in \Phi_N} t^{\,\mathrm{area}(\phi)}, \\ &= \sum_{\ell=0}^{\frac{N(N-1)}{2}} F_N(\ell)\, t^{\frac{N(N-1)}{2} - \ell}, \end{aligned}$$

where $\mathrm{area}(\phi) := \sum_{n=1}^{N} (\phi(n) - n)$ denotes the area under the Dyck path determined by the increasing function ϕ. The generating polynomials mentioned above can be determined using the recurrence relation:

$$P_N(t) = \sum_{n=0}^{N-1} t^n\, P_n(t)\, P_{N-n-1}(t) \tag{4.32}$$

with initial condition $P_0 = 0$, derived in Carlitz and Riordan 1964 (see Blanco and

Petersen 2012 as well, that is a more recent work). Although there is no closed formula for $F_N(\ell)$, the recurrence relation above allows to directly compute these distributions and it can be also established its asymptotic behavior. In the following Table 4.4 $F_N(\ell)$ for some values, that are $2 \leq N \leq 8$ are shown.

N	$F_N(\ell)$
2	(1,1)
3	(1,1,2,1)
4	(1,1,2,3,3,3,1)
5	(1,1,2,3,5,5,7,7,6,4,1)
6	(1,1,2,3,5,7,9,11,14,16,16,17, 14,10,5,1)
7	(1,1,2,3,5,7,11,13,18,22,28,32,37,40,44,43,40,35,25,15,6,1)
8	(1,1,2,3,5,7,11,15,20,26,34,42,53,63,73,85,96,106,113,118,118,115,102,86,65,41,21,7,1)

Table 4.4 – Number $F_N(\ell)$ of functions $\phi \in \Phi_N$ codifying a ϵ-synchronizing subnetworks starting a synchronizing path of length ℓ.

On the other hand, the normalized cumulative distribution, $f_N : [0,1] \to [0,1]$, is defined by:

$$f_N(x) = \frac{1}{C_N} \sum_{n \leq x \times N(N-1)/2} F_N(x), \tag{4.33}$$

where F_N is given by Equation (4.31) and C_N is the N-th Catalan number previously defined. By using the recurrence shown in Equation (4.32), there are numerically computed $f_N(x)$ for increasing values of N, and observe that f_N approaches an absolutely continuous limit distribution $x \mapsto f(x)$ whose density written as $\rho(x) := d\,f(x)/dx$ is closely approached by the curve shown in Figure 4.10. Hence, for N sufficiently large and $\delta > 0$ sufficiently small, the proportion of paths towards synchronization of length $N(N-1)(x \pm \delta)/2$ is approximatively $\rho(x)\,\delta$. As shown in the Figure 4.10, the numerical computation suggests that the function ρ is continuous, unimodal, and negatively skewed.

Recapping, the transition diagram for $L(M_{K_N})$ is composed by levels:

$$\mathrm{L}_0,\ \mathrm{L}_1, \ldots,\ \mathrm{L}_{\frac{N(N-1)}{2}},$$

in such a way that each path towards synchronization passes through levels of increasing index until reaching level $N(N-1)/2$ which is composed solely of the complete graph K_N, representing the full ϵ-synchronization. Besides, a typical initial condition starting at L_n, will take $N(N-1)/2 - n$ steps to attain the complete graph. Furthermore, the number of subnetworks at level $n = N(N-1)/2 - \ell$ is given by $F_N(\ell)$, defined by Equation (4.31). Then, the number of ϵ-synchronized subnetworks at each level increases monotonously from 1 to the following expression:

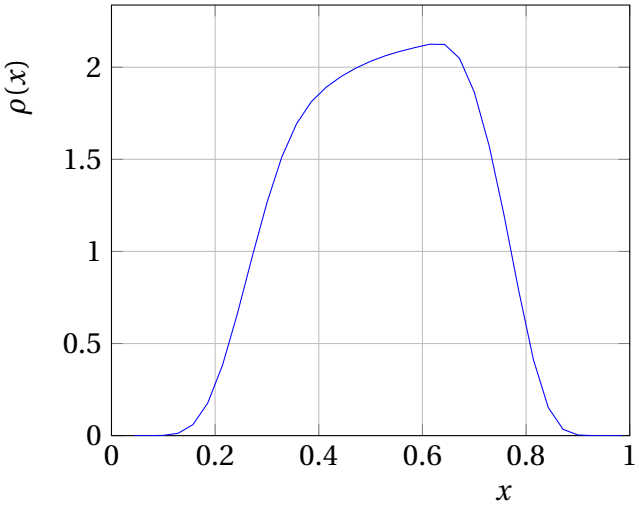

Figure 4.10 – Probability density function $\rho(x)$ of the normalized length asymptotic distribution of a path towards synchronization in the $L(M_{K_N})$ transition diagram.

$$\begin{aligned} \text{mode}_N(\ell) &:= \max_{1\leq\ell\leq N(N-1)/2} F_N(\ell), \\ &\approx 0.632\,\frac{N(N-1)}{2}, \end{aligned} \tag{4.34}$$

and then decreases monotonically to 1 as shown in Figure 4.10. Therefore, since the distribution of these path lengths is negatively skewed, the mean length of the paths towards synchronization is smaller than the most frequent length. Thus, we can conclude that:

$$\begin{aligned} \langle\ell\rangle_N &:= \frac{\sum_{\ell=1}^{N(N-1)/2} \ell\, F_N(\ell)}{C_N}, \\ &\approx 0.523\,\frac{N(N-1)}{2}, \\ &< \text{mode}_N(\ell). \end{aligned}$$

From the calculations shown in this section, an idea of some characteristics of a typical synchronization path in the Laplacian system of the complete graph K_N can be obtained, for example, if a random ordered initial condition $x \in \mathbb{R}^N$ is taken, then its associated synchronization path would most likely be of length as in Equation (4.34).

In addition, under the approach of increasing functions, the degree distributions for the $L(M_{K_N})$ transition diagram are given by the Narayana triangle described by the

Equation (2.26) read by lines. In the OEIS sequence A001263 it is also defined.

By setting the dimension $N = 100$, the following histogram shown in Figure 4.11 it is generated which is unimodal and symmetric.

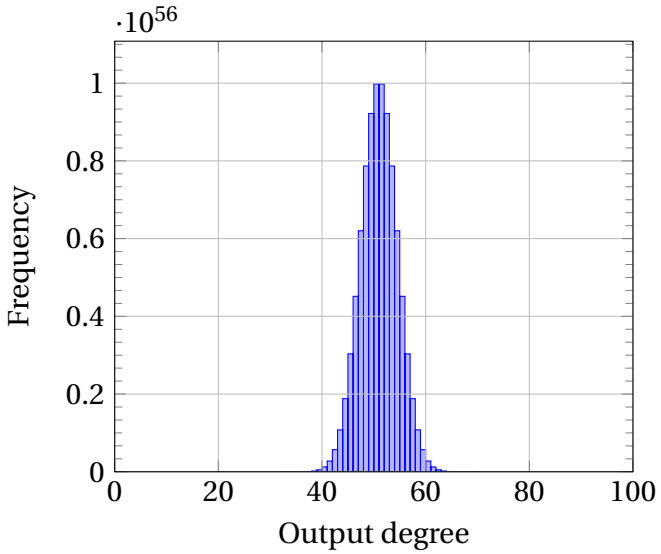

Figure 4.11 – $L(M_{K_{100}})$ transition diagram degree distribution. The degree distribution for the $L(M_{K_N})$ transition diagram, is given by the Narayana triangle described by the Equation (2.26) read by lines, in this case, when $N = 100$ the distribution is shown.

As a conclusion of this section, there are two different types of paths that can be generated from sequences of increasing functions that satisfy that are greater than another by one unit at a single coordinate value. When they only meet this condition are called admissible paths, moreover, when they satisfied a specific order dictated by the differences between the coordinates then, they are realizable paths. This is a famous problem equivalent to compute the number of combinatorially distinct Golomb rulers, for which there is no closed formula, and it seems to be a NP-hard problem. Despite of this, bounds of its growth with respect to the dimension N can still be given. On the other hand, it is shown that the longest path that can be found in the transition diagram of $L(M_{K_N})$ precisely matches the number of edges of K_N. Furthermore, the number of paths towards synchronization of size ℓ is given by the number of Dyck paths of order N with length $2N$ and area $N^2 - \ell$, which its probability density function for N sufficiently large is given, and from which the behavior for the mode and the mean path length is obtained. Finally, the degree distribution of the transition diagram of $L(M_{K_N})$ is given by the lines of the Narayana triangle. Once again, the coding done through the increasing functions allow to formally describe the behavior of this transition diagram.

4.1.4 Discussion

In this section it is formally and rigorously analyzed the behavior of the transition diagram of the Laplacian system applied to the complete graph of dimension N. To achieve this objective, a coding of the subgraphs of K_N was proposed, which preserves the dynamics of the system and turns out to be very useful because it transforms it into a combinatorial problem that has been widely studied before.

One of the advantages of using this coding is that it automatically generates the subgraphs that are feasible for a set of initial conditions. Despite of this, it was considered pertinent to give the two conditions that a subgraph of K_N must meet to be feasible by an initial condition, the first is that it must not strictly contain forks or 3-stars and the second is that it must not induce holes or C_k for $k \geq 4$, this with the aim of giving an idea of how many states that could be thought to be feasible for K_N actually are not.

Moreover, two key simplifications are made for the analytical study of the transition diagram of $L(M_{K_N})$. The first is when defining the coding of the subgraphs that are formed from initial conditions, whose coordinates are in strictly increasing order, then, that the set of associated ϵ-synchronized subnetworks have a bijection with the set of increasing functions. This simplification allows to focus the attention on the diversity of states generated by considering a single symmetry of the complete graph. On the other hand, the second simplification made in this section is when the typical initial conditions in the space $\mathbb{R}^N$ are considered, that is, when the differences between the coordinates are different from zero and pairwise different. This type of initial conditions faithfully represents space, because for example, if they were generated randomly, on the one hand, the probability of finding an initial condition with two or more exactly equal coordinates is zero, and on the other hand, the probability that two differences of the coordinates coincide is also zero. Typical initial conditions generate typical paths, which are the ones with the longest lengths, that is, if they start forming the totally disconnected subgraph, then they will reach synchronization in $N(N-1)/2$ steps.

By considering these two simplifications in the space of initial conditions, it is possible to establish the two rules by which two increasing functions will be consecutive on a path towards synchronization. The first is that an increasing function will follow another if they differ by only one coordinate and only by one unit. From this condition admissible paths are generated. The second condition is that the sequence of increasing functions must correspond to a specific order of the increments of a typical initial condition. This second condition generates feasible paths.

The problem of counting how many realizable paths there are in each dimension is equivalent to counting the number of combinatorially distinct Golomb rulers, which

is a famous open problem, for which some analytical and numerical bounds have been provided. Furthermore, the number of combinatorially distinct Golomb rulers has only been possible to calculate up to dimension nine, due to the great memory demand that the computation of the Golomb rulers requires.

To end this discussion, it should be noted that having this coding allow to associate characteristics of the combinatorial objects that have a relevant meaning in terms of the study of the transition diagram, which are listed below.

Combinatorial concept	**Transition diagram property**
Catalan number	Possible states
Combinatorially different Golomb rulers	Number of paths towards synchronization
Number of Dyck paths of order N and area $N^2 - \ell$	Number of synchronized sequences of length ℓ
N-th line of Narayana triangle	Degree distribution of $L(M_{K_N})$

4.2 The transition diagram of $L(M_{K_{N,N}})$

In this section it is formally and rigorously analyzed the behavior of the transition diagram of the Laplacian system applied to the complete bipartite graph of dimension N. This study is organized as follows: to begin with, the coding used to describe the states and the paths towards synchronization are presented, which respects the monotonic dynamics of the system. Then, the unfeasible subgraphs that the complete bipartite graph has been shown, which imply the states that cannot have the initial conditions in the transition diagram. Finally, the way to generate the paths to synchronization in the Laplacian flow over the complete bipartite graph, an estimation of the diversity of paths and their distribution are exposed.

4.2.1 Coding

The coding of the subgraphs of the complete bipartite graph and the monotonic dynamics that follow on their path to synchronization was carried out taking advantage for the subset of the space for which the differences of the flow of the coordinates monotonically tend to zero, the following shows how this process occurs. It is recalled that the Laplacian matrix of corresponding to $K_{N,N}$ has the following entries

$$L(i,j) = \begin{cases} 1, & \text{if } N < i \leq 2N \text{ and } 0 < j \leq N \\ & \text{or } N < j \leq 2N \text{ and } 0 < i \leq N, \\ -N, & \text{if } i = j,\ 1 \leq i, j \leq 2N, \\ 0, & \text{otherwise.} \end{cases}$$

As it was said in Section 2.1.2, an eigenbasis can be computed in terms of the canonical basis of $\mathbb{R}^{2N}$ and written as the set:

$$\mathscr{B} = \{u^m, v^n, w^n :\ 1 \leq m \leq 2,\ 1 \leq n \leq N-1\}.$$

Where:

$$\begin{aligned} u^1 &= \sum_{k=1}^{2N} \mathrm{e}^k, \\ u^2 &= \sum_{k=1}^{N} (\mathrm{e}^k - \mathrm{e}^{k+N}), \end{aligned}$$

and for each $n \geq 1$,

$$\begin{aligned} v^n &= \mathrm{e}^{n+1} - \mathrm{e}^1, \\ w^n &= \mathrm{e}^{N+n+1} - \mathrm{e}^{N+1}, \end{aligned}$$

In this section the Laplacian matrix of $K_{N,N}$ will be written as $L := L(M_{K_{N,N}})$. It acts on this basis as follows:

$$\begin{aligned} Lu^1 &= 0, \\ Lu^2 &= -2N\,u^2, \\ Lv^n &= -N\,v^n, \\ Lw^n &= -N\,w^N, \end{aligned}$$

for each $n = 1, 2, \ldots, N-1$.

An initial condition $x \in \mathbb{R}^{2N}$ can be decomposed as:

$$x = \bar{x}\,u^1 + (\bar{x}_1 - \bar{x})\,u^2 + \sum_{n=1}^{N-1} \left((x_{n+1} - \bar{x}_1)\,v^n + (x_{N+n+1} - \bar{x}_2)\,w^n \right).$$

Where:

$$\bar{x} := \frac{\sum_{n=1}^{2N} x_n}{2N},\ \bar{x}_1 := \frac{\sum_{n=1}^{N} x_n}{N} \text{ and } \bar{x}_2 := \frac{\sum_{n=1}^{N} x_{N+n}}{N}. \tag{4.35}$$

Therefore, for all $t \in \mathbb{R}$:

$$\begin{aligned} x(t) &= \bar{x}\,u^1 + e^{-2Nt}(\bar{x}_1 - \bar{x})\,u^2 + e^{-Nt} \sum_{n=1}^{N-1} \left((x_{n+1} - \bar{x}_1), v^n + (x_{N+n+1} - \bar{x}_2)\,w^n \right), \\ &= \sum_{n=1}^{N} \left(\left(1 - e^{-Nt}\right) \left(\bar{x} - e^{-Nt}\bar{x}_1\right) + e^{-Nt} x_n \right) \mathrm{e}^n \\ &\qquad + \sum_{n=1}^{N} \left(\left(1 - e^{-Nt}\right) \left(\bar{x} - e^{-Nt}\bar{x}_2\right) + e^{-Nt} x_{N+n} \right) \mathrm{e}^{N+n}. \end{aligned}$$

From here it follows that:

$$\begin{aligned} x_n(t) - x_{N+m}(t) &= e^{-Nt} \left(x_n - x_{N+m} + \left(1 - e^{-Nt}\right) (\bar{x}_1 - \bar{x}_2) \right), && (4.36) \\ x_n(t) - x_m(t) &= e^{-Nt} (x_n - x_m), && (4.37) \\ x_{N+n}(t) - x_{N+m}(t) &= e^{-Nt} (x_{N+n} - x_{N+m}), \end{aligned}$$

for all $t \in \mathbb{R}$ and each $1 \le m, n \le N$.

Hence, the distance between coordinates in the same part of the complete bipartite graph $K_{N,N}$ decreases monotonously, while the distances between coordinates at different parts oscillates at most once, and then decreases to zero. It is important to note that all the differences decreases monotonously if and only if the initial condition $x \in \mathbb{R}^{2N}$ satisfies $\bar{x}_1 = \bar{x}_2$. In this case, the edges (n, m) would be included in the

ϵ-synchronized subnetwork $G_{x(t)}$ for all:

$$t \geq t_{n,m} := \frac{\log|x_n - x_{N+m}| - \log(\epsilon)}{N}.$$

Without loss of generality, assume that the initial condition is ordered as $x_1 \leq x_2 \leq \cdots \leq x_N$, $x_{N+1} \leq x_{N+2} \leq \cdots \leq x_{2N}$, that is, each of its parts is ordered in an increasing way. By Equation (4.37), ensures that $x_1(t) \leq x_2(t) \leq \cdots \leq x_N(t)$ and $x_{N+1}(t) \leq x_{N+2}(t) \leq \cdots \leq x_{2N}(t)$ for all $t \in \mathbb{R}$. Also assume, when convenient, that $\bar{x}_1 = \bar{x}_2$, the initial condition $x \in \mathbb{R}^{2N}$ that satisfies this condition is called *balanced*. In Figure 4.12, in (a), an initial condition where each of the parts that make up the bipartite graph are not balanced is shown, the dashed line represents the average of both coordinates. In (b), an initial condition that is effectively balanced is shown, which are the ones that will be studied in this section.

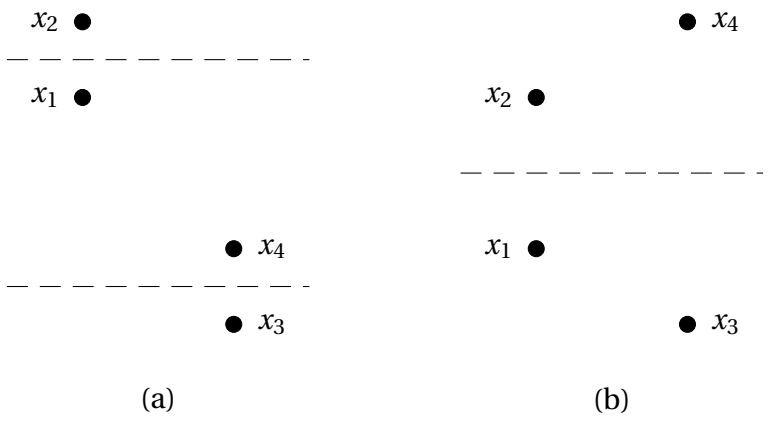

Figure 4.12 – Example of the balanced and not balanced initial conditions. In (a) and (b) examples of initial conditions in $\mathbb{R}^4$ are shown. The value varies depending on its height and are grouped by the same party that they are in $K_{2,2}$, also with dashed lines the average of each pair is drawn. In (a), it is observed that the averages of both parts are different and in (b), it is observed that both averages coincide. Initial conditions that satisfy the case shown in (b) are called balanced initial conditions.

Similarly to Section 4.1.1, in order to utilize the property that the Laplacian flow preserves the coordinate order within each component, the transition diagram is defined based on combinatorial objects that encode the ϵ-synchronized subnetworks while respecting this order. This simplifies the description of the transition diagram, especially in the case of monotonicity, which is achieved when the initial condition $x \in \mathbb{R}^{2N}$ is balanced, meaning $\bar{x}_1 = \bar{x}_2$.

In this occasion, the ϵ-synchronized subnetwork G_x defined by $x_1 \leq x_2 \leq \cdots \leq$

x_N, $x_{N+1} \leq x_{N+2} \leq \cdots \leq x_{2N}$, is encoded by the couple of functions $\alpha_x, \omega_x : \{1,2,\ldots,N\} \to \{0,1,2,\ldots,N+1\}$ given by:

$$\alpha_x(n) = \begin{cases} \min\{\ell \leq N : x_n - \epsilon \leq x_{N+\ell}\} & \text{if } x_{2N} \geq x_n - \epsilon, \\ N+1 & \text{if } x_{2N} < x_n - \epsilon, \end{cases} \tag{4.38}$$

$$\omega_x(n) = \begin{cases} \max\{\ell \leq N : x_n + \epsilon \geq x_{N+\ell}\} & \text{if } x_{N+1} \leq x_n + \epsilon, \\ 0 & \text{if } x_{N+1} > x_n + \epsilon. \end{cases} \tag{4.39}$$

It should be noted that $\text{im}(\alpha_x) \subset [1, N+1]$ while $\text{im}(\omega_x) \subset [0, N]$. Both functions are increasing and such that $\alpha_x(n) \leq \omega_x(n) + 1$ for each $1 \leq n \leq N$. An example of the construction of the increasing functions from a given initial condition is presented in Figure 4.13. Firstly in (a), an example of the relative position of the coordinates of $x = (x_1, x_2, x_3, x_4)$ for each of its parts on different sides with black dots is illustrated, the first two coordinates to the left and the last two coordinates to the right. The angles formed by the first two coordinates indicate their respective ϵ-neighborhoods. To construct the subgraph G_x, as described in Equation (4.41), it is sufficient to observe that x_3 lies within the ϵ-neighborhood of x_1, and x_4 lies within the ϵ-neighborhood of x_2. Consequently, in (b), vertices 1 and 3 are connected, as well as vertices 2 and 4. Finally, in (c), the increasing functions determined by $x \in \mathbb{R}^4$ are depicted. The first function, denoted as α_x, encodes the fact that x_3 is the first coordinate of the second part within the angle opening from x_2, and similarly for x_4 with respect to x_2. On the other hand, the second function, denoted as ω_x, indicates that x_3 is the last coordinate of the second part within the angle opening from x_1, and similarly for x_4 with respect to x_2. Therefore, the two increasing functions associated with the initial condition are built.

Now the following set of increasing functions is defined. Note that the domain of the increasing function has dimension N and the image has dimension $N+2$.

$$I_N := \{\phi : \{1,\ldots,N\} \to \{0,\ldots,N+1\} : \phi(n+1) \geq \phi(n) \text{ for all } 1 \leq n < N\}.$$

From I_N, it can be defined the following collection of pairs of increasing functions:

$$\begin{aligned} \Phi_{N,N} := \{&(\alpha,\omega) \in I_N \times I_N : \text{im}(\alpha) \subset [1, N+1], \\ &\text{im}(\omega) \subset [0, N] \text{ and } \alpha \leq \omega + 1\}, \end{aligned} \tag{4.40}$$

and it codes all the ϵ-synchronized subnetworks of $K_{N,N}$ compatible with an ordered initial conditions $x_1 \leq x_2 \leq \cdots \leq x_N$, $x_{N+1} \leq x_{N+2} \leq \cdots \leq x_{2N}$. The correspondence is given as follows: For each $(\alpha,\omega) \in \Phi_{N,N}$, the subnetwork $G_{(\alpha,\omega)} \subset K_{N,N}$ is constructed with edges in the set

$$E_{(\alpha,\omega)} = \{(n, N+m) : 1 \leq n, m \leq N, \text{ and } \alpha(n) \leq m \leq \omega(n)\}, \tag{4.41}$$

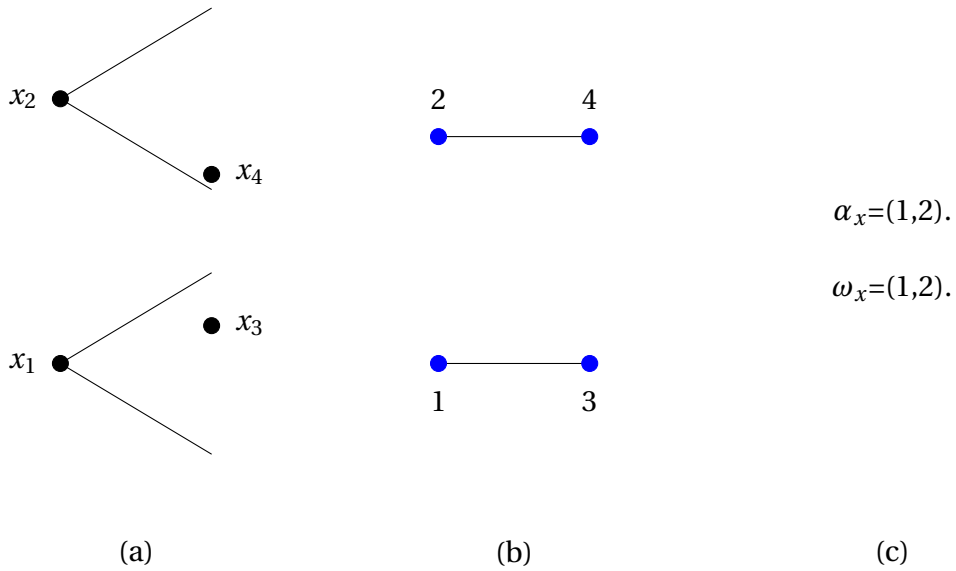

Figure 4.13 – Construction of the increasing functions α_x and ω_x from a given initial condition $x \in \mathbb{R}^4$. In (a), a representation of the values of an initial condition $x \in \mathbb{R}^4$ are shown, and these values are grouped in the same parts for their sites in $K_{2,2}$. Furthermore, at the coordinates x_1 and x_2 a fan is opened that is projected to the second group, this is to represent the ϵ-neighborhood around them, because x_1 and x_3 are within the same neighborhood. Then, in (b), an edge joining the corresponding vertices is drawn, and the same happens with the coordinates x_2 and x_4. For the construction of increasing functions in (c) it is enough to note the following: the first function α_x codified the fact that x_3 is the first coordinate of the second part inside the angle opening from x_2 and similarly x_4 with respect to x_2. On the other hand, the second function ω_x, indicates that x_3 is the last coordinate of the second part inside the angle opening from x_1 and analogously x_4 with respect to x_2.

is associated, which is consistent with the fact that $(\alpha,\omega) = (\alpha_x,\omega_x)$ if and only if $G_{(\alpha,\omega)} = G_x$. The correspondence in Equation (4.41) establishes a mapping from $\Phi_{N,N}$ to the collection of ϵ-synchronized subnetworks defined by ordered initial conditions. In other words, it is the mapping λ associated with Equation (2.29).

Each pair of increasing functions $\alpha,\omega : 1,\ldots,N \to 0,1,\ldots,N+1$ is compatible with some $x \in \mathbb{R}^{2N}$ according to Equations (4.38) and (4.39), and therefore codifies an ϵ-synchronized subnetwork, provided that $\mathrm{im}(\alpha) \subset [1,N+1]$, $\mathrm{im}(\omega) \subset [0,N]$, and $\alpha \leq \omega + 1$. This initial condition $x \in \mathbb{R}^{2N}$ can be constructed as follows.

Firstly, for each $1 \leq n \leq N$ the set:

$$\mathscr{A}_n := \{1 \leq m \leq N : \alpha(n) \leq m \leq \omega(n)\},$$

is defined. Now, the partition:

$$\{1,2,\ldots,N\} = \bigsqcup_{k=1}^{\ell} I_k,$$

where for each $1 \leq k \leq \ell$ can be written. Then, $I_k = \{n_k, n_k+1, \ldots, m_k\}$ is such that $\mathscr{A}_n \cap \mathscr{A}_{n+1} \neq \emptyset$ for each $n_k \leq n < m_k$ and it is a maximal element in the sense of inclusion ($I_k \subsetneq I \Rightarrow \bigcup_{n\in I_k} \mathscr{A}_n$ is not an interval). Note that $n_1 = 1$ and that $I_k = \{n_k\}$ whenever $\alpha(n_k) = \omega(n_k)+1$.

The next step is that for each $1 < k \leq \ell$, let $\Delta : I_k \to I_k$ be such that

$$\Delta(n) = \max\{m \in I_k : \mathscr{A}_n \cap \mathscr{A}_m \neq \emptyset\}.$$

It is easy to observe that $\Delta(n) \geq n$, and $\Delta(n) = n$ if and only if $n = n_k = m_k$. To each Δ, we can associate a directed tree T_k with vertices in I_k, rooted at m_k, and arrows given by $n \mapsto \Delta(n)$. The structure of these trees is similar to the trees described in Section 4.1 for the complete graph K_N.

Additionally, let:

$$n_k \mapsto \Delta(n_k) \mapsto \cdots \mapsto \Delta^j(n_k) \mapsto \cdots \mapsto m_k = \Delta^{h_k}(n_k),$$

be the maximal path in T_k and for each $1 \leq j \leq l_k$ let $V_j = \Delta^{-j}(\{m_k\})$ be the j-th level of T_k. Clearly:

$$\min V_j = \Delta^{h_k - j}(n_k) \text{ and } \max V_j < \min V_{j-1},$$

for each $0 \leq j \leq h_k$.

Now assume that x_{n_k} is given. It defines:

$$n_{k,j} := \min V_j \text{ and } x_{n_{k,j}} := x_{n_k} + j\epsilon,$$

for each $1 \leq j \leq h_k$. Now, for $n_{k,j} \leq n < n_{k,j-1}$, let:

$$x_n = x_{n_{k,j}} + \frac{(n - n_{k,j})\,\epsilon}{n_{j-1} - n_{k,j}}.$$

With:

$$\delta_k := \frac{1}{2} \min_{n_k \leq n < m_k} (x_{n+1} - x_n),$$

for each $n_k \leq n < m_k$ and $\alpha(n) \leq m < \alpha(n+1)$, let:

$$x_{N+m} = x_n - (\epsilon - \delta_k).$$

For $n_{k,1} \leq n < n_{k,0} \equiv m_k$ and $\omega(n) < m \leq \omega(n+1)$, let:

$$x_{N+m} = x_n + (\epsilon - \delta_k).$$

Furthermore, for $\alpha(m_k) \leq m \leq \omega(n_{k,1})$, define:

$$x_{N+m} = \frac{x_{n_{k,1}} + x_{m_k}}{2}.$$

In order to complete the specification of all the coordinates, fix $x_1 = x_{n_1} = 0$ and for each $1 \leq k \leq \ell$ let:

$$x_{n_k} := x_{m_{k-1}} + 3\epsilon.$$

Finally, for each $m \notin \bigcup_{n=1}^{N} \mathscr{A}_n$, let:

$$k(m) := \min\{1 \leq k \leq \ell : \alpha(n_k) > m\}$$

and define:

$$x_{N+m} := x_{N+\alpha(n_k)} - 3\frac{\epsilon}{2}.$$

If $\omega(N) < N$, then define:

$$x_{N+m} := x_{m_\ell} + 3\frac{\epsilon}{3}.$$

With this, the construction of the initial condition associated with the two increasing functions is finalized.

The pairs of increasing functions in $\Phi_{N,N}$ can be related to combinatorial objects, the parallelo-polyminoes inscribed in a rectangle. Formally, the number of parallelo-polyminoes in the lattice of size $p \times q$ is given by the Narayana number Barcucci, Frosini, and Rinaldi 2005 and the dependency is like the following Equation (4.42), as described in Section 2.1.5.

$$T_q^{p+q-1} = \frac{1}{p+q-1}\binom{p+q-1}{q}\binom{p+q-1}{q-1}. \tag{4.42}$$

Furthermore, to each couple of increasing functions $(\alpha, \omega) \in \Phi_{N,N}$ a parallelo-polyminoe in $\{0,1,\ldots,N+1\} \times \{0,1,\ldots,N+1\}$ with border functions $L, U : \{1,\ldots,N+1\} \to \{0,1,\ldots,N+1\}$ can be associated, such that:

$$L(n) = \begin{cases} 0 & \text{for } n = 1, \\ \alpha(n-1) - 1 & \text{for } 2 \leq n \leq N+1, \end{cases} \tag{4.43}$$

And:

$$U(n) = \begin{cases} \omega(n) + 1 & \text{for } 1 \leq n \leq N, \\ N+1 & \text{for } n = N+1. \end{cases} \tag{4.44}$$

In this way, an injective correspondence between parallelo-polyminoes and couples of increasing functions in $\Phi_{N,N}$ is established, from which the cardinality of this set can be calculated, which is expressed in the following equation.

$$|\Phi_{N,N}| = T_{N+1}^{2N+1} = \frac{1}{2N+1}\binom{2N+1}{N+1}\binom{2N+1}{N}. \tag{4.45}$$

To end, as a conclusion of this section, making a simplification of the initial conditions in $\mathbb{R}^{2N}$, through one of the symmetries that the complete bipartite graph $K_{N,N}$ has (the two groups of coordinates are in increasing order, and considering that they are balanced), which describes a section of space that corresponds to where the behavior is monotonic, allows to establish a coding of the ϵ-synchronized subnetworks through pairs of increasing functions, with which the concepts already established in the literature describe one of the most important properties of the transition diagram of $L(M_{K_{N,N}})$, that is: the number of pairs of increasing functions corresponds to the number of possible states in the transition diagram.

4.2.2 Unfeasible subgraphs of $K_{N,N}$

Given the characteristics of the pairs of increasing functions and the way they consistently codes ordered and balanced initial conditions in the sense of ϵ-synchronized subnetworks, it turns out that some subgraphs of $K_{N,N}$ remain uncoded, precisely because they are not feasible by no initial condition. Initially, it can be thought that all the subgraphs of $K_{N,N}$ are feasible by initial conditions, which unfortunately is not true, below are described these types of subgraphs.

To begin, an interesting note is that for the complete bipartite graph case, unlike the case exposed in Section 4.1.2, initial conditions in the form of a fork or a hole can be feasible, since this kind of subgraphs of $K_{N,N}$ does not lead to any contradiction when an initial condition is on it. As is shown in Figure 4.14, there are two subgraphs of the complete bipartite graph $K_{3,3}$, which, in principle, are unfeasible if they are considered as subgraphs of the complete graph K_6, but in $K_{3,3}$ are feasible. For example, fixing the corresponding $\epsilon > 0$ to build the subgraph depicted in (a), means that $|x_1 - x_5| \leq \epsilon$, $|x_2 - x_5| \leq \epsilon$ and $|x_3 - x_5| \leq \epsilon$, and there is no constraint, for instance, $|x_2 - x_1| \leq \epsilon$, in case, it is not necessary to draw any edge between vertices 1 and 2, because this edge does not exist in $K_{3,3}$, an explicit initial condition for constructing this subgraph is when $x_1 = x_2 = x_3 = x_5$ and $|x_5 - x_4| = |x_5 - x_6| = 3\epsilon$. In the case of (b), there are a similar argument, fixing the corresponding $\epsilon > 0$ such that the conditions to have the subgraph represented in that image, implies that $|x_1 - x_5| \leq \epsilon$, $|x_2 - x_5| \leq \epsilon$, $|x_2 - x_4| \leq \epsilon$ and $|x_1 - x_4| \leq \epsilon$, and there are any constraints saying that, for instance $|x_1 - x_2| \leq \epsilon$, in this case, but since the edge joining vertices 1 and 2 does not exist in $K_{3,3}$, then it is not drawn, an explicit initial condition for constructing this subgraph is when $x_1 = x_2 = x_4 = x_5$ and $|x_5 - x_3| = |x_5 - x_6| = 3\epsilon$.

Although these two subgraphs are feasible in the case of the complete bipartite graph in any dimension, there is another subgraph that is unfeasible, the hole of dimension 6 with all permutations of its vertex labels, an example of this subgraph

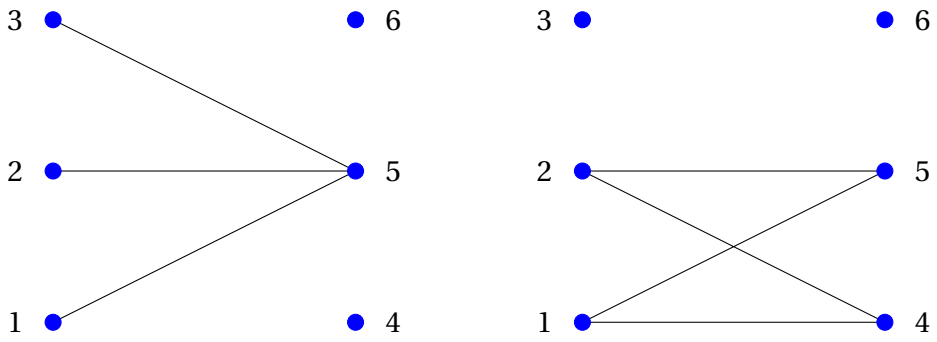

(a) (b)

Figure 4.14 – Feasible subgraphs of $K_{3,3}$. The subgraphs presented in (a) and (b) correspond to the fork and the hole respectively considering as subgraphs of $K_{3,3}$, there is no impediment to build it, then, they are performed by an initial condition on $\mathbb{R}^6$, unlike if they are considered as subgraphs of the complete graph of dimension 6 K_6.

is shown in Figure 4.15. If there were an initial condition $x = (x_1, x_2, x_3, x_4, x_5, x_6) \in \mathbb{R}^6$ that could perform it, the edges present would mean on the one hand that $|x_6 - x_1| \leq \epsilon$, $|x_6 - x_3| \leq \epsilon$, $|x_5 - x_2| \leq \epsilon$, $|x_5 - x_3| \leq \epsilon$, $|x_4 - x_1| \leq \epsilon$ and $|x_4 - x_2| \leq \epsilon$. And on the other hand, that $|x_6 - x_2| > \epsilon$, $|x_5 - x_1| > \epsilon$ and $|x_4 - x_3| > \epsilon$. Also, there is no restriction for the distances $|x_3 - x_1|$, $|x_3 - x_2|$, $|x_2 - x_1|$, $|x_6 - x_4|$, $|x_6 - x_5|$ and $|x_5 - x_4|$, since this graph is considered a subgraph of $K_{3,3}$.

Suppose x_1 is the smallest coordinate of x, then x_4 is to its right, that is $x_4 = x_1 + \epsilon_1$ such that $\epsilon_1 \leq \epsilon$. Then x_6 must also be to the right of x_1, that means $x_6 = x_1 + \epsilon_2$ such that $\epsilon_2 \leq \epsilon$. If $x_4 < x_6$, since $|x_4 - x_2| \leq \epsilon$, then $|x_6 - x_2| \leq \epsilon$, which is a contradiction. Therefore $x_4 > x_6$, and x_2 is to the right of x_4, that is $x_2 = x_4 + \epsilon_3$ such that $\epsilon_3 \leq \epsilon$. If $x_5 > x_2$, and then $x_3 > x_5$, then $|x_6 - x_3| > \epsilon$, which is also a contradiction. If $x_5 > x_2$, then $x_3 < x_5$, but $x_3 > x_2$, then also $|x_6 - x_3| > \epsilon$. If $x_5 > x_2$, then $x_3 < x_5$, but $x_3 < x_2$, then $|x_4 - x_3| \leq \epsilon$, which is a contradiction. The only remaining case is that $x_5 < x_2$, such that $x_5 > x_1 + \epsilon$, that is, is to the right of x_4. To finish, x_3 need to be placed. If $x_3 > x_5$, and $x_3 > x_2$, then $|x_6 - x_3| > \epsilon$, which is a contradiction. If $x_3 > x_5$, and $x_3 < x_2$, then $|x_4 - x_3| \leq \epsilon$, which is also a contradiction. Finally, if $x_3 < x_5$, then also $|x_4 - x_3| \leq \epsilon$. It is concluded that there is no suitable place to put x_3 and thus, there is no initial condition that can perform this subgraph. This same procedure is also followed to verify all possible symmetries. Therefore, an important observation is that not all subgraphs of $K_{N,N}$ are realizable by an initial condition when $N \geq 3$.

The important fact to highlight in this section is that not all the subgraphs of the

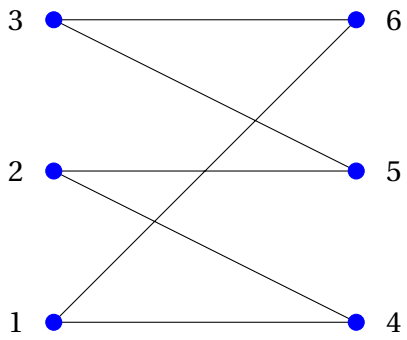

Figure 4.15 – Unfeasible subgraph of $K_{3,3}$. This case corresponds to the hole of dimension 6, seen as a subgraph of $K_{N,N}$ or as a subgraph of K_N is unfeasible by some initial condition with dimension greater than 6.

complete bipartite graph $K_{N,N}$ (when the dimension is greater than 6), are feasible for some initial condition, therefore, establish how many states its transition diagram has is not a trivial problem, which could be calculated exactly in Section 4.2.1, when a symmetry of the graph and balanced initial conditions are considered.

4.2.3 Paths towards synchronization

In this section the paths towards the synchronization of the Laplacian system applied to the complete bipartite graph of dimension $2N$ are studied, from the coding established in Section 4.2.1. To begin with, the conditions that the pairs of increasing functions must fulfill to they can be consecutive to form a path towards synchronization are mentioned. In addition, concrete example for dimensions four are presented. It needs to be noted that the transition diagram contains all the paths towards synchronization starting at balanced initial conditions, but it also contains paths which are not compatible with any balanced initial condition. In general, a bound is presented for the number of paths towards synchronization in the Laplacian system applied to the complete bipartite graph of dimension $2N$ transition diagram. Finally, two types of distributions associated to path lengths in the transition diagram of $L(M_{K_N})$ are shown.

Given the correspondence established by Equation (4.4), each sequence of ϵ-synchronized subnetworks defined by an ordered and balanced initial condition can be accurately represented by the corresponding sequences of increasing function pairs given by Equations (4.38) and (4.39). As discussed in Section 4.2.1, for a balanced initial condition $x \in \mathbb{R}^{2N}$, the differences $x_{N+m}(t) - x_n(t)$ converge monotonically to 0 at the same rate. In this case, the maps $t \mapsto \alpha_{x(t)}$ and $t \mapsto \omega_{x(t)}$ are both coordinate-wise monotonically non-decreasing, and they converge to the constant functions $\mathbf{1}(n) = 1$ and $\mathbf{N}(n) = N$ at time:

$$t_{1,N} := \frac{\log|x_1 - x_{2N}| - \log(\epsilon)}{N}.$$

The sequence of switching times $0 < t_1 < t_2 < \cdots < t_\ell$ is such that $(\alpha_{x(t_\tau)}, \omega_{x(t_\tau)}) \neq (\alpha_{x(t_{\tau+1})}, \omega_{x(t_{\tau+1})})$. We denote α_{t_τ} as α_τ and ω_{t_τ} as ω_τ. In a typical initial condition, at each switching time, only one of the functions α_τ or ω_τ changes, and it changes at only one site. The sequence $((\alpha_0,\omega_0),(\alpha_1,\omega_1),\ldots,(\alpha_\ell,\omega_\ell))$ can be determined by the initial couple (α_0,ω_0), the jump sites $n_1, n_2, \ldots, n_\ell \in 1,2,\ldots,N^\ell$, and the binary labels $q_1, q_2, \ldots, q_\ell \in (-1,+1)^\ell$ as follows:

$$(\alpha_{\tau+1},\omega_{\tau+1}) = \begin{cases} (\alpha_\tau - \delta_{n_\tau}, \omega_\tau) & \text{if } q_\tau = -1, \\ (\alpha_\tau, \omega_\tau + \delta_{n_\tau}) & \text{if } q_\tau = +1. \end{cases} \tag{4.46}$$

To the couple $(\alpha_\tau,\omega_\tau)$, a parallelo-polyminoe according to Equations (4.43) and (4.44) can be associated. In the transition $(\alpha_\tau,\omega_\tau) \to (\alpha_{\tau+1},\omega_{\tau+1})$, the area inside the corresponding parallelo-polyminoe increases by one unit until the greatest area. There is an example of this transition in Figure 4.16, the parallelo-polyminoes only differ by one unit of area.

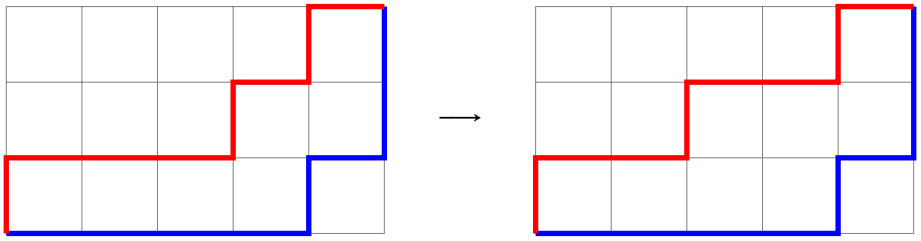

$U = (1,1,1,2,3)$.
$L = (0,0,0,0,1)$.

(a)

$U = (1,1,2,2,3)$.
$L = (0,0,0,0,1)$.

(b)

Figure 4.16 – Example of the transition between parallelo-polyminoes. In (a) and (b), two parallelo-polyminoes and their respective increasing functions that generate them U (red line) and L (blue line) are shown. From the parallelo-polyminoe shown in (a), there is a step to the parallelo-polyminoe shown in (b). In its U-functions, there is only one unit increase in one coordinate. Which translates to an increase of an area unit between them, in other words, this is how it looks the transition between parallelo-polyminoes.

Realizable sequences $((n_1,q_1),(n_2,q_2),\ldots,(n_\ell,q_\ell))$ are those that are compatible with a balanced initial condition $x \in \mathbb{R}^{2N}$ and can be completely determined by the differences:

$$\Delta_{n,m} := x_{N+m} - x_n,$$

with $1 \leq n, m \leq N$ as follows.

For $\epsilon < |\Delta_{n_1,m_1}| < |\Delta_{n_2,m_2}| < \cdots < |\Delta_{n_{N^2},m_{N^2}}|$ the sequence:

$$((n_1, q_1), (n_2, q_2), \ldots, (n_{N^2}, q_{N^2})),$$

where $q_\tau = \text{sign}(\Delta_{n_\tau,m_\tau})$ for each $1 \leq \tau \leq N^2$.

All the possible orderings:

$$\Delta := \{\Delta_{n,m} : 1 \leq n, m \leq N\},$$

are compatible with an initial condition $x \in \mathbb{R}^{2N}$, not necessarily balanced. Assuming that the dynamics towards synchronization is solely determined by this ordering, similar to the balanced case, a transition diagram can be constructed. The vertices of this diagram belong to the set $\Phi_{N,N}$ and the maximal paths start at couples (α, ω) (representing the disconnected subnetwork) and end at the couple $(\mathbf{1}, \mathbf{N})$ (representing the complete bipartite graph $K_{N,N}$). This directed graph encompasses all the paths towards synchronization starting from balanced initial conditions. However, it is important to note that it also includes paths that are not compatible with any balanced initial condition.

For instance, in the case of $N = 2$, there are a total of 20 possible orderings $\Delta_{n,m} :, 1 \leq n, m \leq N$ that are realizable. These orderings, along with their corresponding paths towards synchronization, are presented in Table 4.5 and illustrated in the transition diagram shown in Figure 4.18. However, it is important to note that out of these 20 orderings, there are 4 that are incompatible with a balanced initial condition. These incompatible orderings are indicated in red color. The two-digit strings used to represent the functions α and ω encode each ordering.

In the transition diagram, the underlined starting configurations represent the disconnected network, while the ending vertex (11,22) corresponds to the couple representing the complete bipartite graph $K_{2,2}$. By removing the starting couples indicated in red, which are incompatible with a balanced initial condition, the resulting transition diagram represents all the paths towards synchronization for balanced initial conditions.

In Figure 4.17, the coordinate arrangements that are incompatible with a balanced initial conditions are shown. In (a), for $x_1 < x_2 < x_3 < x_4$ and, in (b), for $x_3 < x_4 < x_1 < x_2$ are depicted. In general, there are 2 arrangements of initial conditions, $x_1 < \cdots < x_N < x_{N+1} < \cdots < x_{2N}$ and $x_{N+1} < \cdots < x_{2N} < x_1 < \cdots < x_N$, which are incompatible with a balanced initial condition. These arrangements define maximal

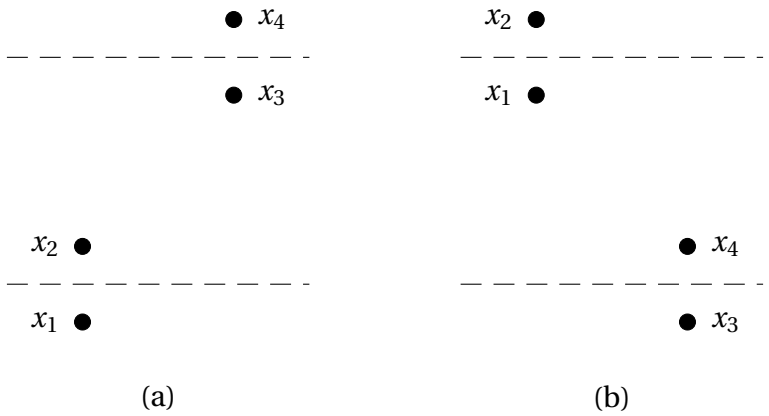

Figure 4.17 – Arrangements incompatible with a balanced initial conditions in $\mathbb{R}^4$. Of all the arrays of 4 components $(x_1, x_2, x_3, x_4) \in \mathbb{R}^4$ that can be generated that satisfy $x_1 < x_2$ and $x_3 < x_4$, there are two arrays that cannot be generated by balanced initial conditions. In (a), the case in which $x_1 < x_2 < x_3 < x_4$ is shown. In (b)m the case $x_3 < x_4 < x_1 < x_2$ is shown. It can be observed that the average of the two parts can not be the same.

paths starting at vertices (**1**, **0**) and (**N+1**, **N**), which for the case $N = 2$, that is for $L(M_{K_{2,2}})$ transition diagram, is indicated in red in the following Figure 4.18.

Coordinates	Differences	Signs
$x_1 < x_2 < x_3 < x_4$	$\lvert\Delta_{2,1}\rvert < \lvert\Delta_{2,2}\rvert < \lvert\Delta_{1,1}\rvert < \lvert\Delta_{1,2}\rvert$	$(+1,+1,+1,+1)$
	$\lvert\Delta_{2,1}\rvert < \lvert\Delta_{1,1}\rvert < \lvert\Delta_{2,2}\rvert < \lvert\Delta_{1,2}\rvert$	$(+1,+1,+1,+1)$
$x_1 < x_3 < x_2 < x_4$	$\lvert\Delta_{2,1}\rvert < \lvert\Delta_{2,2}\rvert < \lvert\Delta_{1,1}\rvert < \lvert\Delta_{1,2}\rvert$	$(-1,+1,+1,+1)$
	$\lvert\Delta_{2,2}\rvert < \lvert\Delta_{2,1}\rvert < \lvert\Delta_{1,1}\rvert < \lvert\Delta_{1,2}\rvert$	$(+1,-1,+1,+1)$
	$\lvert\Delta_{2,2}\rvert < \lvert\Delta_{1,1}\rvert < \lvert\Delta_{2,1}\rvert < \lvert\Delta_{1,2}\rvert$	$(+1,+1,-1,+1)$
	$\lvert\Delta_{2,1}\rvert < \lvert\Delta_{1,1}\rvert < \lvert\Delta_{2,2}\rvert < \lvert\Delta_{1,2}\rvert$	$(-1,+1,+1,+1)$
	$\lvert\Delta_{1,1}\rvert < \lvert\Delta_{2,1}\rvert < \lvert\Delta_{2,2}\rvert < \lvert\Delta_{1,2}\rvert$	$(+1,-1,+1,+1)$
	$\lvert\Delta_{1,1}\rvert < \lvert\Delta_{2,2}\rvert < \lvert\Delta_{2,1}\rvert < \lvert\Delta_{1,2}\rvert$	$(+1,+1,-1,+1)$
$x_1 < x_3 < x_4 < x_2$	$\lvert\Delta_{1,1}\rvert < \lvert\Delta_{2,2}\rvert < \lvert\Delta_{1,2}\rvert < \lvert\Delta_{2,1}\rvert$	$(+1,-1,+1,-1)$
	$\lvert\Delta_{2,2}\rvert < \lvert\Delta_{1,1}\rvert < \lvert\Delta_{2,1}\rvert < \lvert\Delta_{1,2}\rvert$	$(-1,+1,-1,+1)$
$x_3 < x_4 < x_1 < x_2$	$\lvert\Delta_{1,2}\rvert < \lvert\Delta_{1,1}\rvert < \lvert\Delta_{2,2}\rvert < \lvert\Delta_{2,1}\rvert$	$(-1,-1,-1,-1)$
	$\lvert\Delta_{1,2}\rvert < \lvert\Delta_{2,2}\rvert < \lvert\Delta_{1,1}\rvert < \lvert\Delta_{2,1}\rvert$	$(-1,-1,-1,-1)$
$x_3 < x_1 < x_4 < x_2$	$\lvert\Delta_{1,2}\rvert < \lvert\Delta_{1,1}\rvert < \lvert\Delta_{2,2}\rvert < \lvert\Delta_{2,1}\rvert$	$(+1,-1,-1,-1)$
	$\lvert\Delta_{1,1}\rvert < \lvert\Delta_{1,2}\rvert < \lvert\Delta_{2,2}\rvert < \lvert\Delta_{2,1}\rvert$	$(-1,+1,-1,-1)$
	$\lvert\Delta_{1,1}\rvert < \lvert\Delta_{2,2}\rvert < \lvert\Delta_{1,2}\rvert < \lvert\Delta_{2,1}\rvert$	$(-1,-1,+1,-1)$
	$\lvert\Delta_{1,2}\rvert < \lvert\Delta_{2,2}\rvert < \lvert\Delta_{1,1}\rvert < \lvert\Delta_{2,1}\rvert$	$(+1,-1,-1,-1)$
	$\lvert\Delta_{2,2}\rvert < \lvert\Delta_{1,2}\rvert < \lvert\Delta_{1,1}\rvert < \lvert\Delta_{2,1}\rvert$	$(-1,+1,-1,-1)$
	$\lvert\Delta_{2,2}\rvert < \lvert\Delta_{1,1}\rvert < \lvert\Delta_{1,2}\rvert < \lvert\Delta_{2,1}\rvert$	$(-1,-1,+1,-1)$
$x_3 < x_1 < x_2 < x_4$	$\lvert\Delta_{1,1}\rvert < \lvert\Delta_{2,2}\rvert < \lvert\Delta_{1,2}\rvert < \lvert\Delta_{2,1}\rvert$	$(-1,+1,+1,+1)$
	$\lvert\Delta_{2,2}\rvert < \lvert\Delta_{1,1}\rvert < \lvert\Delta_{2,1}\rvert < \lvert\Delta_{1,2}\rvert$	$(+1,-1,-1,+1)$

Table 4.5 – Increment orders at opposite parties, and corresponding signs for typical initial conditions in $\mathbb{R}^4$. The twenty different orderings of the differences between coordinates at opposite parties, and corresponding signs, for a typical initial conditions in $\mathbb{R}^4$.

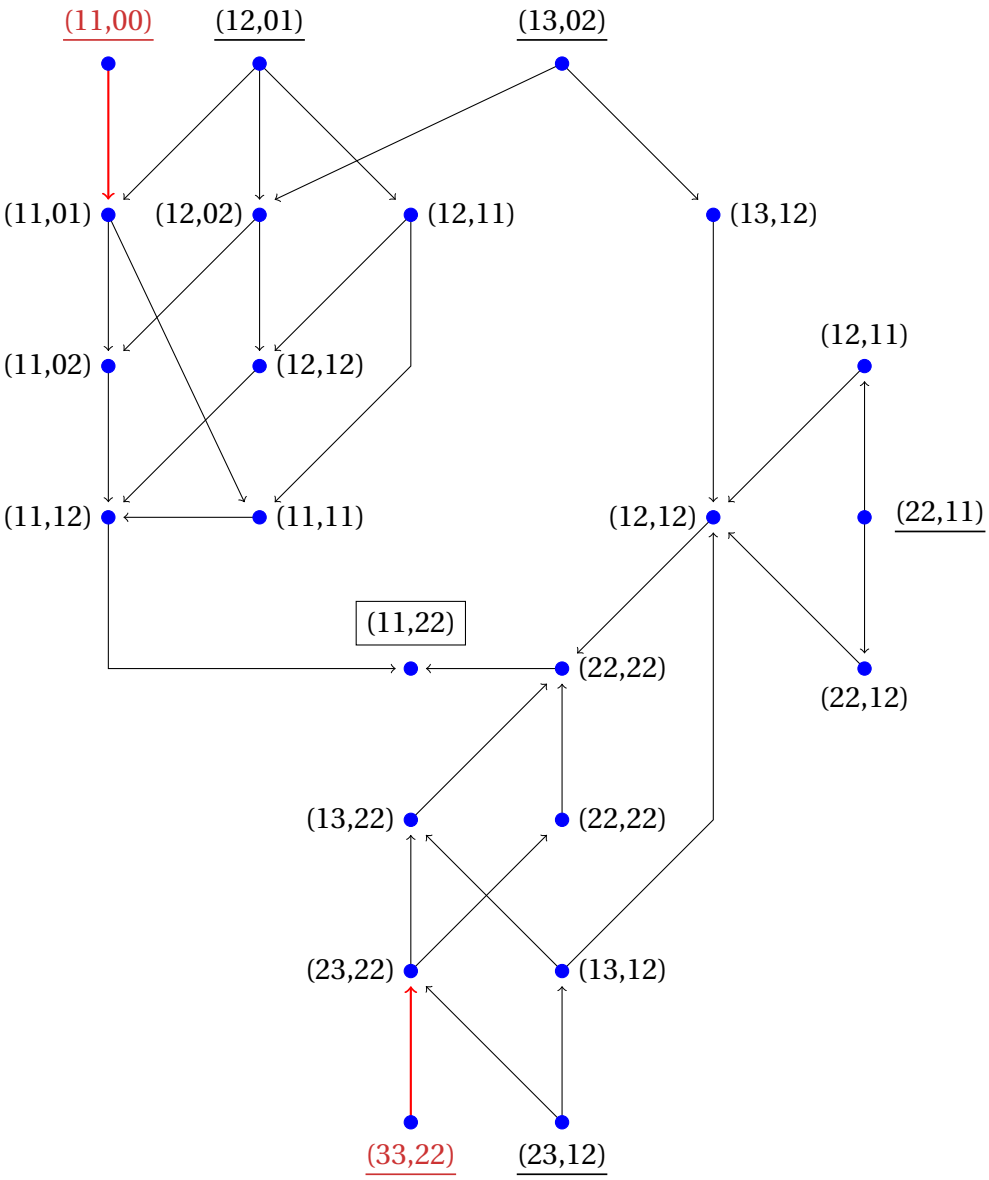

Figure 4.18 – Transition diagram of $L(M_{K_{2,2}})$ with labels assigned by the corresponding increasing functions is shown. This is composed of 23 vertices and 31 edges. The vertices where a path can start (so that it is as long as possible), are underlined, and are $(22,11),(12,01),(13,02),(23,12),(11,00),(33,22)$. The vertices that are in red are those that correspond to initial conditions that are not balanced. And in the middle, the vertex $(1,1,2,2)$ that corresponds to the complete bipartite graph $K_{2,2}$, is placed. This transition diagram corresponds to the ordered initial conditions $x = (x_1, x_2, x_3, x_4) \in \mathbb{R}^4$ such that $x_1 < x_2$ and $x_3 < x_4$, which are the ones that keep the monotony.

Now, the number of paths towards synchronization in the Laplacian flow over the complete bipartite graph $K_{N,N}$ is estimated. Firstly, an easy upper bound for the number of paths towards synchronization starting at typical balanced initial conditions $x \in \mathbb{R}^{2N}$ is written below in Equation (4.47). For each arrangement $x_{i_1} < x_{i_2} < \cdots < x_{i_{2N}}$, obtained by interplacing the first N coordinates with respect to the last N coordinates while maintaining the order within each group, there are Golomb$(2N)$ different orderings for the differences $x_{i_k} - x_{i_\ell}$. Each of these orderings corresponds to a path towards synchronization. However, in this case, the path does not depend on the differences between coordinates within the same group (i.e., first N or last N coordinates).

It is important to note that there are two coordinate arrangements that are incompatible with a balanced initial condition: one where $x_1 < x_2 < \cdots < x_{2N}$ and another where $x_{N+1} < x_{N+2} < \cdots < x_{2N} < x_1 < x_2 < \cdots < x_N$. Therefore, the number of paths towards synchronization in this case is upper bounded by the expression:

$$\sharp\text{Paths towards sync in } L(M_{K_{N,N}}) \leq \left(\binom{2N}{N} - 2\right)\text{Golomb}(2N). \tag{4.47}$$

Once again, the growth of the number of paths towards synchronization with respect to N defines a complexity function analogous to the topological complexity Farber 2003 as a function of time.

Similar to the case presented in Section 4.1, the number of paths towards synchronization of a given length, in this case written as $F_{N,N}(\ell)$, is given by the number of pairs of increasing functions $(\alpha,\omega) \in \Phi_{N,N}$ such that the corresponding parallelopolyminoe has an interior area of $(N+1)^2 - \ell$ units. Hence,

$$F_{N,N}(\ell) := \left|\left\{(\alpha,\omega) \in \Phi_{N,N} : \sum_{n=1}^{N+1} (U(n) - L(n)) = (N+1)^2 - \ell\right\}\right|. \tag{4.48}$$

Here, $L, U : \{1,\ldots,N+1\} \to \{0,1,\ldots,N+1\}$ are the polyminoe border functions defined from the couple of increasing functions (α,ω) by the Equations (4.44) and (4.43), mentioned before. In the Table 4.6 the numbers that generate the distributions $F_{N,N}(\ell)$ for the first dimensions $2 \leq N \leq 8$ are shown.

For each N and $0 \leq \ell \leq N$, the integer $F_{N,N}(\ell)$ coincides with the ℓ-th term of the sequence of Sloans (it can be found by writing the entry A000712 of the On-line Encyclopedia of Integer Sequences Sloane 2022), which among other things, counts the number of couples of integer partitions $P = (p_1 \geq p_2 \geq \cdots \geq p_k)$, $Q = (q_1 \geq q_2 \geq \cdots \geq q_r)$, such that

$$\sum_{i=1}^{k} p_i + \sum_{j=1}^{r} q_j = \ell. \tag{4.49}$$

N	$F_{N,N}(\ell)$
2	(1,2,5,6,6)
3	(1,2,5,10,16,24,31,36,30,20)
4	(1,2,5,10,20,32,53,78,111,146,187,216,243,240,210,140,70)
5	(1,2,5,10,20,36,61,98,153,228,327,454,611,798,1005,1236,1466,1688,1862,1980, 1971,1850,1540,1120,630,252)
6	(1,2,5,10,20,36,65,106,173,268,409,600,867,1212,1671,2244,2966,3826,4868, 6056,7422,8906,10519,12166,13830,15352,16704,17656,18133,17890,16903, 14966,12306,8988,5670,2772,924)
7	(1,2,5,10,20,36,65,110,181,288,449,680,1013,1474,2107,2958,4088,5558,7450, 9842,12820,16488,20932,26246,32507,39790,48116,57538,67984,79414,91653, 104578,117806,131096,143865,155692,165779,173530,177877,178282,173616, 163632,147855,127092,102060,75432,49434,27720,12012,3432)
8	(1,2,5,10,20,36,65,110,185,296,469,720,1093,1618,2369,3400,4824,6732,9296, 12654,17054,22694,29912,38976,50333,64320,81489,102242,127219, 156850, 191841,232602,279832,333830,395204,464030,540737,625028,716966,815766, 920990,1031168,1145253,1260882,1376172,1487820,1593022,1687242,1766791, 1826112,1860845,1865122,1834995,1765746,1656541,1506540,1320987,1106748, 877470,647592,437118,260832,132132,51480,12870)

Table 4.6 – Number $F_{N,N}(\ell)$ of couples $(\alpha,\omega) \in \Phi_{N,N}$ codifying a ϵ-synchronized sub-networks starting in a path towards synchronization of length ℓ.

Indeed, to each couple of integer partitions (P,Q), it can be associated a unique couple $L,U : \{1,2,\ldots,N+1\} \to \{0,1,\ldots,N+1\}$ of upper and lower border functions such that $U(i) = N+1-p_i$ and $L(N+2-j) = q_j$.

Clearly the previous sum presented in Equation (4.49), occurs if and only if the area of the parallelo-polyminoe with border functions L and U is exactly $(N+1)^2 - \ell$.

The correspondence between integer partitions and border functions cannot go further than $\ell = N$, since for $\ell = N+1$ the couple $((N+1),(0))$ of partitions does not define admissible border functions in the considered rectangle.

On the opposite extreme, $F_{N,N}(N^2)$ counts all the parallelo-polyminoes in $\{0,1,\ldots,N+1\} \times \{0,1,\ldots,N+1\}$ composed of $2N+1$ squares. These squares are arranged in a path going from $(0,0)$ to $(N+1,N+1)$, the next square place at the left or on top of the previous one. In Figure 4.19 an example for $N = 4$ is depicted, of this array of squares a path from $(0,0)$ to $(5,5)$ which is made up of 9 squares is shown, which coincides with the notes mentioned above.

Each one of these arrangements can therefore be codified into a sequence:

$$(a_1, a_2, \ldots, a_{2N}) \in \{L, T\}^{2N},$$

with exactly N entries equal to T. From this an exact formula can be written.

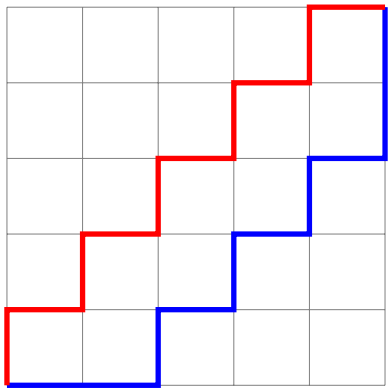

$U = (1,2,3,4,5)$.
$L = (0,0,1,2,3)$.

Figure 4.19 – Example of parallelo-polyminoe in a path from $(0,0)$ to $(5,5)$. Parallelo-polyminoe in a path from $(0,0)$ to $(5,5)$ and the functions U and L that form it are shown. If $N = 4$ is fixed, and it is constructed such that the next square place at the left or on top of the previous one, it is verified that is made up of $2N+1 = 9$ squares.

$$F_{N,N}(N^2) = \binom{2N}{N}. \tag{4.50}$$

On the other hand, the normalized cumulative distribution, $f_{N,N} : [0,1] \to [0,1]$, is given by:

$$f_{N,N}(x) = \frac{1}{|\Phi_{N,N}|} \sum_{n \leq x \times N^2} F_{N,N}(x), \tag{4.51}$$

where the number $F_{N,N}$ is given by Equation (4.48) and the number $|\Phi_{N,N}|$ is already defined in Equation (4.45). In this case, there are numerically computed $f_{N,N}(x)$ for increasing N, and observe how it approaches a limit distribution $x \mapsto \mathrm{f}(x)$ whose density $\varrho(x) := d\ \mathrm{f}(x)/dx$ approaches the curve depicted in Figure 4.20, which means that for N sufficiently large and $\delta > 0$ sufficiently small, the number of paths of length $N^2(x \pm \delta)/2$ is approximatively $\varrho(x)\,\delta$. As in the case of the Laplacian flow applied to the complete graph K_N, the numerical computation suggests that ϱ is continuous, unimodal, and negatively skewed.

Throughout this section, it is emphasized that in the case of $K_{N,N}$ there is not complete panorama of its paths towards synchronization, since this methodology, and therefore this analysis, is limited to the initial conditions that are balanced, because they are the initial conditions that keep the monotony of the system. Furthermore, it is worth noting that currently there are no known combinatorial results that facilitate the calculation of these distributions for arbitrary large sizes N. However, by directly computing and analyzing these distributions for small dimensions, it is observed that

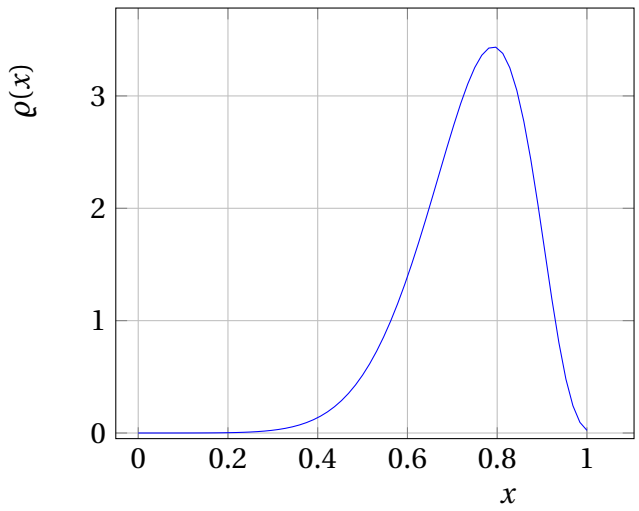

Figure 4.20 – The probability density function $\varrho(x)$ of the asymptotic distribution of the normalized length of a path towards synchronization.

the normalized distribution $f_{N,N}$ converges rapidly. A unimodal distribution with has a maximum at:

$$\begin{aligned} \text{mode}_{N,N}(\ell) &:= \max_{1\leq\ell\leq N^2} F_{N,N}(\ell), \\ &\approx 0.74118\, N^2. \end{aligned} \tag{4.52}$$

as it is depicted in Figure 4.20 can be obtained. The distribution is negatively skewed, and the mean length of these paths being larger than the most frequent length, as it is shown in the following expression:

$$\begin{aligned} \langle \ell \rangle_{N,N} &:= \frac{\sum_{\ell=1}^{N^2} \ell\, F_{N,N}(\ell)}{T(2N+1, N+1)}, \\ &\approx 0.8125\, N^2, \\ &> \text{mode}_{N,N}(\ell). \end{aligned} \tag{4.53}$$

The estimations shown in Equations (4.52) and (4.53) were obtained by using a relatively low ($N = 8$) dimension. As mentioned above, despite this low dimension an accurate qualitative behavior of the asymptotic distribution can be obtained. Which means that it is possible to qualitatively describe a typical synchronization path for the Laplacian of the complete bipartite graph $L(M_{K_{N,N}})$, starting at a random balanced ordered initial condition $x \in \mathbb{R}^{2N}$. For instance, this kind of path towards synchronization would most likely be of the length indicated in Equation (4.52).

As a conclusion of this section, for two pairs of increasing functions to be consecu-

tive on a path towards synchronization then, respective two of them must be equal and the other pair must differ by one unit of area (if it corresponds to the upper function, it must go up, and if it corresponds to the lower function, must go down), in this way a sequence of jump sites and the direction (up or down) are assigned. These realizable sequences are compatible with balanced initial conditions and are completely determined by the differences between the two parties of the coordinates, of which clearly not all correspond to balanced initial conditions. Then the famous problem that computes the number of combinatorially distinct Golomb rulers in dimension $2N$, is necessary to make an adjustment to constrain the paths to synchronization bound (in the case of the Laplacian flow applied to the complete bipartite graph). Furthermore, the number of paths towards synchronization of size ℓ is computationally given for the first eight dimensions, which its probability density function for N sufficiently large is given, and from which the behavior for the mode and the mean path length is obtained. Once again, the coding done through the couples of increasing functions allow to formally describe a part of the space of initial conditions by their transition diagram.

4.2.4 Discussion

In this section it is formally and rigorously analyzed the behavior of the transition diagram of the Laplacian system applied to the complete bipartite graph of dimension $2N$. To achieve this objective, a coding of the subgraphs of $K_{N,N}$ was proposed, which preserves the monotonic dynamics of the system and turns out to be very useful because it transforms it into a combinatorial problem that has been widely studied before.

One of the advantages of using this coding is that it automatically generates the subgraphs that are feasible for a set of initial conditions. Despite of this, it was considered pertinent to give the examples that show that not all the subgraphs of $K_{N,N}$ are feasible. Then, it can be stated that when $N \geq 3$ not all subgraphs of the complete bipartite graph are feasible for some initial condition on the respective space $\mathbb{R}^{2N}$.

Moreover, two key simplifications for the analytical study of the transition diagram of $L(M_{K_{N,N}})$ are made. The first, defining the coding of the subgraphs that are formed from initial conditions, for whose two groups of coordinates are in strictly increasing order, such that, the set of associated ϵ-synchronized subnetworks have a relation with the set of the couples of increasing functions. This simplification allows to focus the attention on the diversity of states generated by considering a single symmetry of the complete bipartite graph. On the other hand, the second simplification made in this section is: balanced initial conditions in the space $\mathbb{R}^{2N}$ are considered (that is, the mean of the two parts of the coordinates are equal). This type of initial conditions represents all the monotonous dynamics of space. As in the previous case, typical initial conditions generate typical paths, which are the ones with the longest lengths, that is, if they start forming the totally disconnected subgraph, then they will reach

synchronization in N^2 steps.

By considering these two simplifications in the space of initial conditions, it is possible to establish the rules by which two pairs of increasing functions will be consecutive on a path towards synchronization. That is, respective two of them must be equal and the other pair must differ by one unit of area, if it corresponds to the upper function, it must go up, and if it corresponds to the lower function, must go down, in this way a sequence of jump sites and the direction (up or down) are assigned.

These realizable sequences are compatible with balanced initial conditions, and they are completely determined by the differences between the two parties of the coordinates. Clearly, not all correspond to balanced initial conditions. The problem of counting how many realizable paths there are in each dimension $2N$ is equivalent to counting the number of combinatorially distinct Golomb rulers (but in this case, with an adjustment), which is a famous open problem. Some analytical and numerical bounds have been provided in low dimensions (due to the great memory demand that the computation of the Golomb rulers requires).

To end this discussion, it should be noted that having this coding allow to associate characteristics of the combinatorial objects that have a relevant meaning in terms of the study of the transition diagram, which are listed below.

Combinatorial concept	**Transition diagram property**
Narayana number	Possible states
Combinatorially different Golomb rulers	Number of paths towards synchronization
Number of parallelo-polyminoe with interior area $(N+1)^2-\ell$	Number of synchronized sequences of length ℓ

4.3 About other transition diagrams

In this section it is briefly formally and rigorously analyzed the behavior of the transition diagrams of the Laplacian system applied over the cycle graph of dimension N and of the Kuramoto model applied over the complete graph of dimension N. The formal and rigorous analyzes concerning these two systems are presented with the aim of giving a perspective and a starting point for future research.

4.3.1 The transition diagram of $L(M_{C_N})$

In this section it is formally and rigorously analyzed the behavior of the transition diagram of the Laplacian system applied to the cycle graph of dimension N. This study is organized as follows: to begin with, the two dynamics are shown in the Laplacian system with respect to the dimension. Then, the feasible subgraphs that the cycle graph has been shown. Finally, a bound for the maximum length of the paths that are observed in the associated transition diagram is presented.

As mentioned in the Section 2.1 (specifically in Equations (2.12) and (2.13)), the eigensystem of the Laplacian system applied to the cycle graph $L(M_{C_N})$ (in this Section it is written just as L), has the symmetries inherited by the graph in question, besides there is a difference in the behavior of the system depending on the parity of the dimension N. When the system has an even dimension, it behaves in one way, and when it has an odd dimension, it behaves in another way. This can be inferred when the flow of an initial condition of the space is analyzed, as it is done in the following.

To begin, any initial condition $x \in \mathbb{R}^N$ can be written as a linear combination of the eigenbasis $\mathscr{B}_L = \{v_1, v_2, ..., v_N\}$ of $L(M_{C_N})$, for some coefficients $\alpha_i \in \mathbb{R}$, where $1 \leq i \leq N$, as the following expression:

$$x = \sum_{i=1}^{N} \alpha_i \, |v_i\rangle \, .$$

On the other hand, its flow meets:

$$\begin{aligned} x(t) &= \sum_{i=1}^{N} \alpha_i e^{\lambda_i t} \, |v_i\rangle \, , \\ &= \sum_{i=1}^{N-1} \alpha_i e^{\lambda_i t} \, |v_i\rangle + \alpha_N \, |v_N\rangle \, , \\ &= \alpha_N \, |v_N\rangle + \sum_{i=1}^{\lfloor \frac{N-1}{2} \rfloor} e^{\lambda_i t} (\alpha_i \, |v_i\rangle + \alpha_{N-i} \, |v_{N-i}\rangle) \\ &\quad + \alpha_{i^*} e^{\lambda_{i^*} t} \, |v_{i^*}\rangle \, . \end{aligned}$$

Where the i^* term only appears when the dimension N is even, and is defined as following:

$$i^* = \frac{N}{2} + 1.$$

Therefore, with this fact, it can be inferred that depending on the parity of the dimension N, the Laplacian system applied to the cycle graph have a different dynamic.

On the other hand, the flow at each coordinate meets:

$$\begin{aligned} x_j(t) &= \alpha_N + \sum_{i=1}^{\lfloor \frac{N-1}{2} \rfloor} e^{\lambda_i t}(\alpha_i v_i^j + \alpha_{N-i} v_{N-i}^j) + \alpha_{i^*} e^{\lambda_{i^*} t} v_{i^*}^j, \\ &= \alpha_N + \sum_{i=1}^{\lfloor \frac{N-1}{2} \rfloor} e^{\lambda_i t}\left(\alpha_i \cos\left(\frac{2\pi ji}{N}\right) + \alpha_{N-i}\cos\left(\frac{2\pi j(N-i)}{N}\right)\right) \\ &\quad + \alpha_{i^*} e^{\lambda_{i^*} t} v_{i^*}^j, \\ &= \alpha_N + \sum_{i=1}^{\lfloor \frac{N-1}{2} \rfloor} e^{\lambda_i t}\cos\left(\frac{2\pi ji}{N}\right)(\alpha_i + \alpha_{N-i}) + \alpha_{i^*} e^{\lambda_{i^*} t} v_{i^*}^j. \end{aligned}$$

And also, by the symmetry of the function $\cos(x)$ and the considered interval $\left(0, \frac{2\pi(N-1)}{N}\right)$, the eigenvectors are equal by couples as the following relation $v_i = v_{N-i}$ for $1 \leq i \leq \lfloor \frac{N-1}{2} \rfloor$. The symmetry of the eigenvalues and the eigenvectors make that the flow of the coordinates also have a symmetric behavior.

One of the most important notes related to the dynamics of the cycle graph is that all its subgraphs are feasible for some initial condition. Hence:

$$\sharp\text{Vertices in the transition diagram of } L(M_{C_N}) = 2^{N-1}. \tag{4.54}$$

The simplest way to construct an initial condition $x \in \mathbb{R}^N$ that meets the requirements of a given subgraph is: if vertex i is connected to vertex j, then $x_i = x_j$ and make sure that when there is no edge, the vertices are further apart than the corresponding $\epsilon > 0$.

On the other hand, due to the way in which the eigenvalues and eigenvectors in the spectrum of $L(M_{C_N})$ are defined, the differences of the coordinates are not monotone, then, they are crossings between them. This causes that the flow of the transition diagram is not in a single direction (as it has been observed in the two previous cases, whichever vertex was chosen at the beginning, the next step was closer to the node that represents complete synchronization), that is, there are cycles or returns from low levels to high levels. Also, for this reason, the number of steps towards synchronization often exceeds the total number of edges of C_N which is $N-1$.

As a conclusion of this section, since the Laplacian system applied to the cycle graph does not have a monotone dynamic quickly to find, it was not possible to provide a coding in terms of increasing functions as in the previous cases. However, it was possible to provide the number of possible states, and a lower bound for the depth of the transition diagram. It is hoped that in the future a good coding will be achieved in such a way that it will be possible to describe its transitory dynamics in a combinatorial way.

4.3.2 The transition diagram of the Kuramoto model

In this section it is formally and rigorously analyzed the behavior of the transition diagram of the Kuramoto model applied to the complete graph of dimension N and the complete bipartite graph of dimension $2N$. This study is organized as follows: first, a discussion is made of why and when it is possible to use the same coding in terms of increasing functions from the case of the Laplacian system to the case of the Kuramoto model in the complete graph. Finally, in the same way, it is discussed, and the conditions to use the same coding in terms of pairs of increasing functions from the case of the Laplacian system to the case of the Kuramoto model in the complete bipartite graph are given.

Although the above presented results in Section 4.1 concern the Laplacian flow, they can be applied in a particular region when the Kuramoto flow is considered. In the case of the complete graph K_N, the transition diagram resulting from the Kuramoto flow captures a significant portion of the paths towards synchronization that originate from a small neighborhood around the diagonal. In this region, the same coding scheme for ϵ-synchronized subnetworks, as described in Section 4.1.1, can be applied. This is because the order of the coordinates is preserved by the Kuramoto flow, allowing us to use the set of increasing functions in Φ_N for coding purposes. In fact, based on Equation (2.25), where is the Kuramoto model applied on a network with a coupling strength σ, then for a couple of index $1 \leq n, m \leq N$:

$$\begin{aligned} \frac{d(x_n - x_m)}{dt} &= \sigma \left(\sum_{j=1}^{N} \sin\big(x_j - x_n\big) - \sin\big(x_j - x_m\big) \right), \\ &= \sigma\, r \left(\sin(\Theta - x_n) - \sin(\Theta - x_m) \right), \end{aligned}$$

where $r\, e^{i\Theta} = \left(\sum_{j=1}^{N} \cos\big(x_j\big) \right) + i \left(\sum_{j=1}^{N} \sin\big(x_j\big) \right)$, by expanding the Equation (2.22). Hence, whenever $x_n = x_m$,

$$\frac{d}{dt}(x_n - x_m) = 0,$$

which implies that the order in the coordinates is preserved under the flow since no crossing of coordinates is possible.

Assume that:

$$\max\{|x_n - \bar{x}| : 1 \leq n \leq N\} < \frac{\pi}{4},$$

where $\bar{x} = \sum_{n=1}^{N} x_n(0)$.

In this case:

$$|\Theta - \bar{x}| \leq \frac{\pi}{4} \quad \text{and} \quad \frac{d}{dt}(x_n - x_m) = 0,$$

if and only if $x_m = x_n$.

Furthermore, in this case, the sign of $(\sin(\Theta - x_n) - \sin(\Theta - x_m))$ is the same as the sign of $(x_m - x_n)$, and therefore $|x_n - x_m|$ decreases monotonously for all initial conditions $x \in \mathbb{R}^N$.

Numerical calculations have shown that the transition diagram obtained from the Laplacian system applied to the complete graph K_N is preserved by the Kuramoto flow when considering a sufficiently small value of ϵ with respect to $\pi/4$, and initial conditions $x \in (S^1)^{|V|}$ such that $|x_n - \bar{x}| < \pi/4$ for all $1 \leq n \leq N$.

On the other hand, for the case of the complete bipartite graph $K_{N,N}$, the order of the coordinates at each of the two parts is preserved by the Kuramoto flow. For this, it can be proceed as in an analogous way, which was exposed before, that is, to explore the behavior between each couple $1 \leq n, m \leq N$ of coordinates, and obtain:

$$\begin{aligned} \frac{d(x_n - x_m)}{dt} &= \sigma\, r_2 \left(\sin(\Theta_2 - x_n) - \sin(\Theta_2 - x_m)\right), \\ \frac{d(x_{N+n} - x_{N+m})}{dt} &= \sigma\, r_1 \left(\sin(\Theta_1 - x_n) - \sin(\Theta_1 - x_m)\right), \end{aligned}$$

in this case, there is: $r_1\, e^{i\Theta_1} = \left(\sum_{j=1}^N \cos(x_j)\right) + i\left(\sum_{j=1}^N \sin(x_j)\right)$ and similarity, $r_2\, e^{i\Theta_2} = \left(\sum_{j=1}^N \cos(x_j)\right) + i\left(\sum_{j=1}^N \sin(x_j)\right)$.

From this it follows that if $x_n = x_m$ then:

$$\frac{d}{dt}(x_n - x_m) = 0,$$

and similarly for $x_{N+n} - x_{N+m}$,

$$\frac{d}{dt}(x_{N+n} - x_{N+m}) = 0.$$

The preservation of order in the coordinates at each part under the Kuramoto flow enables us to utilize the same coding scheme for ϵ-synchronized subnetworks that was initially defined for the Laplacian flow on the complete bipartite graph $K_{N,N}$. This means that the coding scheme based on increasing functions can be applied consistently to represent and analyze ϵ-synchronized subnetworks in both the Laplacian and Kuramoto systems.

As there is mentioned Section 4.2, the transition diagram defined for the Laplacian flow over the complete bipartite graph $K_{N,N}$, describes only the paths towards synchronization corresponding to balanced initial conditions. In Figure 4.18, the red markings indicate the ϵ-synchronized subnetworks that are incompatible with balanced initial conditions. The complete transition diagram, including these subnetworks, allows

for non-monotonic paths. Additionally, for unbalanced initial conditions $x \in \mathbb{R}^{2N}$, the flow does not preserve the order in the differences between coordinates.

As a conclusion of this section, it is possible to use the two codes that were used in the case of the Laplacian system to apply them in the study of the transitory dynamics of the Kuramoto model, when certain conditions are considered. In the case of the complete graph, when initial conditions close to the diagonal are considered. In the case of the complete bipartite graph, when the initial conditions are balanced (that is, the same conditions that are considered for the linear case). The fact that the codes can be reused allows to think of more general conditions to use them, for example, for the complete graph it would be enough that the system that synchronizes is monotonic, and its differences are monotonic. This generalization is expected to be made formally in future works.

Conclusions

In this thesis, I have studied the transition behavior of systems that synchronize. Also, I have proposed a new approach to understand the paths towards synchronization, especially for two concrete systems: the Laplacian system and the Kuramoto model, which I applied in four different types of graphs: the complete graph, the complete bipartite graph, the cycle graph, and the ring lattice family.

Two types of analysis were carried out in this thesis. The first is an exploratory study based on computational calculations and simulations, to find the most important characteristics of the two systems studied, applied on four types of graphs. The main objective of this type of analysis was to recognize the behavior patterns that follow the random generated initial conditions with the change of parameters (that is, systems and graphs). In the second type of analysis presented in this thesis, a formal, rigorous, and complete description was made, based on propositions, of the characteristics and properties of the transitory state of these systems for typical initial conditions, which completes the first analysis and thus includes the observations made.

The results of the exploratory study presented in this thesis, first, allowed to know how the transitory state of the Laplacian system acts on the complete graph, the bipartite graph, the cycle graph, and the ring lattice family, to distinguish and analyze the features that make them different. In this way, the exploratory study allowed to know that, from the ring lattice $C(N,k)$ (that has N vertices, and each of them is connected with its k neighbors to the left, and its k neighbors to the right), is possible to generalize the behavior of the analyzed graphs, that goes from the complete graph to the cycle graph. It is possible because when the parameter k is varied, the density of the graph edges changes, and the transition from a highly connected to a not so connected graph behavior can be observed, and what features appear or change (as internal directed cycles or monotonicity).

On the one hand, thanks to the monotonic behavior of the Laplacian flow in the complete graph K_N, it was possible to completely describe the behavior of their transient dynamics, using a codification of the ϵ-synchronized subnetworks by increasing functions above the diagonal, which are well known and studied. On the other hand, in the case of the transitory behavior of the complete bipartite graph $K_{N,N}$, a similar codification was presented, but it is limited only to synchronizing paths which start at special type of initial conditions, the balanced ones, which preserve a monotonous behavior, and therefore, this methodology can be applied.

On the contrary, in the case where there is no monotony in the flow towards synchronization, specifically when considering the cycle graph and most of the members of the ring lattice family, arguments and discussion about the behaviors observed in the experimental studies were provided.

In all cases, I obtained a closed formula for the number of realizable states, and in the monotonical cases, their states are given by combinatorial objects that codify all the feasible ϵ-synchronized subnetworks. In contrast, determining a closed-form expression for the number of paths towards synchronization in Laplacian systems still poses a challenge. Nevertheless, it is feasible to establish bounds or conduct computational calculations that can provide insights into their growth rate. From these results about complexity, it can be concluded that with little information, that is, from a small-dimensional system, an immense number of paths can be found. Although it is known that in finite time, these systems converge to the synchronized state, the number of ways in which the initial conditions reach the asymptotic state grows at a factorial rate.

It is important to discuss the difference between the experimental study, in which randomly generated initial conditions were considered, and the rigorous study, in which typical initial conditions were considered for the monotonical cases. In the rigorous study, it has been said that randomly generating a non-typical initial condition has zero probability, and then, the paths to synchronization for the typical initial conditions would be the longest possible (in terms of the edges number of the considered graph). On the other hand, in the experimental study, when the initial conditions are randomly generated, the results indicate that the generated paths are not the longest, as expected. This behavior is due to the threshold $\epsilon > 0$ that is considered when the simulations were made, then, when this threshold $\epsilon \to 0$ decreases, the behavior tends to the one observed for the typical initial conditions.

The probability density functions of the asymptotic distribution of the normalized length of a path towards synchronization in both the complete bipartite graph $K_{N,N}$ and the complete graph K_N exhibit similar characteristics. They are continuous, unimodal, and negatively skewed. However, the typical length, relative to the longest path, is larger for the case of the complete bipartite graph $K_{N,N}$ compared to the complete graph K_N.

In the case of the transitory behavior of the Kuramoto model applied on the complete graph K_N, it can be implemented the already defined methodology used to describe the Laplacian system on the same graph in a neighborhood around the diagonal. For this reason, the dynamics in this region can be studied in a complete way. In the other case, the description of transition diagram for the Laplacian flow over $K_{N,N}$, the same codification used to study the linear case for the balanced initial conditions can be implemented. The full dynamics of this system would be the subject of future work.

Finally, it is worth noting that the ϵ-synchronizing sequences discussed in this thesis can be viewed as a way of partitioning the basin of attraction of a particular attractor, which in this case is the fully synchronized state. These sequences effectively divide the space of initial conditions into different regions, with each region corresponding to a specific ϵ-synchronized subnetwork. Since, for a given finite $\epsilon > 0$, the final ϵ-synchronized subnetwork will be reached in a finite time $\tau(\epsilon, N)$, if the space of initial conditions has a finite volume, the entire space-time trajectory will also be bounded. Therefore, these sequences serve to effectively partition the full space-time around the diagonal.

Moreover, by associating each sequence with an ensemble of initial conditions that realizes that sequence, it becomes possible to measure and assign weights (measures) to each sequence. This provides a means to further characterize the space-time complexity by quantifying the distribution and properties of these ensembles. By considering the ensemble measures, it becomes possible to gain deeper insights into the structure and behavior of the space of initial conditions and their corresponding trajectories towards synchronization.

Below are some perspectives and future work regarding the analysis of the transient state of systems that synchronize.

As has been said and remembered throughout this thesis, there are different asymptotic states that a system that describes the synchronization phenomenon can reach, for example, in the Kuramoto model there is a phase locking state, in which the difference between the phases of the N oscillators is equal to a fraction of the complete angle, which is also an attractor. Given $\epsilon > 0$, adjusting the definition of ϵ-synchronized neighbors in the graph $G = (V, E)$ for vertices $u, v \in V$, from being

$$|x_u - x_v| \leq \epsilon,$$

to

$$|x_u - x_v| \mod \left(\frac{2\pi}{|V|}\right) \leq \epsilon,$$

the transitory state can be studied before reaching the phase locking of the initial condition, with the same methodology. This is recommended to study the behavior of the family of graphs called ring lattice, when the Kuramoto model is applied, because when the proportion of edges with respect to the number of edges of the complete graph tends to zero (that is, when N grows and k remains constant), it is more likely to find this state of phase locking than global synchronization state.

Some perspectives, regarding the formal and rigorous study of the cycle graph C_N and the family of the ring lattices $C(N, k)$ in the Laplacian system are mentioned. In the first case, it is still necessary to find an encoding in which some degree of monotony

is found, if possible, to continue with the approach presented in this manuscript. It is possible that by observing the symmetry of the spectrum, which implies that the i-th component tends to have the same behavior as the $N+1-i$-th component, then, $N/2$ increasing functions might be needed to describe the neighborhood in which they behave monotonically (following the same intuition that was used to solve the bipartite complete graph case). In the second case, since the family of ring lattices can take from the complete graph to the cycle graph by varying the connectivity parameter k, then an area of opportunity is to exploit the concept and investigate in depth the transition between these types of graphs.

Most of these results are published in España, Leoncini, and Ugalde 2022, and in a second article now in preparation.

Bibliography

[Ace+05] Juan A. Acebrón, L. L. Bonilla, Conrad J. Pérez Vicente, et al. “The Kuramoto model: A simple paradigm for synchronization phenomena”. In: *Rev. Mod. Phys.* 77 (1 Apr. 2005), pp. 137–185. DOI: 10.1103/RevModPhys.77.137 (cit. on p. 11).

[AZ03] V. Afraimovich and G. M. Zaslavsky. “Space-Time Complexity in Hamiltonian Dynamics”. en. In: *arXiv* 2003.0 (2003) (cit. on p. 11).

[Are+08] Alex Arenas, Albert Diaz-Guilera, Jurgen Kurths, et al. “Synchronization in complex networks”. English. In: *Physics Reports* 469.3 (Dec. 2008), pp. 93–153. ISSN: 0370-1573. DOI: 10.1016/j.physrep.2008.09.002 (cit. on p. 11).

[ADP06] Alex Arenas, Albert Díaz-Guilera, and Conrad J. Pérez-Vicente. “Synchronization Reveals Topological Scales in Complex Networks”. In: *Phys. Rev. Lett.* 96 (11 Mar. 2006), p. 114102. DOI: 10.1103/PhysRevLett.96.114102 (cit. on p. 12).

[BYL18] Dianbin Bao, Kisung You, and Lizhen Lin. *Network Distance Based on Laplacian Flows on Graphs*. 2018. DOI: 10.48550/ARXIV.1810.02906. URL: https://arxiv.org/abs/1810.02906 (cit. on p. 39).

[BFR05] Elena Barcucci, Andrea Frosini, and Simone Rinaldi. “On directed-convex polyominoes in a rectangle”. In: *Discrete Mathematics* 298.1 (2005). Formal Power Series and Algebraic Combinatorics 2002 (FPSAC’02), pp. 62–78. ISSN: 0012-365X. DOI: https://doi.org/10.1016/j.disc.2005.01.006 (cit. on p. 117).

[BJB13] Peter Baudains, Shane D. Johnson, and Alex Maves Braithwaite. “Geographic patterns of diffusion in the 2011 London riots”. In: *Applied Geography* 45 (2013), pp. 211–219. ISSN: 0143-6228 (cit. on p. 9).

[BBP11] Matthias Beck, Tristram Bogart, and Tu Pham. “Enumeration of Golomb Rulers and Acyclic Orientations of Mixed Graphs”. In: (2011). DOI: 10.48550/ARXIV.1110.6154. URL: https://arxiv.org/abs/1110.6154 (cit. on p. 37).

[BA09] Nooshin Bigdeli and Karim Afshar. “Characterization of Iran electricity market indices with pay-as-bid payment mechanism”. In: *Physica A-statistical Mechanics and Its Applications* 388 (2009), pp. 1577–1592 (cit. on p. 9).

[BP12] Saúl A. Blanco and T. Kyle Petersen. "Counting Dyck Paths by Area and Rank". In: *Annals of Combinatorics* 18 (2012), pp. 171–197 (cit. on pp. 35, 106).

[CR64] L. Carlitz and John Riordan. "Two element lattice permutation numbers and their q-generalization". In: *Duke Mathematical Journal* 31 (1964), pp. 371–388 (cit. on p. 106).

[CDS95] Dragos M. Cvetkovic, Michael Doob, and Horst Sachs. "Spectra of graphs : theory and application". In: 1995 (cit. on pp. 20, 29).

[Das04a] K.Ch. Das. "The Laplacian spectrum of a graph". In: *Computers and mathematics with Applications* 48.5 (2004), pp. 715–724. ISSN: 0898-1221. DOI: https://doi.org/10.1016/j.camwa.2004.05.005. URL: https://www.sciencedirect.com/science/article/pii/S0898122104003074 (cit. on p. 20).

[Das04b] Kinkar Ch. Das. "Sharp lower bounds on the Laplacian eigenvalues of trees". In: *Linear Algebra and its Applications* 384 (2004), pp. 155–169 (cit. on p. 20).

[Dav+13] Toby P. Davies, Hannah Fry, Alan Wilson, et al. "A mathematical model of the London riots and their policing". In: *Scientific Reports* 3 (2013) (cit. on p. 9).

[DJD19] Robin Delabays, Philippe Jacquod, and Florian Dörfler. "The Kuramoto Model on Oriented and Signed Graphs". In: *SIAM Journal on Applied Dynamical Systems* 18.1 (2019), pp. 458–480. DOI: 10.1137/18M1203055. eprint: https://doi.org/10.1137/18M1203055. URL: https://doi.org/10.1137/18M1203055 (cit. on pp. 11, 33).

[DE16] Lee DeVille and Bard Ermentrout. "Phase-locked patterns of the Kuramoto model on 3-regular graphs." In: *Chaos* 26 9 (2016), p. 094820 (cit. on pp. 11, 33).

[Dim02] Apostolos Dimitromanolakis. *Analysis Of The Golomb Ruler And The Sidon Set Problems And Determination Of Large Near-Optimal Golomb Rulers*. Tech. rep. 2002 (cit. on p. 37).

[Eps02] Joshua M. Epstein. "Modeling civil violence: An agent-based computational approach". In: *Proceedings of the National Academy of Sciences* 99.suppl_3 (2002), pp. 7243–7250. DOI: 10.1073/pnas.092080199. eprint: https://www.pnas.org/doi/pdf/10.1073/pnas.092080199. URL: https://www.pnas.org/doi/abs/10.1073/pnas.092080199 (cit. on p. 9).

[ELU22] A España, X Leoncini, and E Ugalde. *Combinatorics of the paths towards synchronization*. 2022. DOI: 10.48550/ARXIV.2205.05948. URL: https://arxiv.org/abs/2205.05948 (cit. on p. 140).

[Far03] Michael Farber. "Topological Complexity of Motion Planning". In: *Discrete & Computational Geometry* 29 (2003), pp. 211–221 (cit. on pp. 104, 126).

[FA18] J D da Fonseca and Celso Vieira Abud. “The Kuramoto model revisited”. In: *Journal of Statistical Mechanics: Theory and Experiment* (2018) (cit. on pp. 11, 31).

[GJ12] Zhong-Ke Gao and Ning-De Jin. “A directed weighted complex network for characterizing chaotic dynamics from time series”. In: *Nonlinear Analysis: Real World Applications* 13.2 (2012), pp. 947–952. ISSN: 1468-1218. DOI: https://doi.org/10.1016/j.nonrwa.2011.08.029. URL: https://www.sciencedirect.com/science/article/pii/S146812181100263X (cit. on p. 9).

[Giu+02] Alessandro Giuliani, Romualdo Benigni, Joseph Zbilut, et al. “Nonlinear Signal Analysis Methods in the Elucidation of Protein Sequence-Structure Relationships”. In: *Chemical reviews* 102 (June 2002), pp. 1471–92. DOI: 10.1021/cr0101499 (cit. on p. 9).

[Gol72] Solomon W. Golomb. “How to number a graph”. In: *Graph Theory and Computing*. Ed. by RONALD C. READ. Academic Press, 1972, pp. 23–37. ISBN: 978-1-4832-3187-7. DOI: https://doi.org/10.1016/B978-1-4832-3187-7.50008-8. URL: https://www.sciencedirect.com/science/article/pii/B9781483231877500088 (cit. on p. 102).

[GMA07] Jesús Gómez-Gardeñes, Yamir Moreno, and Alex Arenas. “Paths to synchronization on complex networks.” In: *Physical review letters* 983 (2007), p. 034101 (cit. on p. 33).

[Gro59] D. M. Grobman. “Homeomorphisms of systems of differential equations”. In: *Doklady Akademii Nauk SSSR* (1959), pp. 880–881 (cit. on p. 34).

[Har60] Philip Hartman. “A lemma in the theory of structural stability of differential equations”. In: *Proceedings of the American Mathematical Society* 11 (1960), pp. 610–620 (cit. on p. 34).

[Hil07] Roland Hildebrand. “Positive partial transpose from spectra”. In: *Physical Review A* 76.5 (Nov. 2007), 052325:1–052325:5 (cit. on p. 105).

[HSL15] Lvlin Hou, Michael Small, and Songyang Lao. “Dynamical Systems Induced on Networks Constructed from Time Series”. In: *Entropy* 17 (2015), pp. 6433–6446 (cit. on p. 9).

[Joh14a] Nathaniel Johnston. *A237749*. https://oeis.org/A237749. “[Online; accessed 04-May-2022]". 2014 (cit. on pp. 37, 105).

[Joh14b] Nathaniel Johnston. *Counting the Possible Orderings of Pairwise Multiplication*. http://www.njohnston.ca/2014/02/counting-the-possible-orderings-of-pairwise-multiplication/. “[Online; accessed 04-May-2022]". 2014 (cit. on p. 104).

[Kur75] Yoshiki Kuramoto. "Self-entrainment of a population of coupled non-linear oscillators". In: *International Symposium on Mathematical Problems in Theoretical Physics*. Ed. by Huzihiro Araki. Berlin, Heidelberg: Springer Berlin Heidelberg, 1975, pp. 420–422. ISBN: 978-3-540-37509-8 (cit. on p. 10).

[KV05] Catherine Kyrtsou and Constantinos E. Vorlow. "Complex Dynamics in Macroeconomics: A Novel Approach". In: 2005 (cit. on p. 9).

[LZ02] X. Leoncini and G. M. Zaslavsky. "Jets, Stickiness and Anomalous Transport". In: *Physical Review E : Statistical, Nonlinear, and Soft Matter Physics* 65 (2002). 17 pages, 17 figures, p. 046216 (cit. on p. 11).

[Liu+15] Hongxiao Liu, Maxim Dolgushev, Yi Qi, et al. "Laplacian spectra of a class of small-world networks and their applications". In: *Scientific Reports* 5 (Mar. 2015), p. 9024. DOI: 10.1038/srep09024 (cit. on p. 20).

[Mar+02] Norbert Marwan, Niels Wessel, Udo Meyerfeldt, et al. "Recurrence-plot-based measures of complexity and their application to heart-rate-variability data". In: *Physical review. E, Statistical, nonlinear, and soft matter physics* 66 2 Pt 2 (2002), p. 026702 (cit. on p. 9).

[MT17] Georgi S. Medvedev and Xuezhi Tang. "The Kuramoto model on power law graphs". In: *arXiv: Adaptation and Self-Organizing Systems* (2017) (cit. on pp. 11, 33).

[Mer94] Russell Merris. "Laplacian matrices of graphs: a survey". In: *Linear Algebra and its Applications* 197-198 (1994), pp. 143–176. ISSN: 0024-3795. DOI: https://doi.org/10.1016/0024-3795(94)90486-3. URL: https://www.sciencedirect.com/science/article/pii/0024379594904863 (cit. on p. 20).

[MP04] Yamir Moreno and Amalio F. Pacheco. "Synchronization of Kuramoto oscillators in scale-free networks". In: *EPL* 68 (2004), pp. 603–609 (cit. on pp. 11, 33).

[Nar79] T. V. Narayana. "Lattice Path Combinatorics With Statistical Applications". In: 1979 (cit. on p. 35).

[NJZ09] Xiao-Hui Ni, Zhi-Qiang Jiang, and Wei-Xing Zhou. "Degree distributions of the visibility graphs mapped from fractional Brownian motions and multifractal random walks". In: *Physics Letters A* 373.42 (Oct. 2009), pp. 3822–3826. DOI: 10.1016/j.physleta.2009.08.041 (cit. on p. 9).

[Pan02] James Pantaleone. "Synchronization of metronomes". In: *American Journal of Physics* 70 (2002), pp. 992–1000 (cit. on p. 10).

[PRK01] Arkady Pikovsky, Michael Rosenblum, and Jürgen Kurths. "Synchronization - A Universal Concept in Nonlinear Sciences". In: *Cambridge Nonlinear Science Series*. 2001 (cit. on p. 10).

[Rob08] David C. Roberts. “Linear reformulation of the Kuramoto model of self-synchronizing coupled oscillators”. In: *Phys. Rev. E* 77 (3 Mar. 2008), p. 031114. DOI: 10.1103/PhysRevE.77.031114. URL: https://link.aps.org/doi/10.1103/PhysRevE.77.031114 (cit. on p. 11).

[Sie09] David A. Siegel. “Social Networks and Collective Action”. In: *American Journal of Political Science* 53.1 (2009), pp. 122–138. DOI: https://doi.org/10.1111/j.1540-5907.2008.00361.x (cit. on p. 9).

[Slo21] N. J. A. Sloane. *A001263*. https://oeis.org/A001263. “[Online; accessed 12-May-2022]". 2021 (cit. on p. 35).

[Slo22] N. J. A. Sloane. *A000712*. https://oeis.org/A000712. “[Online; accessed 04-May-2022]". 2022 (cit. on p. 126).

[Slo] N. J. A. Sloane. *A000108*. https://oeis.org/A000108. “[Online; accessed 12-May-2022]" (cit. on p. 36).

[SE19] Yury Sokolov and G. Bard Ermentrout. “When is sync globally stable in sparse networks of identical Kuramoto oscillators?” In: *Physica A: Statistical Mechanics and its Applications* (2019) (cit. on p. 11).

[SF99] Richard P. Stanley and Sergey Fomin. *Enumerative Combinatorics*. Vol. 2. Cambridge Studies in Advanced Mathematics. Cambridge University Press, 1999. DOI: 10.1017/CBO9780511609589 (cit. on pp. 35, 90).

[Str00] Steven H. Strogatz. “From Kuramoto to Crawford: exploring the onset of synchronization in populations of coupled oscillators”. In: *Physica D: Nonlinear Phenomena* 143.1 (2000), pp. 1–20. ISSN: 0167-2789. DOI: https://doi.org/10.1016/S0167-2789(00)00094-4. URL: https://www.sciencedirect.com/science/article/pii/S0167278900000944 (cit. on p. 11).

[Thr52] R. M. Thrall. “A combinatorial problem.” In: *Michigan Mathematical Journal* 1.1 (1952), pp. 81–88. DOI: 10.1307/mmj/1028989731. URL: https://doi.org/10.1307/mmj/1028989731 (cit. on p. 104).

[vW93] J. L. van Hemmen and W. F. Wreszinski. “Lyapunov function for the Kuramoto model of nonlinearly coupled oscillators”. In: *Journal of Statistical Physics* 72.1-2 (July 1993), pp. 145–166. DOI: 10.1007/BF01048044 (cit. on p. 11).

[Wan+16] Yanjun Wang, Jian Bu, Ke Han, et al. “A novel network approach to study communication activities of air traffic controllers”. In: *Transportation Research Part C Emerging Technologies* 68 (May 2016), pp. 369–388. DOI: 10.1016/j.trc.2016.04.017 (cit. on p. 9).

[WSG] Jianjun Wu, Huijun Sun, and Ziyou Gao. “Mapping to Complex Networks from Chaos Time Series in the Car Following Model”. In: *Traffic and Transportation Studies (2008)*, pp. 397–407. DOI: 10.1061/40995(322)37. eprint: https://ascelibrary.org/doi/pdf/10.1061/40995283222937. URL: https://ascelibrary.org/doi/abs/10.1061/40995283222937 (cit. on p. 9).

[Yu+15] Fei Yu, An Zeng, Sebastien Gillard, et al. “Network-based recommendation algorithms: A review”. In: *ArXiv* (2015) (cit. on p. 9).

[Zar16] María Zarauza Martínez. *Estudio de las transiciones de fase en un modelo de sincronización macroscópica*. http://hdl.handle.net/10902/9216. “[Online; accessed 10-May-2022]". July 2016 (cit. on p. 10).

[ZA05] G. M. Zaslavsky and V. Afraimovich. “Working with Complexity Functions”. In: *Chaotic Dynamics and Transport in Classical and Quantum Systems*. Ed. by P. Collet, M. Courbage, S. Métens, et al. Dordrecht: Springer Netherlands, 2005, pp. 73–85. ISBN: 978-1-4020-2947-9 (cit. on p. 11).